DIRECT PRODUCTION OF LOWER OLEFINS FROM SYNTHESIS GAS USING SUPPORTED IRON CATALYSTS

Directe productie van lagere olefines uit synthesegas met gedragen ijzerkatalysatoren

(met een samenvatting in het Nederlands)

PROEFSCHRIFT

ter verkrijging van de graad van doctor aan de Universiteit Utrecht op gezag van de rector magnificus, prof. dr. G. J. van der Zwaan, ingevolge het besluit van het college voor promoties in het openbaar te verdedigen op maandag 23 september 2013 des middags te 12.45 uur

door

Hirsa María Torres Galvis

geboren op 5 mei 1979 te Bogotá, Colombia

Promotores: Prof. dr. ir. K. P. de Jong
Prof. dr. J. H. Bitter

This research was carried out under project number 053.62.012 in the framework of the ACTS-ASPECT program of The Netherlands Organization for Scientific Research (NWO).

Al que todo me ha dado
y a mis padres

"Unos y otros flaquean, y caen por tierra, pero nosotros nos mantenemos erguidos y en pie."

Salmo 20:8

Gracias Abue…

ISBN: 978-90-393-5995-2
Cover design by the author
Printed by Gildeprint Drukkerijen

Table of contents

Chapter 1

General introduction

The Fischer-Tropsch process: Historical background and current state

The fast development and growth of transport industry during the 1920s spurred research on alternative processes for the production of liquid fuels, especially by countries with limited access to crude oil and available coal resources. Germany led the industrial development of coal-based fuels with the invention of a coal liquefaction process by Friedrich Bergius in 1913 in Rheinau-Mannheim *(1)* and the Fischer-Tropsch process invented by Franz Fischer and Hans Tropsch in 1926 during their work at the Kaiser Wilhelm Institute for Coal research in Müllheim *(2)*.

The Fischer-Tropsch process is the catalytic conversion of synthesis gas, a mixture of H_2 and CO, into mainly hydrocarbons. The conversion of carbon monoxide and hydrogen mixtures to liquid hydrocarbons in the presence of a heterogeneous metal catalyst was first reported by Mittasch and Schneider in 1913. The process was not further developed or commercialized at that time due to the complexity of the products mixture obtained from the reaction instead of a single defined product *(3)*. Fischer and Tropsch recognized the value of liquid hydrocarbon mixtures as transportation fuels and developed promoted metal catalysts for their production from coke-oven off-gases. The industrialization and commercialization of the Fischer-Tropsch (FT) technology was first accomplished by Ruhrchemie AG in 1936 *(4)*. By 1945 the industrial capacity of the FT process in Germany was approximately 600 x 10^3 t per year *(5)*. Other FT plants were built during the 1940s in France, Japan and Manchuria under Ruhrchemie licenses and they remained in operation until 1945.

In the immediate post-World War II years the interest in the FT process persisted in view of the rapidly increasing oil consumption, the concerns about its limited reserves, and the forecasted high oil prices. During the late 1940s and mid-1950, three FT plants were built in the United States but they shut down in the 1950s mainly forced by a sharp increase in the price of methane for the production of syngas *(2,6)*. The construction of the Sasol FT plant, Sasol 1, began in 1952 in Sasolburg, South Africa. Before the construction of the Sasol plant was completed, large oil reserves were discovered in the Middle East, the North Sea, Alaska and other areas thus reducing the competitiveness of coal-based processes. The Sasol plant was the only commercial coal-based FT plant that was operational between the 1960s and

the early 1970s *(2)*. The energy crises in the 1970s revived the interest in the Fischer-Tropsch technology because of increasing prices of crude oil, prompting Sasol to start the construction of Sasol 2 at Secunda in 1976. By the mid-1980s, Sasol had yet built a third FT plant summing up to a total capacity of 6000 x 10^3 t per year.

In the early 1990s two FT plants based on natural gas-derived syngas came on stream: the Mossgas plant (PetroSA) in Mossel Bay, South Africa, and the Shell plant in Bintulu, Malaysia, with capacities of 1000 x 10^3 and 500 x 10^3 t per year, respectively. The commercial expansion of the gas-to-liquids (GTL) process continued during the 2000s to present with the construction and operation of the ORYX (Sasol/Chevron/QP) and Pearl (Shell/QP) plants in Qatar with nameplate capacities of 1.7 x 10^6 and 7 x 10^6 t per year, respectively *(4)*.

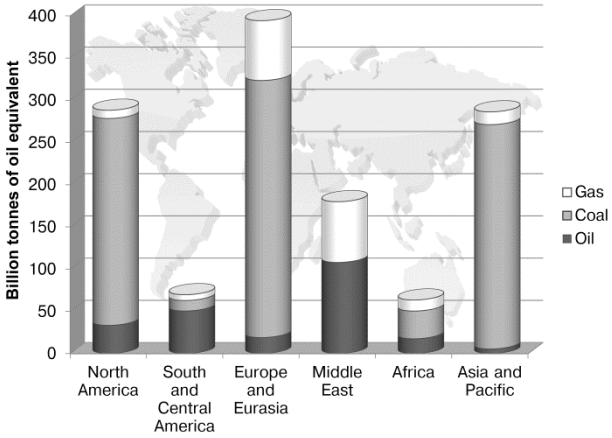

Figure 1. Proven reserves of fossil fuels by the end of 2011 *(7)*.

The coal-to-liquids (CTL) process has been gaining importance in the latest years in countries with large coals reserves, particularly in China *(8)*. In these regions (Figure 1), coal has a relatively low cost in comparison to natural gas, making the coal-based processes economically competitive. The advances in carbon capture and storage have also contributed to further the potential of fuel production using coal as feedstock *(9)*.

The production of transportation fuels from biomass or BTL process (biomass-to-liquids) has been presented as an alternative to produce clean and carbon-neutral diesel *(10)*. Research efforts in the development of BTL are mainly

directed to the design of catalysts with longer lifetimes that can withstand the presence of poisons present in biomass-derived syngas.

The development of XTL processes (X: natural gas, coal or biomass) has been fostered by high oil prices, environmental concerns and the strategic necessity of many countries to reduce their reliance on imported oil for the production of transportation fuels. For similar reasons, there is a growing interest in the development of alternative processes for the production of chemicals from non-oil based sources.

Several processes for the conversion of syngas into commodity chemicals such as lower olefins (ethylene, propylene and butylenes) have been developed *(11,12)*. Two processes based on the Fischer-Tropsch reaction have been proposed for the production of C_2-C_4 olefins: cracking of liquid hydrocarbons produced via traditional FT synthesis *(13)* and the Fischer-Tropsch-to-olefins route (FTO) which is a direct process to convert natural gas, coal or biomass-based syngas into lower olefins *(14,15)* .

The Fischer-Tropsch reaction

The formation of hydrocarbon products from synthesis gas in the Fischer-Tropsch reaction involves the addition of one carbon atom at a time with the simultaneous production of water according to the following overall reaction:

Hydrocarbons: $$n\mathrm{CO} + 2n\mathrm{H_2} \rightarrow (-\mathrm{CH_2}-)_n + n\mathrm{H_2O} \quad [1]$$

During the Fischer-Tropsch process, not only the formation of alkenes and alkanes takes place but also other parallel reactions occur:

Alcohols: $$n\mathrm{CO} + 2n\mathrm{H_2} \rightarrow \mathrm{C}_n\mathrm{H}_{2n+2}\mathrm{O} + (n-1)\mathrm{H_2O} \quad [2]$$

Water-gas shift (WGS): $$\mathrm{CO} + \mathrm{H_2O} \leftrightarrow \mathrm{CO_2} + \mathrm{H_2} \quad [3]$$

Methanation: $$\mathrm{CO} + 3\mathrm{H_2} \rightarrow \mathrm{CH_4} + \mathrm{H_2O} \quad [4]$$

Boudouard reaction: $$2\mathrm{CO} \leftrightarrow \mathrm{C} + \mathrm{CO_2} \quad [5]$$

The formation of methane (Equation 4) and carbon deposits (Equation 5) are thermodynamically favored between 200°C and 400°C *(11)*. These reactions are highly undesirable as they have a negative impact on catalytic performance; on the one hand, the production of methane during the Fischer-

Tropsch synthesis is unwanted as this is a low-value product that is formed at the expense of more desirable products. On the other hand, carbon deposition or carbon lay-down is one of the main deactivation mechanisms of Fischer-Tropsch catalysts *(16-18)* and it is also the cause of attrition problems at the nanoscale when using bulk iron catalysts at high temperatures *(19,20)*.
The Fischer-Tropsch synthesis can be identified as a surface polymerization reaction that consists of different reaction steps:

1. Adsorption of the reactants
2. Formation of the chain initiator
3. Chain growth or propagation
4. Chain termination
5. Product desorption

In view of the nature of the FT reaction, a range of hydrocarbons with different carbon-chain lengths is obtained rather than a single product. The chain length distribution of the hydrocarbon products can be described using the Anderson-Schulz-Flory (ASF) model *(11)*:

$$\ln\left(\frac{W_n}{n}\right) = n \ln \alpha + \ln\left[\frac{(1-\alpha)^2}{\alpha}\right] \qquad [6]$$

Where W_n is the weight fraction of the product with n carbon atoms and α is the chain growth probability.
The FT product stream in general comprises mixtures of alkanes, alkenes and oxygenates, such as alcohols, esters, aldehydes and carboxylic acids. Product selectivity can be tuned by changing the composition of the catalyst and the reaction conditions.
Several reaction mechanisms have been proposed to explain the product distribution of the Fischer-Tropsch synthesis. The most widely accepted is the 'alkyl' mechanism or surface carbide mechanism (in the case of iron-based catalysts) *(9,17)*.
In this reaction mechanism (Figure 2) the chain initiator is formed by dissociative adsorption of CO and posterior removal of surface oxygen by reaction with adsorbed hydrogen to form water or with adsorbed CO to form CO_2. The surface carbon is subsequently hydrogenated to form CH, CH_2 (monomer) and CH_3 (chain initiator) surface species. Carbon-chain growth

proceeds via insertion of CH_2 species and termination occurs either via β-hydride abstraction to yield α-olefins or by hydrogenation to produce paraffins. Simplified schemes of other reaction mechanisms proposed for the Fischer-Tropsch synthesis are shown in Figures 3 and 4.

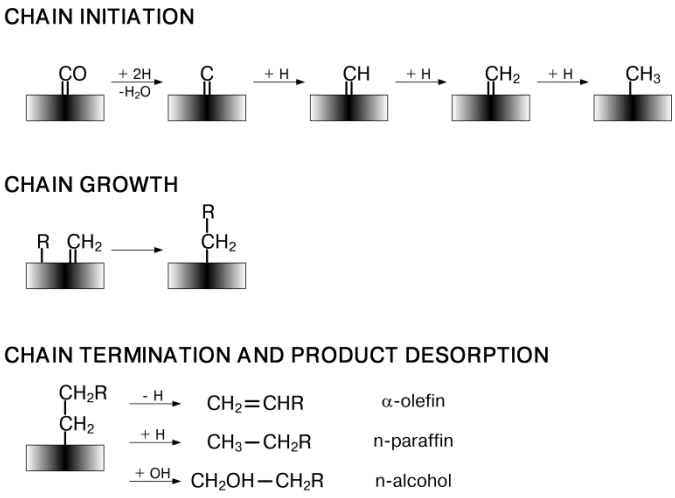

Figure 2. Alkyl mechanism

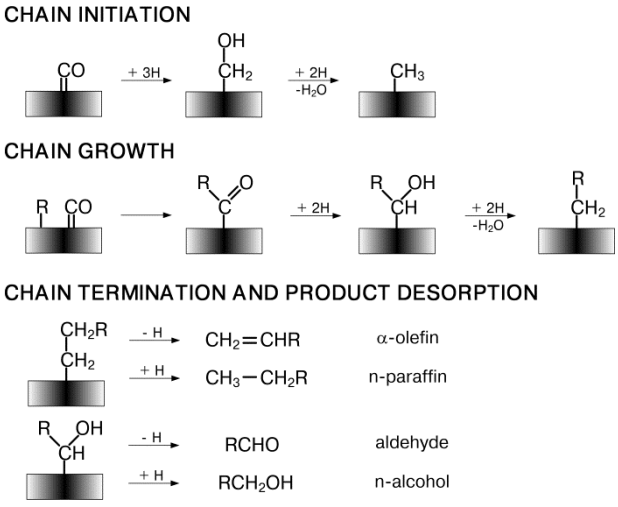

Figure 3. CO insertion mechanism

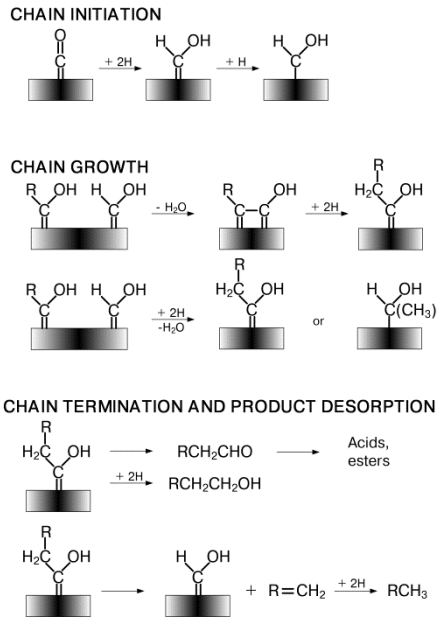

Figure 4. Enol mechanism

Fischer-Tropsch catalysts: Iron versus cobalt

Iron and cobalt catalysts are both industrially used for the conversion of syngas into hydrocarbons. Cobalt is used in low temperature FT synthesis to produce diesel, waxes, lubricants and gasoline. Iron-based catalysts are used for the production of waxes in the low temperature Fischer-Tropsch process (LTFT, 220 to 240°C) while in the high temperature process (HTFT, 320 to 350°C) they are used for the production of light alkenes and liquid fuels, primarily gasoline but also diesel fuel range.

Cobalt is much more expensive than iron, however, Co-based catalysts exhibit higher productivities at high conversions and longer lifetimes *(21)*. Cobalt catalysts prepared using oxidic supports are more attrition resistant than bulk iron catalyst. Co catalysts are more sensitive to deactivation by poisoning by contaminants (N, S) than Fe-based catalysts.

Iron and cobalt catalysts are not directly comparable as they have different operating ranges. However, it is generally observed that cobalt yields a product rich in alkanes (Figure 5) whereas α-olefins are preferentially formed when using Fe catalysts.

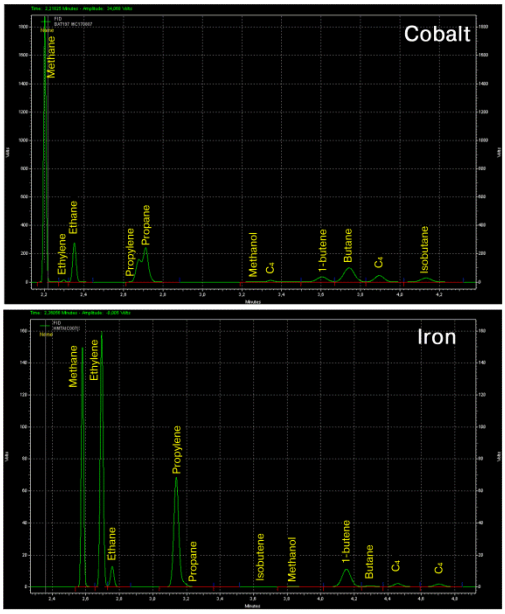

Figure 5. Comparison of product selectivity between iron and cobalt catalysts (GC chromatograms)

Iron possesses a high activity for the water gas shift (WGS) reaction. Synthesis gas derived from coal, which has a high CO content, can be used directly for the FT reaction on Fe-based catalysts, eliminating the need of an upstream shift reactor to increase the H_2/CO ratio. Additionally, processes using syngas with high CO_2 contents, *e.g.* biomass-derived gas, could benefit from the reverse WGS reaction *(2)*.

Iron and cobalt have different responses to changes in process parameters. For iron, the increase of reaction temperature results in a decrease of the carbon chain length of the products without affecting the olefin-to-paraffin ratio. In the case of cobalt, not only the chain growth probability decreases with increasing temperature but also methane production increases significantly and the extent of secondary hydrogenation and isomerization reactions is enhanced.

Promoted iron catalysts exhibit moderate to low methane selectivity even when the reaction is carried out at high temperatures (> 300°C) in the presence of CO-rich syngas. Fe-based catalysts allow the production of low molecular weight hydrocarbons by increasing reaction temperature without excessive methane selectivity.

In view of its properties, iron is the obvious metal of choice for the development of catalysts for the Fischer-Tropsch synthesis of lower olefins from coal or biomass-derived syngas. However, one of the major challenges faced when using iron-based catalysts at high temperatures for the conversion of CO-rich syngas is their stability. The formation of iron carbide, the active phase for the Fischer-Tropsch reaction, induces changes in the morphology of iron-containing particles resulting in fragmentation, in particular of so-called 'bulk catalysts', and the nucleation of carbon filaments.
The catalyst design strategy in the present work comprises the use of inert supports to stabilize Na plus S-promoted iron nanoparticles. Carrier materials with weak metal-support interaction allow the formation of the active carbide phase to achieve high catalytic activity while limiting the sintering and posterior fragmentation of iron-containing particles thus improving catalyst stability.

Scope of the thesis

The main aims of this work are the design and development of highly active, selective and stable Fe-based catalysts for the direct synthesis of lower olefins from synthesis gas and the systematic study of the factors that determine their catalytic performance. **Chapter 2** highlights the relevance of non-petroleum-based processes for the production of C_2-C_4 olefins and surveys research conducted on catalysts proposed for the Fischer-Tropsch synthesis of these major chemical building blocks. The newly developed catalysts and their performance in the Fischer-Tropsch-to-olefins (FTO) process are described in **Chapter 3**. Emphasis is made on the influence of the nature of the support on catalytic activity and stability. **Chapter 4** comprises a study of the effect of iron (carbide) nanoparticle size on activity and selectivity of promoted and unpromoted catalysts using carbon nanofibers as support material. In **Chapter 5**, α-alumina supported Fe catalysts were used to investigate the influence of sodium and sulfur on C_2-C_4 and methane selectivities, catalytic performance and carbon deposition. Na plus S-promoted and unpromoted catalysts supported on α-alumina were prepared using different iron precursors to establish a comparison between catalysts with different extent of aggregation of iron-containing particles. The results of this study are discussed in **Chapter 6**. **Chapter 7** summarizes the most important findings of the present work and provides perspectives on the further development and optimization of FTO catalysts.

References

1. S. W. Weller, *Energy Fuels* **8**, 415-420 (1994).
2. B. H. Davis, M. L. Occelli, Eds., *Fischer-Tropsch Synthesis, Catalysts and Catalysis (Series: Studies in surface science and catalysis No. 163)* (Elsevier, Amsterdam, 2007).
3. J. L. Casci, C. M. Lok, M. D. Shannon, *Catal. Today* **145**, 38-44 (2009).
4. D. Leckel, *Energy Fuels* **23**, 2342-2358 (2009).
5. H. Schulz, *Appl. Catal. A* **186**, 3-12 (1999).
6. M. E. Dry, *Catal. Today* **71**, 227-241 (2002).
7. BP Statistical Review of World Energy June 2012. http://www.bp.com/statisticalreview.
8. X. Hao, G. Dong, Y. Yang, Y. Y. Xu, Y. W. Li, *Chem. Eng. Technol.* **30**, 1157-1165 (2007).
9. A. P. Steynberg, M. E. Dry, Eds., *Fischer-Tropsch Technology (Series: Studies in surface science and catalysis No. 152)* (Elsevier, Amsterdam, 2004).
10. E. van Steen, M. Claeys, *Chem. Eng. Technol.* **31**, 655-666 (2008).
11. C. Wang, L. Xu, Q. Wang, *J. Nat. Gas Chem.* **12**, 10-16 (2003).
12. M. Janardanarao, *Ind. Eng. Chem. Res.* **29**, 1735-1753 (1990).
13. T. V. M. Rao, X. Dupain, M. Makkee, *Microporous Mesoporous Mater.* **164**, 148-163 (2012).
14. E. Schwab, A. Weck, J. Steiner, K. Bay, *Oil Gas Eur. Mag.* **1**, 44-47 (2010).
15. C. López, A. Corma, *ChemCatChem* **4**, 751-752 (2012).
16. N. E. Tsakoumis, M. Rønning, Ø. Borg, E. Rytter, A. Holmen, *Catal. Today* **154**, 162-182 (2010).
17. E. de Smit, B. M. Weckhuysen, *Chem. Soc. Rev.* **37**, 2758 (2008).
18. C. H. Bartholomew, *Appl. Catal. A* **212**, 17 (2001).
19. D. B. Bukur, W. P. Ma, V. Carreto-Vazquez, *Top. Catal.* **32**, 135-141 (2005).
20. D. S. Kalakkad, M. D. Shroff, S. D. Köhler, N. B. Jackson, A. K. Datye, *Appl. Catal. A* **133**, 335-350 (1995).
21. A. Y. Khodakov, W. Chu, P. Fongarland, *Chem. Rev.* **107**, 1692-1744 (2007).

Chapter 2

Catalysts for production of lower olefins from synthesis gas: A review

Abstract

C_2 to C_4 olefins are traditionally produced from steam cracking of naphtha. The necessity for alternative production routes for these major commodity chemicals via non-oil based processes has driven research in past times during the oil crises. Currently, there is a renewed interest in producing lower olefins from alternative feedstocks such as coal, natural gas or biomass, in view of high oil prices, environmental regulations and strategies to gain independence from oil imports. This review describes the major routes for the production of lower olefins from synthesis gas with an emphasis on a direct or single step process, the so called FTO or Fischer-Tropsch to Olefins process. The different catalysts for FTO are outlined and compared and the key issues and requirements for future developments are highlighted. Iron-based catalysts are prevailing for FTO and reproducible lower olefin selectivities of 50 wt% of hydrocarbons produced have been realized at CO conversions higher than 70% for 60 to 1000 h on stream. Remarkably the high selectivity to lower olefins has been achieved over a broad range of process conditions (P, T, H_2/CO ratio, GHSV). A major challenge for further development and application of FTO catalysts is the suppression of carbon lay-down to enhance catalyst lifetime and to preserve their physical integrity under demanding reaction conditions.

Adapted with permission from H. M. Torres Galvis and K. P. de Jong, *Catalysts for production of lower olefins from synthesis gas: A review*, ACS Catal. (2013) http://dx.doi.org/10.1021/cs4003436.

Introduction

Lower olefins

Ethylene, propylene and butylenes are key building blocks in the chemical industry. Throughout this review we refer to C_2-C_4 olefins as lower or light olefins. These base chemicals are among the organic chemicals with the largest production volumes worldwide (Table 1). Their broad spectrum of derivatives result in a very diverse end market ranging from packing materials and synthetic textiles to anti-freezing agents, solvents and coatings.

Table 1. Production of organic chemicals in 2010 in thousands of metric tons *(1)*

	U.S.A.	ASIA[a]	CHINA	EUROPE
Ethylene	23975	18237	14188	19968
Propylene	14085	14295	n.a.	14758
Ethylene dichloride	8810	3222[d]	n.a.	1323
Benzene	6862[b]	10889	5530	5107
Ethyl benzene	4240	n.a.	n.a.	1226
Cumene	3478	n.a.	n.a.	n.a.
Ethylene oxide	2664	845[d]	n.a.	2619
Butadiene	1580[c]	2715	n.a.	2020
Methanol	n.a.	n.a.	15740	n.a.

n.a.: Information not available; [a]Japan, South Korea and Taiwan; [b]Thousands of liters; [c]1,3-Butadiene rubber grade; [d]Japan only.

Ethylene is the largest-volume petrochemical produced worldwide. It is used to produce intermediate chemicals of high importance in industry such as ethyl benzene, ethylene oxide and ethylene dichloride, which were listed, along with ethylene, in the top 30 highest volume chemicals in the United States in 2000 *(2)*. The major chemicals derived from ethylene and their derivatives are shown in Figure 1. Ethylene is mainly used by the plastics industry. In 2010, approximately 61% of the total consumption of ethylene was for production of polyethylene in the Western European countries (Figure 2). Ethylene is also used in the production of other plastics such as polystyrene (PS), polyethylene terephthalate (PET), and polyvinyl chloride (PVC), which are widely used in the packaging, textile and construction industries.

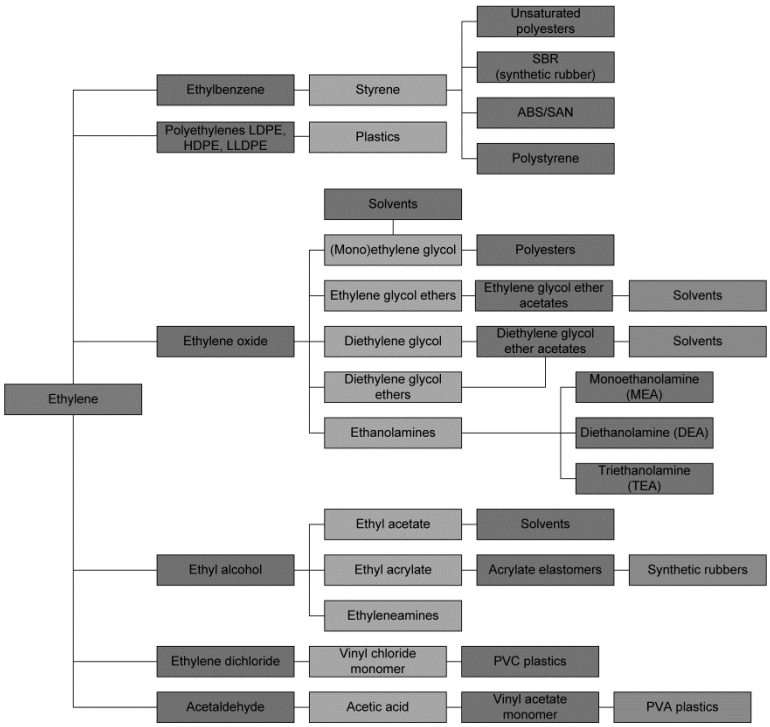

Figure 1. Ethylene and its derivatives

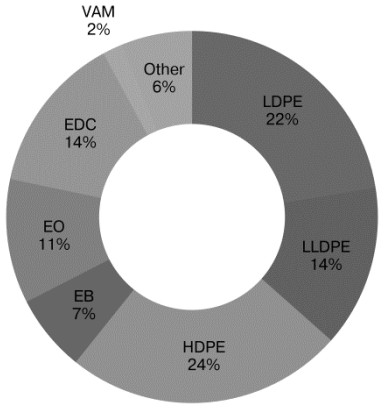

Figure 2. Ethylene consumption over different products in the Western European countries. LDPE: low-density polyethylene; LLDPE: linear low-density polyethylene; HDPE: high-density polyethylene; EB: ethyl benzene; EO: ethylene oxide; EDC: ethylene dichloride; VAM: vinyl acetate monomer. Statistics of 2010 *(3)*.

The commercial ethylene production is mainly based on steam cracking of a broad range of hydrocarbon feedstocks. In Europe and Asia, ethylene is obtained mainly from cracking of naphtha, gasoil and condensates, while in U.S., Canada and the Middle East ethylene is produced by cracking of ethane and propane. Naphtha cracking is the major source of ethylene worldwide; however, gas cracking has being gaining importance in recent years.

Propylene is a versatile petrochemical which has even more derivatives than ethylene. However, the tremendous growth of polypropylene consumption over the last 15 years has been the main driver of the large increase of the demand of propylene. In 2010, more than 55% of propylene consumption was dedicated to the production of polypropylene in the Western European countries. Approximately 13% of the propylene was used in the production of propylene oxide which is a chemical precursor for the synthesis of propylene glycol and polyols. The rest of the production was used in the synthesis of cumene (about 8%), acrylonitrile, isopropyl alcohol and many other industrially relevant chemicals *(3)*.

Traditionally, propylene is produced as a byproduct of steam cracking of naphtha for ethylene production or it is recovered from refinery processes, especially from Fluid Catalytic Cracking (FCC). During steam cracking it is possible to tune the propylene/ethylene ratio by varying the severity of the cracking process. A low severity cracking process yields less ethylene and more byproducts. Although the normal condition is moderately high severity cracking to achieve ethylene maximization, the necessity to increase the production of high value byproducts such as propylene, may dictate lowering the severity during short-term optimization.

Refinery propylene is primarily derived from FCC, visbreaking/thermal cracking and coking. For all of these processes propylene is obtained as a diluted stream in propane. FCC-derived propylene accounts for approximately 30% of the global supply and this percentage tends to increase as the steam cracking-derived propylene decreases as a result of the growth of ethylene production from ethane-based cracking *(4)*. In recent years, the production of propene via dehydrogenation of propane (PDH) has grown in view of the availability of low-priced propane in shale gas *(5)*.

The C_4 olefins fraction is composed by butadiene, isobutylene and n-butenes which are used in fuel and chemical applications. Butadiene is mainly used as raw material for the production of different types of synthetic rubber (SBR, polybutadiene rubber, etc.). These synthetic rubbers are in high demand all

over the world, especially in Asia, for the manufacture of finished goods in the electronics and automotive sectors. Butadiene is also used for the production of ABS (acrylonitrile-butadiene-styrene), SB (styrene-butadiene) copolymer latex and block copolymers, and nitrile rubbers (NBR).

One of the most important applications of butylenes is in the fuel industry accounting for approximately 85% of the butylenes world production. They are used for the production of gasoline alkylate, polymer gasoline and dimersol, which are gasoline blending components. Isobutylene is a raw material for the synthesis of methyl tert-butyl ether (MTBE) and ethyl tert-butyl ether (ETBE), which are used as octane enhancers, and for the production of isooctane by dimerization and subsequent hydrogenation.

n-Butenes have a smaller chemical market compared with butadiene and isobutylene. They are used as comonomers for polyethylene, for the production of sec-butyl alcohol, which is a raw material in the synthesis of MEK (methyl ethyl ketone), and for the synthesis of higher olefins.

Approximately 95% of the butadiene world production is a byproduct of the steam cracking of naphtha and gas oil for the production of ethylene and propylene. Butadiene is then recovered from the C_4 cracker stream by extractive distillation. Other processes for the production of butadiene involve further processing of the C_4 stream, *e.g.* recycle co-cracking with and without selective or full dehydrogenation.

Alternative feedstocks

The constantly growing demand for lower olefins has caused the global production capacity to double over the past 15 years. During 2008 and 2009, ethylene demand decreased due to the slow global economic growth, nevertheless, analysts predict that the demand will grow after 2012 (Figure 3). It is expected that new steam crackers will provide sufficient ethylene to meet the growing demand. Propylene production will increase as well; however, according to experts the production capacity will be insufficient to cover the demand *(6)*.

The growth of the demand for lower olefins will inevitably increase the demand for the feedstocks required in the petrochemical industry. With the recent high oil prices, research has been directed to the development of processes based on alternative feedstocks for the production of lower olefins.

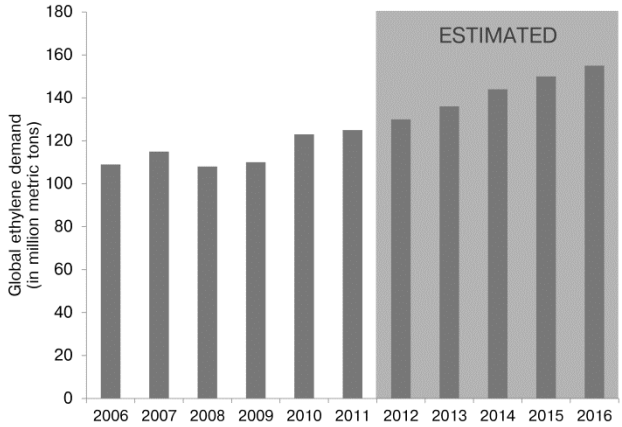

Figure 3. Ethylene demand in the period 2006-2011. Forecast for the period 2012-2016. Source: CMAI.

Apart from high oil prices, there are some other drivers in the search of alternative routes and feedstocks:

- The production of lower olefins via steam cracking is one of the ten most energy-consuming processes of the chemical and petrochemical industry *(7)*.
- There is a growing awareness of the depletion of conventional oil reserves. Some analysts suggest that the oil consumption will surpass the discovery of new reserves followed by the depletion of known reserves *(8)*.
- The oil contained in unconventional reserves is heavy oil in the case of so-called oil sands. The extraction and upgrading of unconventional oil currently may involve higher costs and higher CO_2 emissions in comparison with conventional oil *(9)*.
- There is a pressing necessity to decrease CO_2 emissions *(10)*. Feedstocks such as biomass have lower net CO_2 contribution *(11)*.
- Many countries, among them Japan, China and Brazil, are searching for alternatives to reduce their reliance on imported crude oil and refined products.

Several processes have been developed in an attempt to solve one or more of the challenges encountered by the lower olefins industry. These processes are based on alternative feedstock such as coal, natural gas or biomass.

Although coal has long been used as a feedstock for the chemical industry, for instance, for the production of acetylene via the carbide process and for the synthesis of ammonia, in times of abundant low-cost oil and gas, its role diminished.

The rapid increase of energy demand, the high oil and gas prices and the strategic drive of coal-rich countries to reduce their dependence on imported crude oil, have led to reconsider coal as a primary feedstock for the production of chemicals.

Countries with large coal reserves, such as China, are very active in the research, development and implementation of coal-based projects such as the transformation of syngas to olefins via methanol synthesis (MTO) or via dimethyl ether or SDTO process (Syngas via Dimethyl ether to Olefins). However, there are some challenges in the great potential of the coal-to-olefins industry. Coal gasification generates excess CO_2 that has to be removed from the synthesis gas and discharged from the plant. The environmental pressure to reduce CO_2 emissions may bring about CO_2 sequestration technologies that have to be implemented before coal-based processes are established worldwide.

Biomass gasification has a potential as a source for hydrocarbon products in view of feedstock flexibility and the possibilities to reduce net CO_2 emissions *(12-15)*. The use of biomass for the production of lower olefins might benefit from low feedstock costs and tax incentives. However, the potential for cost reduction in light olefins production is limited by the cost of collection and transportation of biomass in large-scale applications and the production of synthesis gas.

The use of biomass is mainly encouraged by its carbon-neutral nature. Biomass may be transformed through pyrolysis to achieve high energy density and then converted to syngas. The syngas obtained from biomass is CO-rich and in general contains several impurities, as it is the case for coal-based syngas. The syngas derived from these sources requires extensive purification to remove contaminants, such as sulfur, that are detrimental for the catalysts used in syngas transformation processes. For most conversion processes, the H_2/CO ratio needs to be adjusted by means of the water gas shift reaction (WGS). After purification and tuning the H_2/CO ratio, syngas can be used for the production of chemicals and fuels.

With the recent discovery of large shale gas reserves in the U.S. *(16,17)*, new possibilities are open for the transformation of natural gas to olefins. Wet shale

gas can be directly fed to ethane crackers to produce ethylene, while dry shale gas can be used for the production of syngas and thus be transformed directly or indirectly to lower olefins.

The increased availability of natural gas from shale deposits has produced a major shift in the feedstocks used for the production of ethylene in U.S. and consequently it has affected the propylene and butadiene markets. The use of ethane as feedstock for the crackers instead of naphtha results in a tighter supply of C_3 and C_4 olefins and it might increase the prices for those chemicals in the future *(5,18)*. These issues have also opened opportunities for alternative processes for the production of propylene and butylenes.

Large shale gas reserves have been found not only in U.S. but also in other countries such as China, which holds the largest technically recoverable reserves *(19)*. The exploitation of shale gas for energy purposes and for the production of lower olefins is expected to increase dramatically in the years to come in spite of some environmental concerns related to its extraction *(20)* and the high costs involved in the production of shale gas *(21)*.

Production of lower olefins from synthesis gas

Some of the alternative processes for the production of lower olefins are: dehydrogenation of lower alkanes, syngas-based processes and specific processes for target products such as the production of ethylene via dehydration of ethanol derived from renewable sources or propylene synthesis via dehydrogenation of propane obtained as a byproduct of biodiesel production.

Figure 4 displays the different conversion processes that use coal or biomass-based syngas as feedstock. The same scheme applies for H_2-rich syngas although in that case, the step for the adjustment of the H_2/CO ratio is not necessary. The processes for the production of lower olefins via syngas can be divided into two main groups: indirect processes, which require the synthesis of an intermediate such as methanol or dimethyl ether, and direct processes.

Indirect processes

Several indirect processes for the conversion of syngas to lower olefins have been developed in view of the selectivity restriction posed by the Anderson-Schulz-Flory product distribution that governs the Fischer-Tropsch synthesis *(22-25)*. The Methanol-to-Olefins process (MTO) has been developed and

commercialized in places where the technology has an economical advantage over naphtha cracking and other natural gas conversion processes.

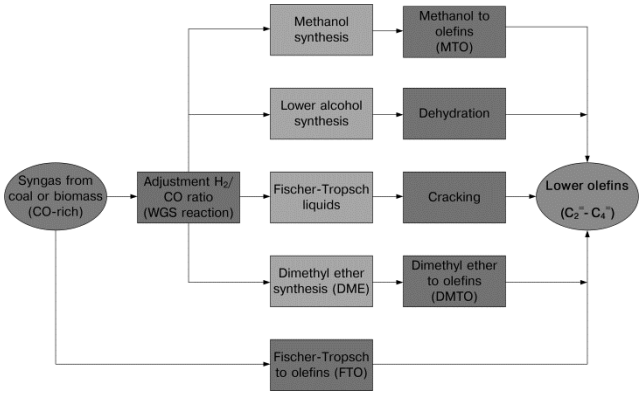

Figure 4. Processes for the transformation of CO-rich synthesis gas into lower olefins

Mobil synthesized the ZSM-5 zeolite and used it for the Methanol-to-Gasoline process (MTG) *(26)*. Later, the MTO process was developed by UOP/Hydro to produce a mixture of C_2-C_4 olefins from methanol using a zeolite-based catalyst. The main product of MTO is ethylene when the process is performed using a SAPO-34 catalyst. The MTO UOP/Hydro process produces up to 90% of light olefins from methanol but the SAPO-34 catalyst can be rapidly deactivated (in the order of minutes to hours) by coke formation depending on reaction conditions and crystal size *(27)*.

High selectivities to propylene have not been reported for the MTO process using SAPO-34 *(28)*. For this reason, the Methanol-to-propylene (MTP) process was developed by Lurgi to selectively produce propylene obtaining gasoline, fuel gas and LPG as byproducts. The ZSM-5-based Lurgi process produces up to 70% propylene from methanol via recycling of byproducts *(29)*.

Liu *et al.* (22) reported on a pilot plant for MTO using two reactors: the first reactor contained γ-Al2O3 to dehydrate methanol to dimethyl ether (DME) and the second one used ZSM-5 for the conversion of DME to light olefins. They obtained a C_2-C_4 olefin selectivity of 85 wt% (C_2H_4: 24 wt%; C_3H_6: 40 wt%) with a methanol conversion of 100%. The catalyst showed a good stability during the 1500 h of the test.

Another indirect process that has been developed is the Dimethyl ether-to-Olefins process (DMTO) that is also known as SDTO (Syngas-via-Dimethyl

ether-to-Olefins) or simply DTO. In principle this process could be more efficient than MTO as the synthesis of dimethyl ether (DME) from syngas has more favorable thermodynamics in comparison with methanol synthesis. The process uses two types of catalysts: in a first reactor the DME synthesis is carried out using a metal-acid bifunctional catalyst and the DME conversion reaction is performed using a SAPO-34 catalyst in a second reactor. Liu and coworkers *(22)* reported a C_2-C_4 olefin selectivity of 90 wt% (C_2H_4: ~ 60 wt%; C_3H_6: ~ 20 wt%) at a DME conversion of 100%, using a Cu-Zn/ZSM-5 catalyst for the conversion of syngas to DME and a metal-modified SAPO-34 type of molecular sieve for the conversion of DME to lower olefins. Selectivities to other products were not reported. The SAPO-type catalyst had to be regenerated by coke burn-off. The catalyst retained its performance after regeneration and only showed a small decrease in relative crystallinity in the presence of water *(30)*. It has been stated that DMTO should be closely related to MTO because of the fast conversion equilibrium that occurs among methanol, DME and water *(28)*; this has been observed as well by Liu *et al.* when they used methanol instead of DME on their modified SAPO-type catalyst obtaining similar selectivities *(22)*.

Zhao *et al. (28)* investigated the synthesis of light olefins over modified H-ZSM-5 catalysts using DME as feed. They obtained high C_2-C_4 olefin selectivities (up to 75%C) with preferential formation of propylene (~45%C) using zirconia-modified H-ZSM-5.

Some of other indirect processes for the production of lower olefins from synthesis gas that have been reported are:

1. The Texaco process *(31)*: This process consists of two stages: in the first step, syngas is converted into carboxylic acid esters in a homogeneous reaction in the presence of a ruthenium catalyst promoted with quaternary phosphonium salts. The second stage involves the pyrolysis of the aliphatic carboxylic acid esters to alkenes and the parent acid. Product selectivity can be tailored depending on the feed to obtain ethylene or propylene selectivities up to 55%.
2. A process developed by Dow Chemical Company to transform syngas into a mixture of lower alcohols (C_1-C_5) using molybdenum sulfides. The alcohol mix can be subsequently dehydrated to produce lower olefins.
3. The production of lower olefins from FT liquids *(32)*. Hydrocarbons that are produced through the Fischer-Tropsch reaction route can be transformed

into C_2-C_4 olefins through cracking and upgrading using traditional petrochemical processes.

All indirect processes involve more than one step which generates additional costs in terms of equipment and energy consumption. However, processes with high selectivities to ethylene such as MTO or DMTO, or highly selective towards propylene like MTP, can be of great interest for the production of polyethylene or polypropylene in remote areas not linked to chemical complexes *(33,34)*.

Direct processes

The direct conversion of syngas into lower olefins via the Fischer-Tropsch synthesis of Fischer-Tropsch to Olefins (FTO) process is an interesting option compared to cracking of FT liquids, MTO or DMTO *(34)*. The idea of following a direct route for the synthesis of lower olefins from synthesis gas has been considered for more than 50 years and many references can be found in literature about catalytic systems that might be suitable for this application *(24,25,35)*.

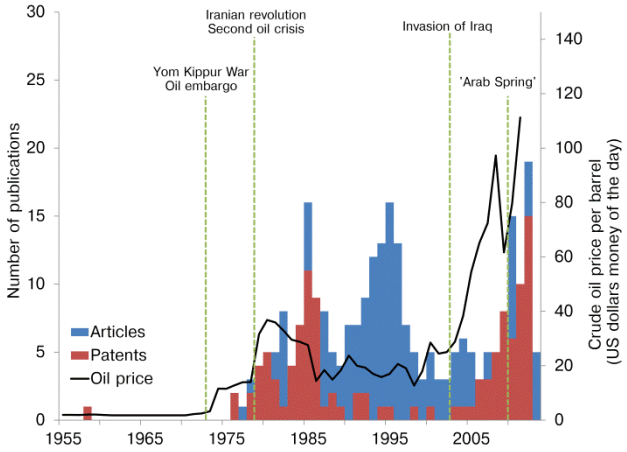

Figure 5. Scientific papers and patents on the direct production of lower olefins via Fischer-Tropsch *(36)* (bars) in 1955 – 2013 in relation to the oil price *(37)* (solid line).

Figure 5 represents the output of research publications and industrial patents on the direct Fischer-Tropsch synthesis of lower olefins since 1955. The increase in the number of publications in this subject was preceded by periods

where oil prices reached peak values. It is also clear that oil prices are strongly dependent on geopolitical issues as depicted in Figure 5.

It is interesting to observe for instance how the number of patents on the direct production of light olefins from syngas reached maximum values after the oil embargo of 1973 and the second oil crisis in 1979. The shortage and of the consequent high cost of oil for the production of light olefins via naphtha cracking increased the urge to develop alternative routes to produce these valuable commodity chemicals via syngas-based processes.

After oil prices dropped to lower levels, between 1987 and 2003, the number of patents on the topic decreased but academic research related to the catalysts and the process was still very active. During this period the scientific publications were mostly dedicated to the influence of chemical promoters and supports on C_2-C_4 olefins selectivity and to the optimization of process conditions to maximize the activity and selectivity towards the target products.

After the invasion of Iraq in 2003 oil prices raised steeply renewing the interest of chemical and petrochemical companies on more efficient catalysts and processes to produce lower olefins using natural gas, coal or biomass as feedstock. Once more in 2010, the oil prices increased dramatically caused by political instability in many oil-producing countries in the Middle East.

Therefore countries such as China and U.S. with large reserves of natural and shale gas or coal, are taking the lead on the research and development of direct processes for the production of C_2-C_4 olefins to ensure a reliable supply of these bulk chemicals and to achieve independence from oil imports. Figure 6 shows the 10 countries with the highest number of research papers and patents on catalysts for the production of lower olefins via Fischer-Tropsch.

Despite of the number of publications on the direct production of lower olefins via the Fischer-Tropsch reaction, there has been no commercial application for this process in view of the low C_2-C_4 olefins selectivity, low mechanical or chemical stability, or high methane production of some of the catalysts proposed up to now.

Researchers have developed different catalytic systems based on metals that exhibit CO hydrogenation activity. Among these metals only iron, cobalt, nickel and ruthenium have been found to be sufficiently active for their application *(38)*. From the commercial standpoint only Fe and Co are used as they are more readily available and less expensive compared to ruthenium. Ni is very active as well but it produces much more methane than Co or Fe and it forms

volatile carbonyls at the reaction conditions at which FT plants operate resulting in continuous loss of the metal. Other metals with moderate FT activity are Rh and Os. The products obtained from FT synthesis when using Rh as catalyst contain large fractions of oxygenates. Mo has also shown some FT activity in the presence of H_2S but it was found to be less active than Fe. Cr has also been investigated as a possible FT catalyst, but its activity is even lower than Mo.

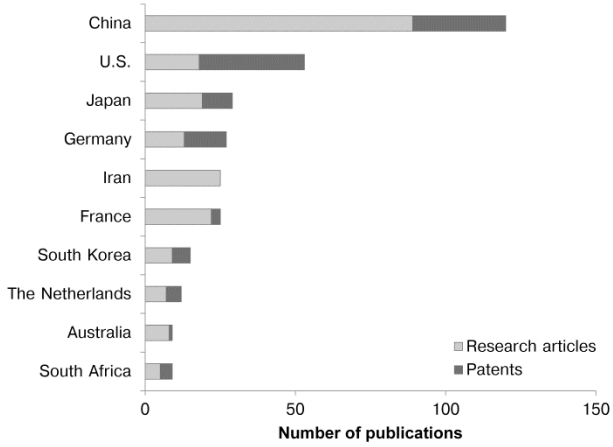

Figure 6. Number of publications on the direct production of lower olefins from synthesis gas from 1955 to 2013 ***(36)*** (Fischer-Tropsch only, top 10 countries).

It has been found that the properties of the FT active metals can be modified by adding chemical promoters to improve selectivity to light olefins or to enhance catalytic activity. Improvements on the mechanical stability of the catalysts might be achieved by addition of structural promoters whereas the surface area of the active metal can be extended by dispersing it on a support or carrier material. The different catalytic systems developed for the FTO process are discussed more in detail in the section dedicated to the Fischer-Tropsch to Olefins process.

To the best of our knowledge, there are no other direct syngas transformation routes to produce lower olefins apart from FTO. Some researchers have designed hybrid processes that use one reactor with two different catalysts such as the development reported by Arakawa *et al. (39)*. In this process the upper part of the catalyst bed consisted of a Rh-Ti-Fe-Ir/SiO_2 catalyst to produce ethanol and the lower part contained H-silicalite for alcohol

dehydration. This process produced approximately 45 %C of ethylene while propylene and butylenes were produced in negligible amounts. Although selectivity to ethylene was high, the selectivity to methane was near 33 %C. Another example is the composite catalyst developed by Denise *et al. (40)* where a physical mixture of a methanol catalyst (Cr_2O_3/ZnO) and dealuminated mordenite produced a mixture of light hydrocarbons (alkenes and alkanes in the C_1-C_5 range).

Other examples of hybrid processes involve the use of a Fischer-Tropsch catalyst to produce hydrocarbons from syngas and further cracking of the products in a second catalyst bed containing a zeolite *(41,42)*. Park *et al. (41)* used a precipitated Fe-Cu-Al_2O_3 catalyst promoted with potassium for the FT synthesis while cracking of the C_{5+} products was performed on ZSM-5. Using this dual bed reactor they obtained a C_2-C_4 olefins selectivity of 41 %C with a low methane production (10%) under high CO conversions (320°C, 10 bar and H_2/CO = 2). Although it could be expected that the stability of the zeolite would be compromised by the presence of water during reaction, Lee *et al. (42)* pointed out that ZSM-5 maintained its hydrothermal stability and activity at least during 100 h time on stream.

Fischer-Tropsch to Olefins process (FTO)

The Fischer-Tropsch synthesis is the reaction of CO and H_2 in the presence of an active catalyst to produce hydrocarbons and alcohols. Due to the nature of the reaction, which may be considered as a surface polymerization reaction, the product stream consists of a range of products instead of a single component. Although the mechanism of the Fischer-Tropsch reaction has been a matter of study for several years, it has not been completely elucidated yet. However, it is widely accepted that the reaction proceeds through a surface carbide mechanism which is shown as a simplified scheme in Figure 7.

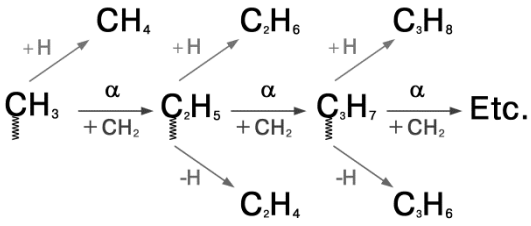

Figure 7. Fischer-Tropsch reaction mechanism (surface carbide mechanism).

The product distribution can be predicted using the Anderson-Schulz-Flory (ASF) model that depends on the chain growth probability α. Different factors have an influence on the alpha parameter such as process conditions, type of catalyst and chemical promoters *(43)*. The ASF product distribution as a function of α is depicted in Figure 8.

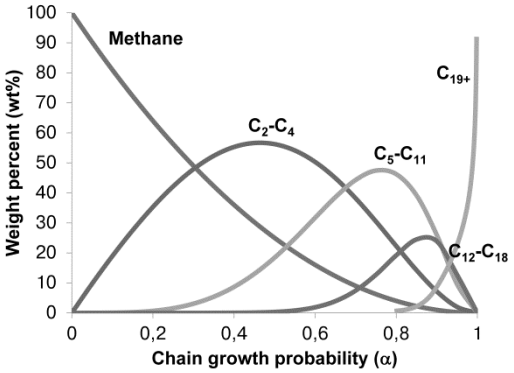

Figure 8. Anderson-Schulz-Flory (ASF) model for the prediction of product distribution.

Since the Fischer-Tropsch reaction has been known for almost a century, there is a vast amount of information related to the fundamentals of the reaction, the industrial process and the FT catalysts, which has been covered in several comprehensive reviews *(38,44-48)*. Other more specific reviews involve the preparation, application and deactivation of iron *(43,49,50)*, cobalt *(51-53)* and nickel *(54)* catalysts in the traditional Fischer-Tropsch process for the production of fuels. For this reason, we will not discuss the general aspects of the Fischer-Tropsch reaction or traditional FT catalysts but we rather focus on the Fischer-Tropsch synthesis of lower olefins or FTO and the catalysts for that purpose.

The primary aims of FTO are to maximize lower olefins selectivity, to reduce methane production and to avoid the formation of excess CO_2. According to the ASF model, the maximum selectivity towards C_2-C_4 olefins is achieved with an alpha value between 0.4 and 0.5. One of the most efficient ways of shifting product selectivity to low alpha values is by increasing reaction temperature. However, a decrease on the chain growth probability results in an increase of methane selectivity as indicated by the ASF product distribution. This effect was long considered a major restriction for the industrial application of the direct conversion of syngas into lower olefins via the Fischer-Tropsch

synthesis *(24,25)*. Negative deviations of the ASF model for methane selectivity have been observed for iron-based catalysts *(34,55)*. Schwab *et al. (34)* proposed that Fe catalysts possess different catalytic sites, some in charge of C-C coupling for the growth of the carbon chain and others responsible for methane formation. According to Schwab, these catalytic sites can be modified independently and controlled by addition of promoters. Torres Galvis *et al. (56)* ascribed the negative deviations of methane selectivity of Na/S-promoted iron catalysts to selective blockage of hydrogenation sites. They put forward that sulfur restricts the termination of carbon chain growth through hydrogenation thus favoring the β-hydride abstraction termination pathway. This proposal not only explains the lower methane selectivity but also the higher light olefins selectivity observed when iron catalysts were promoted with low amounts of sulfur.

The vast majority of the catalysts suggested for FTO contain iron. In comparison to cobalt, iron is less expensive, it has a lower activity, Fe Fischer-Tropsch products have a higher olefin content, as iron is less reactive to secondary hydrogenation reactions, and it displays lower methane selectivity at the high temperatures necessary to drive alpha to lower values. In view of their high water gas shift (WGS) activity, iron catalysts are an attractive option for the conversion of CO-rich syngas derived from coal or biomass because an additional H_2/CO ratio adjustment step is not necessary. Many catalyst formulations containing iron or other FT-active metals have been proposed for the synthesis of light olefins from synthesis gas. In this review we have divided these catalytic systems into two major groups: bulk or unsupported catalysts, including those materials with structural promoter content below 50 wt%, and supported catalysts.

Researchers in the field use different ways to present their catalytic data. The product selectivity for iron-based catalysts is generally reported excluding CO_2. Selectivity can be expressed based on weight (wt%: g of a product * 100 / g of hydrocarbons), molar-based (moles of a product * 100 / total moles of hydrocarbons) or carbon-based (%C: carbon atoms in a product * 100 / total carbon atoms present in hydrocarbons). The conversion of CO can be reported as total CO conversion (including CO_2) or CO conversion to hydrocarbons. Some other authors prefer to mention syngas conversion ($CO + H_2$) instead of CO conversion. In the following sections, product selectivity and CO conversion will be expressed as a percentage (%). The specific details on the

choice of the researchers to report their results can be found in the summary tables (Tables 3 and 4).

Bulk or unsupported iron catalysts

South Africa possesses large coal deposits and limited exploitable oil reserves. For this reason, this country has done its utmost to become independent from oil imports. In view of this necessity, the South African government issued a license to start the oil-from-coal project after the Second World War. Since 1955 SASOL has produced chemicals and gasoline using the so-called Synthol process *(57)*. The main aim of this process is to produce liquid fuels although lower olefins are also obtained depending on the operating conditions and the type of catalysts. The product selectivities obtained by SASOL with the low temperature (LTFT) and the high temperature (HTFT) processes is shown in Table 2.

Table 2. Fischer-Tropsch products of iron-based catalysts *(38)*

	LTFT SLURRY REACTOR T = 240°C 20 Bar	**HTFT FLUIDIZED BED REACTOR T = 340°C 20 Bar**
% Selectivities (C atom basis)		
Methane	4	8
C_2-C_4 paraffins	2.5	6
C_2-C_4 olefins	6	24
C_5-C_8	7	16
C_{7+}	76.5	41
Water soluble oxygenates	4	5
α	0.95	0.70

The catalyst used for the HTFT process in fluidized bed reactors is a fused catalyst containing iron oxide and structural and chemical promoters *(57)*. Table 2 shows that product selectivity towards short-chain hydrocarbons (C_1-C_6) and light olefins for the HTFT process is almost three times higher than for the low temperature process. The shift of product selectivity to short-chain hydrocarbons is reflected in the lower α and the two-fold increase in methane selectivity.

Between the mid 1970's and mid 1980's Ruhrchemie A. G. developed different catalysts for the HTFT process by mixing iron oxide with oxides of

other metals such as Ti, V, Mo, W, or Mn. It was reported by Büssemeier *et al. (58,59)* that mixed oxide catalysts could produce lower olefins with a selectivity of 70% while exhibiting a low methane production (~ 10%) at CO conversions of about 50% (280°C, 10 bar, H_2/CO = 1). They also reported that a catalyst prepared by sintering of Fe, Ti, Zn and K oxides displayed high light olefins selectivity (75%) and low methane selectivity (10%) at high syngas conversion (87%) when tested at 340°C *(60)*. The catalyst life in both cases was mentioned to be some hundreds of hours. This type of catalysts exhibits extensive carbon deposition and difficulties to reproduce the results have been encountered *(55)*.

Roy *et al. (61)* studied catalysts with similar composition as the fused catalysts patented by Ruhrchemie *(60)* but prepared by precipitation of iron nitrate in the presence of titania and further impregnation of the precipitate with Zn and K. The highest selectivity to light olefins they observed with the $Fe\text{-}TiO_2\text{-}ZnO\text{-}K_2O$ catalyst was obtained at a syngas conversion of 45%, 250°C, 2.5 bar and H_2/CO = 1. The selectivity to $C_2\text{-}C_3$ olefins was 68% and no C_4 products were reported while methane selectivity was approximately 20%.

Other mixed oxide catalysts were investigated by Goldwasser *et al. (62)* who prepared perovskite-like oxides by doping a $LaFeO_3$ matrix with K and/or Mn to obtain $La_{1-x}K_xFe_{1-y}Mn_yO_3$ oxides. When these materials prepared by co-precipitation were tested at 280°C, 11 bar and H_2/CO = 2, a high light olefins selectivity (70%) was observed in combination with a low methane production (10%) at low CO conversion (14%).

Although it has been reported that bulk mixed oxide catalysts are quite selective to lower olefins they have not been applied in commercial processes most probably due to their low stability *(55)*. Attempts to improve the stability of these systems included the modification of the catalysts by precipitating the oxides in the presence of a structural promoter such as SiO_2 or Al_2O (63), however, for these modified catalysts the achieved lower olefins selectivity was low (< 30 %C). A summary of the different bulk catalysts proposed for the direct production of lower olefins from synthesis gas is presented in Table 3.

Table 3. Unsupported catalyst for the Fischer-Tropsch to Olefins process

Catalyst -Elements present-	T (°C)	P (bar)	H_2/CO (molar)	CO conv. (%)	CH_4 (wt%)	C_2-C_4 olefins (wt%)	CO conv. to CO_2 (%)	Reference
Fe-Mn	350	15	2	96	30	52	NR	Wang *et al. (23)*
Fe-V-Zn-K	320	10	1	85[a]	12	59	NR	Büssemeier *et al. (59)*
Fe-Mn-Zn-K	320	10	1	86[a]	10	71	NR	Büssemeier *et al. (59)*
Fe-Ti-Zn-K	340	10	1	87[a]	10	75	NR	Büssemeier *et al.(60)*
Fe-Ti-Zn-K	250	2.5	1	45[a]	20	68	NR	Roy *et al. (61)*
La-K-Mn-Fe	280	11	2	14	10	70	30	Goldwasser *et al. (62)*
Fe-Cu-Al (sol-gel)	300	10	2	96	7[c]	21[c]	40	Kang *et al. (64)*
Fe-Au-K	360	10	2	97	16	39	31	Vielstich *et al. (65)*
Fe carbonyl-Na	340	23	1	98	15[d]	44[d]	NR	Hoffer *et al. (66)*
$(Co_{0.73}Fe_{0.27})_{0.58}[Co_{0.69}Fe_{2.31}O_4]$	250	10	1	5	34	52	15	Tihay *et al. (67)*
$(Co_{0.95}Fe_{0.05})_{0.62}[Co_{0.31}Fe_{2.69}O_4]$	230	10	1	2	25	36	25	Tihay *et al.(68)*
Fe/Mn/S	350	1	1	<5	28[d]	45[d] (C_2)	NR	Van Dijk *et al. (69)*
0.59 g Na/0.12 g S/100 g Fe	330	20	4	41[a]	9[d]	39[d]	NR	Crous *et al. (70)*
0.8 g K/0.2 g S/100 g Fe	360	40	4	12[a]	12[d]	37[d]	NR	Crous *et al. (70)*
Fe-Mn poisoned with H_2S feed	450	1	2	18	5-7[d]	60[d,e]	NR	Hadadzadeh *et al. (71)*
Fe-Mn	300	1	1	10	44[c]	26[c]	~ 50	Gónzalez-Cortés *et al. (72)*
Fe-Co-Mn	300	1	1	60	34[c]	25[c]	~50	Gónzalez-Cortés *et al. (72)*
Fe-Co	450	1	4	85	NR	54[d,e]	NR	Mirzaei *et al. (73)*
Fe-Co-Si	450	1	4	92	NR	65[d,e]	NR	Mirzaei *et al. (73)*
Fe-Co-Si-K	450	1	4	88	NR	64[d,e]	NR	Mirzaei *et al. (73)*
Fe-Co-K	260	1	2	64	10[d]	54[d]	5	Feyzi *et al. (74)*
Mn-Fe	285	10	0.7	53	7	52	NR	Kölbel *et al. (75)*
Fe-Mn	298	12	0.6	30[a]	12	29	NR	Deckwer *et al. (76)*
Fe-Mn-K	305	21	1	92	10	34	44	Soled *et al. (77)*
Fe-Mn	300	2.5	1	NR	44	75[f]	NR	Hutchings *et al. (78)*
Fe-Mn	300	6	1	36	14	15[e]	NR	Copperthwaite *et al. (79)*
Co-Mn	190	3.5	1	24	6	9[e]	NR	Copperthwaite *et al. (79)*
Fe-Mn-K-C	330	15	2	98	30	43	21	Zhang *et al. (80)*
Fe-Ti-Mn-Zeolite	450	10	0.5	10	25[d]	49[d]	NR	Sano *et al. (81)*
MoO_3-Al_2O_3-K_2O	300	21	0.5	37	25	26	NR	Murchison *et al. (82)*

Table 3. Unsupported catalyst for the Fischer-Tropsch to Olefins process (continuation)

Catalyst -Elements present-	T (°C)	P (bar)	H_2/CO (molar)	CO conv. (%)	CH_4 (wt%)	C_2-C_4 olefins (wt%)	CO conv. to CO_2 (%)	Reference
In_2O_3-CeO_2	350	0.7	3	55[b]	24[d]	65[d]	45	Arai *et al. (83)*
Mo_2C	300	0.03	1	NR	35[d]	59[e]	NR	Kojima *et al. (84)*
Mo_2C-K	297	1	3	70	NR	55[g]	~50	Park *et al. (85)*
Co-Ce-SiO_2	450	1	2	95	15[d]	51[d]	NR	Mirzaei *et al. (86)*
Co-Th	240	1	2	NR	34[c]	32[d]	NR	Costa *et al. (87)*
Zr-Al	400	17	NR	22	NR	67	NR	Yao et al. *(88)*

Note: Product selectivities are reported excluding CO_2.
[a] Syngas conversion
[b] CO converted to hydrocarbons (%)
[c] Mole percent (%)
[d] Carbon-based selectivity (%C)
[e] $C_2 + C_3$
NR: Not reported
[f] % of alkenes in the C_2-C_4 fraction
[g] C_2-C_5 olefins

Alkali metals and sulfur as promoters

It has been shown by many researchers that the addition of promoters can improve lower olefins selectivity of iron-based catalysts. The promoters that are most commonly used are alkali metals. Potassium has been extensively studied as a promoter for iron catalysts and it has been reported that it increases the chain growth probability and enhances the production of olefinic hydrocarbons. Furthermore, it has been claimed that potassium has an effect on structural properties of bulk catalysts such as surface area and pore size *(89-93)* and that its addition affects the extent of reduction and carbidization *(94,95)*. Similar effects have been observed for sodium *(92,96,97)*.

The effect of alkali promoters on product selectivity and catalytic activity is highly dependent on the concentration of the promoters, the preparation method and the reaction conditions. Kang *et al. (64)* investigated the influence of the synthesis method on the performance of Fe-Cu-Al-K catalysts. They prepared two unsupported catalysts with similar compositions using the co-precipitation and sol-gel methods and two supported catalysts prepared by wet impregnation and impregnation/co-precipitation. The catalysts were tested at 300°C, 10 bar and H_2/CO of 2 for 70 h. The sample prepared with the sol-gel method exhibited the highest C_2-C_4 hydrocarbons selectivity (21%), with a yield of olefins of 11% and low methane selectivity (7%) at high CO conversion (96%). Kang *et al.* observed that C_2-C_4 selectivity and olefinic content decreased with an increase of surface acidity.

Bulk alkali-promoted catalysts have not only been prepared by co-precipitation or sol-gel methods but also by impregnation of preformed iron particles such as polycrystalline iron whiskers *(65)* or iron particles prepared from carbonyl precursors *(66)*. Hoffer *et al. (66)* reported a C_2-C_4 olefins selectivity of 44% with low methane selectivity (15%) at high CO conversion (98%) when Na-promoted Fe particles were tested at 340°C, 23 bar and H_2/CO of 1 (TOS = 60 h).

Although bulk catalysts promoted with Na or K have shown high selectivities to light olefins, their main disadvantage is that they suffer from fragmentation and attrition originated by the formation of carbon deposits or by phase transformations during carbide formation within large iron oxide crystals *(67,68,98)*.

Sulfur has also been used as a chemical promoter to increase lower olefins selectivity. Sulfur is widely known as a very effective poison for Fischer-Tropsch catalysts, especially in the case of cobalt-based systems. However,

some studies have shown that for Fe catalysts sulfur might act as a promoter, enhancing light olefins selectivity, reducing methane formation and even increasing catalytic activity at low concentrations and under specific reaction conditions *(69,99-101)*.

Crous *et al. (70)* filed a patent application for a catalyst with high selectivity to light olefins which consisted of a bulk iron oxide promoted with an alkali metal and a second promoter of the group: Be, Ge, N, P, As, Sb, S, Se and Te. They reported high selectivity to lower olefins (39%) and low methane formation (9%) with a syngas conversion of 41% when a precipitated catalyst promoted with sodium and sulfur was tested in the Fischer-Tropsch reaction at 330°C, 20 bar and a H_2/CO of 4.

Other studies have been performed with sulfur promoted catalysts where the promoter was not added during the preparation of the catalyst but it was incorporated in the catalytic system through exposure to H_2S *(71,102)*. Hadadzadeh *et al. (71)* investigated the effect of H_2S poisoning on catalysts prepared by co-precipitation of Fe and Mn nitrates in the presence of a structural promoter (titania, silica, alumina, magnesia or zeolite). Their results showed that the sulfur-poisoned catalysts exhibited higher ethylene and propylene selectivities and lower methane production and activity when tested at 450°C, 1 bar and H_2/CO of 2. Hadadzadeh and coworkers focused their research on the influence of the different structural promoters and preparation conditions on activity and selectivity but the effect of the promoters on stability was not specifically addressed.

Bimetallic systems

Another strategy used by several researchers to improve the catalytic performance of catalysts for the direct production of lower olefins from synthesis gas is the use of Fe-based bimetallic catalysts. Among them, Co-Fe *(67,68,72-74)* and Fe-Mn *(23,69,71,72,75-80,103)* catalysts are the most studied systems. In the case of Co-Fe catalysts, the researchers intended to improve catalytic stability and activity of the already olefin-selective Fe catalysts by alloying it with a more active Fischer-Tropsch catalyst like Co. The bulk Co-Fe catalysts are generally prepared by co-precipitation and they are usually promoted with chemical promoters such as K, Cu and/or Mn and modified with structural promoters such as SiO_2 or Al_2O_3.

Tihay *et al. (67,68)* reported on Co-Fe catalysts which contained both an alloy and a spinel phase. The catalysts were prepared by co-precipitation of iron and

cobalt chloride solutions with KOH. The highest C_2-C_4 olefins selectivity was observed for a catalyst with a Co/Fe of 0.45. This sample was tested at 250°C, 10 bar and a H_2/CO of 1. At low CO conversion (~ 5%), a light olefin selectivity of 52% was obtained while methane production was high (34%). It was reported that this catalyst was stable for 200 h.

González-Cortés *et al. (72)* studied Mn-promoted Co-Fe catalysts which were prepared as mechanical mixture of the metal oxides. The catalysts were tested at 300°C, 1 bar and a H_2/CO of 1. Under these conditions a catalyst with a molar composition of 100Fe:20Co:20Mn exhibited a C_2-C_4 olefins selectivity of 25% (CO conversion: 60%), which was the highest obtained for the studied Fe-Co-Mn systems. In comparison, an unpromoted Fe catalyst displayed a lower but stable CO conversion (40%) with a light olefins selectivity of ~ 32% and similar methane selectivity (~35%).

Fe-Co oxides prepared by co-precipitation of cobalt and iron nitrates in the presence of a structural promoter (1.5 wt% of TiO_2, SiO_2, Al_2O_3 or La_2O_5) were investigated by Mirzaei *et al. (73)*. After optimization of preparation procedure, catalyst composition and reaction conditions, they reported that a potassium promoted (1.5 wt%) 40Fe:60Co (molar basis) catalyst modified with SiO_2 showed ~ 48% of ethylene and ~ 20% of propylene in its product composition when tested at 450°C, 1 bar and a H_2/CO of 4 (CO conversion ~ 85%). The catalyst was found to be active and stable for 72 h under these reaction conditions and selectivities to other products were not specified.

A recently published work from Feyzi *et al. (74)* on Fe-Co catalysts prepared by co-precipitation of Fe and Co nitrates using the water-oil microemulsion technique reported that a K-promoted (2 wt%) 75Co:25Fe (molar basis) catalyst tested at 260°C, 1 bar and H_2/CO of 2 exhibited a C_2-C_4 olefins selectivity of ~ 54% while maintaining a low methane production at high CO conversion (~ 64%). Increasing the operating pressure from 1 bar to 10 bar resulted in an increase of CO conversion (~ 73%) and in a further decrease in methane selectivity (~ 7%). However, it had a negative impact on light olefins selectivity that decreased to ~33%.

Even though it has been claimed that Mn is an effective promoter to decrease methane selectivity and to increase C_2-C_4 olefins selectivity of Fe-based catalysts, the results reported by different research groups vary depending on the preparation method, catalyst composition, pretreatment and reaction conditions.

Van Dijk *et al. (69)* did not observe any effect of Mn on olefins selectivity when Fe-Mn catalysts were prepared by co-precipitation of Fe and Mn nitrates and when they were tested at 240°C, 1 bar and H_2/CO of 1 (CO conversions were kept below 5%). When reaction temperature was increased to 350°C, the Fe-Mn catalysts produced mainly methane. The impregnation of a Fe-Mn catalyst with a solution of ammonium sulfate resulted in a five-fold more active catalyst that produced olefins more selectively (CH_4: 28%; C_2H_6: 2%; C_2H_4: 45%). The sulfated (Fe_{at}/S_{at} = 200) and unsulfated catalysts exhibited a high extent of carbon deposition. Nevertheless, the sulfated catalysts displayed a lower mechanical strength evidenced by the disintegration of the catalyst particles after few hours. Van Dijk *et al.* indicated that higher quantities of S improved the resistance to carbon deposition, improving mechanical stability while maintaining a high C_2-C_4 olefins selectivity. The sulfur levels were maintained below 1 wt% to avoid catalyst deactivation via poisoning.

Soled *et al. (77)* prepared Fe-Mn catalysts as solid solutions by mixing Mn_3O_4, Fe_2O_3 and Fe powder and sintering the mixture at temperatures above 800°C. The catalysts were promoted by impregnation of potassium carbonate or sulfate. When the catalysts were tested at 300°C, 22 bar and H_2/CO of 1, they exhibited a high CO conversion (> 94%), low methane production and high light olefins selectivity. The catalysts promoted with potassium sulfate displayed a C_2-C_6 olefins selectivity almost two times higher than the sample promoted with potassium carbonate (~ 34%) and a lower methane selectivity (~ 10%).

Manganese promoted Fe and Fe-Co catalysts were compared by González-Cortés *et al. (72)*. In comparison with unpromoted Fe catalysts, Fe-Mn samples displayed lower C_2-C_4 olefins selectivities (~ 26%) and higher methane production (~ 44%) when the reaction was carried out at 300°C, 10 bar and H_2/CO of 1. In general, the Fe-Mn catalysts modified with Co showed higher methane selectivities compared to the catalysts without Co.

Wang *et al. (23)* investigated Fe-Mn catalysts prepared by the sol-gel method or by co-precipitation. Both types of catalysts were tested at 350°C, 15 bar and a H_2/CO of 2 (TOS = 300 h). The highest light olefins selectivity was achieved with a co-precipitated catalysts (15:85 Mn:Fe). At a very high CO conversion (> 90%), this catalyst showed a high C_2-C_4 olefins selectivity (~ 50%) and a methane selectivity of about 30%. They attributed the higher yield of alkenes obtained with co-precipitated catalysts to better carbidization and

reduction properties. The results obtained by Wang *et al.* pointed out that catalyst preparation is a key aspect that can determine the performance during reaction.

Zhang *et al. (80)* added carbon as a structural modifier for their Fe-Mn-K catalysts prepared via the sol-gel method. The catalysts were tested at 330°C, 15 bar and H_2/CO of 2. The highest C_2-C_4 olefins selectivity (~ 43%) was achieved at a high CO conversion (~ 98%) along with a methane selectivity of about 30%. The chain growth probability (α) decreased with an increase of the content of structural modifier while the C_2-C_4 fraction increased achieving a maximum at 5 wt% carbon content. Zhang and coworkers claimed that carbon promoted the formation of nanoparticles which enhanced the selectivity to light olefins.

Other bimetallic iron-based systems have been studied such as the co-precipitated Ni-Fe catalysts modified with alumina *(104)*. Nickel is a well-known methanation catalyst and it is expected that it would have a negative influence on the alkene to alkane ratio due to its high activity for hydrogenation. The research study by Cooper *et al. (104)* showed that the addition of Ni to bulk Fe catalysts results in a low alkene/alkane ratio when the Ni content was below 60%. Contrary to what was expected, bulk Ni-Fe catalysts with 60 or 80 wt% of Ni exhibited an alkene/alkane ratio of approximately 4 or 2, respectively.

A graphical summary of the bulk catalysts with the highest selectivity to lower olefins is displayed in Figure 9.

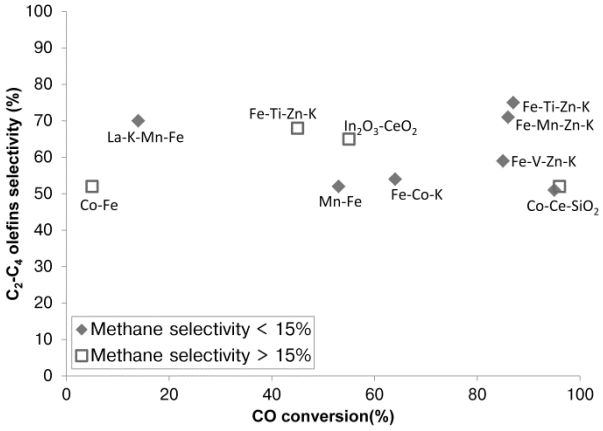

Figure 9. Bulk catalysts for the FTO reaction (C_2-C_4 olefins selectivity > 50%). Catalysts with CH_4 selectivities below 15%: diamonds.

From Figure 9 it can be observed that selectivities to C_2-C_4 olefins up to 75% were obtained using potassium-promoted catalyst. These catalysts were synthesized combining different promoters. The results reported for the Fe-Ti-Zn-K and Fe-Mn-Zn-K catalysts indicated that these catalysts not only had a high selectivity to lower olefins and low methane production but also a high activity (CO conversion ~ 90%). However, these results have been difficult to reproduce *(55,69)* probably originated by the complex structure of the catalyst, the presence of impurities in the precursors or differences in the activation procedure.

Non Fe-based catalysts

Research studies have been performed as well on catalytic systems that do not contain Fe (carbide) as an active phase for the production of light olefins from synthesis gas. These non-Fe based catalysts vary in composition from Co *(105)*, and precipitated K_2MoO_4 *(82)* to multicomponent systems such as Co-Mn *(79)*. Other non Fe-based catalysts have been used for the selective production of ethylene such as co-precipitated Cu-Cr-Co-Al_2O_3 *(106)* or for the preferential synthesis of ethylene and propylene using co-precipitated In_2O_3-CeO_2 *(83)* or Mo_2C *(84)*.

Potassium promoted molybdenum catalysts were developed by Park *et al. (85)*. These catalysts showed C_2-C_5 olefins selectivities up to 60% at high CO conversion (70%) when they were tested under the Fischer-Tropsch reaction at 297°C, 1 bar and $H_2/CO = 3$.

Cobalt based systems have been investigated by different research groups *(86,87,107)*. Mirzaei *et al.* studied the effect of catalyst preparation conditions (Co/metal ratios, ageing time and calcination temperature), structural promoters (titania, silica, alumina or zeolite) and reaction conditions (H_2/CO and reaction temperature) on catalytic performance. A Co-Ce catalyst modified with SiO_2 and tested at 450°C, 1 bar and H_2/CO of 2 exhibited a high C_2-C_4 olefins selectivity (~ 50%) with low methane production (15%) at a CO conversion of 90% (53). Mirzaei *et al. (107)* also reported on a Co-Mn-TiO_2 catalyst with high selectivity to ethylene and propylene (~ 15% and ~ 85%, respectively) at a CO conversion of 65%. Selectivities towards other products were not reported. Their results were obtained at 450°C, 1 bar and $H_2/CO = 3$.

Costa *et al. (87)* reported on a catalyst prepared by mixing dicobalt octacarbonyl and thorium acetylacetonate in a hydrogenated terphenyl. The

solution was heated up at 200°C to decompose the metal precursors forming a slurry catalyst. Syngas with a H_2/CO ratio of 2 was introduced in the catalyst suspension and the reaction was carried out at 240°C and 1 bar. It was reported that 88% of the hydrocarbons formed corresponded to the C_1-C_5 fraction with an olefin content of more than 80%.

A high selectivity to lower olefins was observed by Yao *et al. (88)* when they performed the Fischer-Tropsch reaction at 400°C and 18 bar using a Zr-Al catalyst. They reported a C_2-C_4 olefins selectivity of 67% at a CO conversion of 22%. The H_2/CO ratio used for the reaction and the selectivity to methane and other hydrocarbons were not specified.

Promoted bulk catalysts could be considered as the most interesting option for FTO because of their high selectivity to light olefins, low methane production, low cost and simple synthesis procedures. However, it is known that unsupported iron catalysts that are used for the Fischer-Tropsch reaction at high temperatures (> 300°C) and CO-rich syngas suffer from low mechanical stability. Bulk Fe catalysts tend to fragment due to carbon deposition or to density differences between the oxidic and carbidic phases present in the working catalyst *(98,108)*. In the case of carbon deposition it has been shown that bulk Fe catalyst particles break up and formation of fines may pose problems *(109,110)*. By moving to supported catalysts the carbon is to a certain degree contained in the pores and iron particles are much smaller and fragmentation is delayed or does not occur.

Figure 10 illustrates the structural changes of bulk iron catalysts upon carbidization. The large Fe_2O_3 crystals fragmented upon contact with CO at high temperature due to stress originated inside the particle by the formation of the carbide phase or by nucleation of carbon deposits (Figure 10C). The formation of iron carbide is necessary for the Fischer-Tropsch reaction as it is recognized as the active phase *(108,111)*. Advances in characterization techniques have allowed the investigation of carbides formation in working bulk Fe catalysts under industrially relevant conditions *(112,113)*.

In Figure 10D it is clearly observed that the small carbide particles were covered with a layer of graphitic carbon. In some cases, the carbon deposits grow as fibrils or filaments as observed by Torres Galvis *et al. (55)*.

A strategy to avoid or to restrict the nucleation of carbon deposits on iron-containing particles is to reduce their size from micrometers to nanometers. Small iron nanoparticles do not fragment further when they are put in contact with syngas at high temperatures; however, if they are close together, they

tend to aggregate forming large particles which ultimately nucleate carbon and fragment *(114)*. The use of a support material increases the stability of iron-based catalysts by serving as a mechanical anchor that maintain the nanoparticles separated avoiding the formation of clusters and particle growth. Several supports have been proposed for the dispersion of the active phase of FTO catalysts ranging from oxides and molecular sieves to clays and carbonaceous materials. The supported catalysts that have been used to selectively produce light olefins from synthesis gas are discussed in the following section.

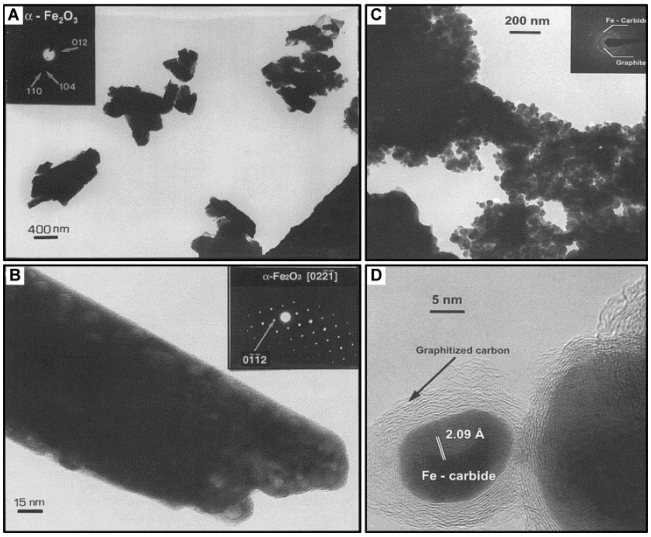

Figure 10. Fragmentation of bulk Fe catalysts upon exposure to CO. A, B: TEM images of a bulk iron catalyst before reaction. Electron diffraction showed that the primary particles were single α-Fe_2O_3 crystals. **C, D:** Micrographs after the catalyst was put in contact with CO at 400°C. The individual particles were identified as iron carbide and were covered by graphitic carbon. Adapted with permission from Kalakkad *et al. (98)*.

Supported Fe catalysts

Support materials are used in the preparation of heterogeneous catalysts to maximize the surface area of the active phase. For this reason, carrier materials with large surface areas such as silica or gamma alumina are traditionally preferred. Catalysts containing highly dispersed iron nanoparticles can be easily prepared by impregnating conventional high surface area supports with inorganic iron salts. The iron-containing nanoparticles of these catalysts have a relatively narrow size distribution and a homogeneous spatial

distribution thus minimizing the formation of aggregates. Nevertheless, iron has a strong interaction with most of the oxidic supports which results in the formation of mixed iron oxides that are not active for the Fischer-Tropsch reaction. It is known that iron aluminates *(115,116)* and iron silicates *(117-119)* are difficult to reduce which hinders the formation of the carbidic active phase. Consequently, catalysts prepared on γ-alumina or silica exhibit lower activities compared with catalysts supported on inert carriers *(55)*. Although a weakly interactive support allows activating the iron phase and facilitates a close contact between iron and chemical promoters, the weak physical binding between its surface and iron nanoparticles does not withstand the reaction conditions. As a result, iron-containing nanoparticles aggregate extensively and the catalyst deactivates due to a reduction in the active surface and to increased coke lay-down *(114)*. A schematic representation of the improved stability achieved when using a support material is shown in Figure 11.

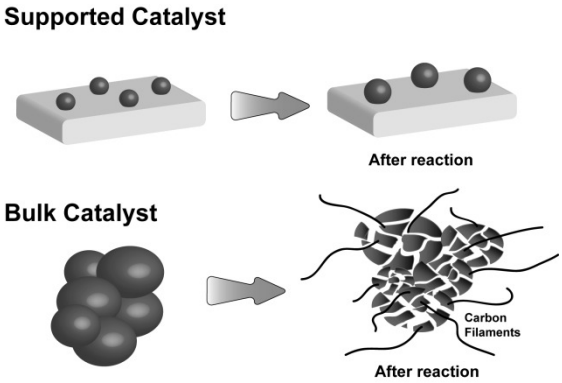

Figure 11. Stabilization of iron-containing nanoparticles using a support.

In view of the importance of the nature of the support and its influence on catalytic performance extensive research has been performed to find an optimal combination of active metal, support and modifiers. In the following sections, we will discuss the different catalysts that have been used for the synthesis of lower olefins via Fischer-Tropsch. The catalytic performance of these materials is summarized in Table 4.

Silica supported catalysts

Bruce *et al. (120)* prepared Fe, Fe/Mn, Fe/K, Fe/Mn/K catalysts by impregnation of silica gel with metal nitrates. For a comparison, they

synthesized also Fe/Mn/K and Fe/Mn supported catalyst using Fe/Mn or Fe/Mn/K carbonyls. The catalysts were tested at 300°C, 2-5 bar and a H_2/CO ratio of 1.5. Under low CO conversion (< 5%), a high selectivity toward lower olefins (64%) and low methane production (25%) was observed for the Fe/Mn/K carbonyl-based catalyst. Bruce and coworkers attributed the higher light olefin selectivity of the carbonyl-derived catalysts to a minimization of secondary hydrogenation reactions. It is expected that the impregnation of organometallic complexes would lead to better iron dispersions in comparison with iron nitrate which rapidly crystallize upon drying *(155)*. However, morphological or chemical differences between nitrate-based and carbonyl-based were not specifically mentioned.

A similar approach was used by Commereuc *et al. (121)* who prepared supported iron catalyst using iron carbonyl precursors and different oxidic supports. A high olefin selectivity (69%) was achieved when using a Fe/SiO_2 catalyst synthesized by impregnation of iron pentacarbonyl. The reaction conditions were 265°C, 10 bar, H_2/CO of 1 and low CO conversion (5%).

Stoop *et al. (122)* reported a high olefin selectivity when performing the Fischer-Tropsch reaction with a Ru/Fe (1:3) silica supported catalyst at 277°C, 1 bar and H_2/CO of 2. At CO conversions below 3%, this bimetallic catalyst exhibited low methane selectivity (10%) and high olefin to paraffin ratios (ethylene/ethane: 3; propylene/propane: 16). The Ru/Fe alloy combined the high olefin selectivity of Fe with the high catalytic activity of Ru. Interestingly, thermogravimetric studies showed that carbon deposition rates of the Ru/Fe (1:3) catalyst were higher than for unpromoted Fe/SiO_2. When reaction temperature was increased to 402°C the amount of carbon deposited increased steeply with time causing severe deactivation.

Table 4. Supported catalyst for the Fischer-Tropsch to Olefins process

Catalyst -Elements present-	T (°C)	P (bar)	H_2/CO (molar)	CO conv. (%)	CH_4 (%wt)	C_2-C_4 olefins (%wt)	CO conv. to CO_2 (%)	Reference
Fe-Mn-K/SiO_2	300	2-5	1.5	<5	25	64	NR	Bruce *et al. (120)*
Fe/SiO_2	265	10	1	5	21[a]	69[a,d]	NR	Commereuc *et al. (121)*
Ru-Fe/SiO_2	277	1	2	<3	26[a]	60[a,b]	NR	Stoop *et al. (122)*
Fe/SiO_2, sil-1 shell	380	10	0.5	21	21	30	NR	Jiang *et al. (123)*
Fe-Ce/ heat treated γ-Al_2O_3	280	8	0.5	3[c]	8	58	NR	Baker *et al. (124)*
Fe-Pr/heat treated γ-Al_2O_3	280	8	0.5	15[c]	7	63	NR	Baker *et al. (125)*
Fe/Al_2O_3	290	9	0.9	5	25	49	NR	Basset *et al. (126)*
Fe/γ-Al_2O_3	500	15	1	18	38	43	NR	Barrault *et al. (127)*
Fe-K/Al_2O_3	260	1	3	1	23[g]	60[g]	NR	Arakawa *et al. (128)*
Fe/Al_2O_3	470	15	1	20	29	41	NR	Barrault *et al. (129)*
Fe-Mn/Al_2O_3	340	15	1	70	19[a]	18[a]	NR	Barrault *et al. (130)*
Fe-S/Al_2O_3	470	15	1	14	28[a]	42[a]	NR	Barrault *et al. (130)*
Fe-Mn-S/Al_2O_3	470	15	1	12	28[a]	34[a]	NR	Barrault *et al. (130)*
Fe-Na-S/α-Al_2O_3	340	20	1	80	11[a]	53[a]	~50	Torres Galvis *et al. (55)*
Fe-K/Silicalite	280	21	0.9	NR	9	36	NR	Rao *et al. (131)*
Fe-Cu-K/Zr-ferrierite	300	10	0.5	96	34[a]	12[a,e]	38	Bae *et al. (132)*
Fe-Cu-K/ZSM-5	300	10	2	81	20[a]	30[a]	36	Kang *et al. (133)*
Fe-Mn-K/Silicalite-2	347	20	2	90	22	70	NR	Xu *et al. (134)*
Fe-Mn/Silicalite-1	275	21	1	10	9	65	3	Das *et al. (135)*
Fe-Cu-K/ZSM-5	300	10	2	81	18	10	38	Kang *et al. (136)*
Fe/K-ZSM-5	300	14	1	9	10	37[f]	NR	Mitsudo *et al. (137)*
Fe-Pd/ZnO	300	7	1	<10	45[g]	30[g]	NR	Gustafson *et al. (138)*
Fe-Mn/MgO	320	20	2	79	23	68	NR	Xu *et al. (139)*
Fe/MgO	176	1	0.5	1	26	58	NR	Hugues *et al. (140)*
Fe/MnO	270	1	1	10	12	59	28	Barrault *et al. (141)*
Fe-Al-laponite	412	1	3	NR	28[a]	43[a]	20	Barrault *et al. (142)*
Fe/O-CNT	340	25	1	50	8	92[h]	24	Schulte *et al. (143)*
Fe-Mn/C	250	1	1	NR	11	53	28	Barrault *et al. (144)*

Table 4. Supported catalyst for the Fischer-Tropsch to Olefins process (continuation)

Catalyst -Elements present-	T (°C)	P (bar)	H_2/CO (molar)	CO conv. (%)	CH_4 (%wt)	C_2-C_4 olefins (%wt)	CO conv. to CO_2 (%)	Reference
FeN-Mn/CNT	300	5	1	12	24	44	36	Yang *et al. (145)*
Fe-Na-S/CNF	340	20	1	88	13[a]	52[a]	~50	Torres Galvis *et al. (55)*
Fe/Activated carbon	350	1	1	2	18	61[f]	NR	Sommen *et al. (146)*
Fe/C	230	1	3	3	40[g]	32[f,g]	NR	Jung *et al. (147)*
K[$MnFe(CO)_9$]/C	290	1	3	1[b]	25[g]	76[g]	NR	Venter *et al. (89)*
Co-Mn/SiO_2	280	1	1	9	19[a]	22[a]	NR	Barrault *et al. (130)*
Co-Zn/TiO_2	240	1	2	65	9[a]	47[a]	2	Feyzi *et al. (148)*
Co/Silicalite-1	275	21	3	49	27	33	12	Das *et al. (149)*
Mo-K/ZrO_2	300	21	1	92	19[a]	65[a,e]	NR	Murchison *et al. (82)*
Ru/TiO_2	**	1	1	1	26	47	NR	Vannice *et al. (150)*
Ru-Na/TiO_2	270	0.5	2	NR	18[a]	68[a]	25	Doi *et al. (151)*
Ru/Al_2O_3	200	0.7	2	10-25	8	70	2	Okuhara *et al. (152)*
Ru/CeO_2	354	21	1	10	16	39	NR	Pierantozzi *et al. (153)*
Ru/V_2O_3	243	1	3	4	45[g]	28[g]	NR	Vannice *et al. (154)*

Note: Product selectivities are reported excluding CO_2.
[a] Carbon-based selectivity (%C)
[b] C_2-C_5
[c] CO converted to hydrocarbons (%)
[d] % olefins in hydrocarbons
NR: Not reported
[e] % of alkenes in the C_2-C_4 fraction
[f] C_2 + C_3
[g] Mole percent (%)
** 262 – 274°C
[h] % of alkenes in the C_2-C_6 fraction

Another bimetallic system was studied by Cooper *et al. (104)*, who investigated Fe/Ni catalysts supported on silica. In contrast with the bulk Fe/Ni catalysts discussed in page 41, the Fe-Ni/SiO_2 catalysts with Ni contents higher than 60% showed low alkene to alkane ratios. At lower Ni loadings, the effect of Ni on olefins selectivity was negligible.

A different approach to improve the light olefins selectivity of Fe/SiO_2 catalysts was proposed by Jiang *et al. (123)* who combined a Fischer-Tropsch active core with a zeolite shell to limit the formation of long hydrocarbons. The Fe/SiO_2 core was prepared by incipient wetness impregnation of iron nitrate and the silicalite-1 shell was synthesized using a secondary growth method. When the composite catalyst was tested at 380°C, 10 bar and H_2/CO of 2 it exhibited a light olefins selectivity of 30%, a CH_4 selectivity of 21% and a CO conversion of 21%. In contrast, under the same reaction conditions the bare Fe/SiO_2 catalyst displayed a lower C_2-C_4 olefins selectivity (20%) but its CO conversion was almost double. The lower catalytic activity of the core-shell catalyst was tentatively attributed to limitations in the diffusion of the reactants and to possible effects on the iron phase by the hydrothermal zeolite synthesis.

Yeh and coworkers *(156)* studied the catalytic performance of silica-supported iron carbides and iron nitrides. The highest selectivity to olefins (~25%) was observed for a Fe-K-nitride/SiO_2 at low CO conversion (~1%), when it was tested under the Fischer-Tropsch reaction at 250°C, 8 bar and a H_2/CO ratio of 1.

Alumina supported catalysts

Baker *et al. (124,125)* prepared iron oxide catalysts using heat-treated gamma alumina modified by impregnation of rare earth oxides. A high C_2-C_4 olefins selectivity (63%) and low methane production (7%) was observed when using a Fe-Pr/heat-treated γ-alumina at 280°C, 8 bar and H_2/CO ratio of 0.5. The highest yield of alkenes was achieved at low H_2/CO ratios (<1). Under these conditions iron-based catalysts exhibit extensive coke lay-down *(146,157)*, however, the researchers claimed that the catalyst had a long active life.

Organometallic compounds have not only been used for the preparation of Fe/SiO_2 but also for the synthesis of alumina supported catalysts. Basset *et al. (126)* filed a patent application on catalysts prepared by deposition of organometallic aggregates of Fe and/or Co and/or Ni on inorganic supports. The highest light olefins selectivity was obtained with a catalyst prepared with

the precursor $Fe_4(CO)_{13}H_2$ which was impregnated on alumina (presumably alpha alumina, surface area 10 m^2/g). The catalyst displayed a lower olefins selectivity of 49% and CH_4 selectivity of 25% at low CO conversion (5%) when used in the Fischer-Tropsch reaction at 9 bar, 290°C and H_2/CO of 0.9.

As previously mentioned, Commereuc *et al. (121)* prepared different iron-based catalyst by impregnation of silica, lantanum oxide, magnesium oxide and alumina with $Fe(CO)_5$ or $Fe_3(CO)_{12}$ diluted in n-pentane. Most of the catalysts showed C_2-C_5 olefins selectivity higher than 40% when the reaction was carried out for 90 h at 10 bar and H_2/CO of 1. γ-alumina supported catalysts prepared using different precursors, $Fe(CO)_5$ or Fe nitrate, displayed different catalytic performance. The catalyst prepared with iron nitrate exhibited a lower olefin selectivity (38%) compared with the sample prepared with iron carbonyl (57%). Commereuc and coworkers attributed the higher light olefins selectivity to a higher dispersion of iron-containing particles. The fresh carbonyl-based catalyst contained 2 nm Fe particles that sintered to form 20-50 nm particles after 90 h of reaction. Fe nanoparticle growth coincided with a decrease in olefins selectivity.

The influence of different alumina supports on catalytic activity was investigated by Barrault *et al. (127)*. The catalysts were synthesized by precipitation of iron nitrate with ammonia in the presence of the carrier material. The reaction was performed at 15 bar, H_2/CO of 1, and the reaction temperature was varied from 280°C to 500°C according to the catalyst activity. The highest selectivity to light olefins (43%) was observed for a γ-alumina supported catalyst (400 m^2/g). This catalyst showed a low activity at 280°C and it was necessary to increase reaction temperature to 500°C to achieve a similar level of CO conversion (20%) than for catalysts prepared with aluminas with lower surface areas. Under these reaction conditions, the catalyst with the highest C_2-C_4 olefins selectivity displayed the highest methane selectivity (38%). The comparison of the catalytic properties of alumina supported catalysts showed that the most active catalysts were the least selective.

A Na and S-promoted/α-alumina catalyst with a high selectivity to light olefins was designed by Torres Galvis *et al. (55)*. A homogeneous distribution of iron-containing nanoparticles is difficult to achieve in supports with low interaction toward iron such as α-alumina with a low surface area (~10 m^2/g). Fe/α-alumina catalysts prepared by impregnation of aqueous solutions of iron nitrate exhibit a poor distribution of iron nanoparticles *(114)*. To achieve a more

homogeneous spatial distribution of the particles, the researchers used ammonium iron citrate, a chelated iron complex, as a precursor. The catalysts were tested at 340°C, 20 bar and H_2/CO of 1. A high selectivity to light olefins (53%) and a low methane selectivity (11%) were achieved by introducing Na and S as chemical promoters *(56)*. The catalysts supported on inert carriers showed a higher activity in comparison with samples prepared with high surface area supports such as γ-alumina and silica. After 64 h or reaction, Na-S-Fe/α-alumina displayed a stable catalytic activity, limited sintering and relatively low coke lay-down (<10%). In a further study, Koeken *et al. (157)* investigated the influence of process conditions on catalytic performance and the deactivation of Na-S-Fe/α-alumina catalysts. Koeken and coworkers showed that the formation of carbon deposits can be suppressed for these catalysts by using higher H_2/CO ratios without affecting the catalyst selectivity.

Zeolite-supported catalysts

Many research groups have explored the use of zeolites *(22,81,131-137,139)* and aluminophosphate molecular sieves *(158)* as supports for iron-based FTO catalysts.

Rao *et al. (131)* filed a patent application on a Fe-K/silicalite catalyst prepared by impregnation of K and Fe nitrates. The catalyst was tested at 280°C, 21 bar and a H_2/CO ratio of 0.9 and under these conditions a light olefin selectivity of 36% was obtained with a methane production of 9%. A Fe-Cu-K/zeolite catalyst developed by Bae *et al. (132)* was prepared using a proton type ferrierite zeolite impregnated with a solution containing Fe and Cu nitrates and K carbonate. The reaction was carried out at 350°C, 9.8 bar and a H_2/CO of 2. The catalyst exhibited a C_2-C_4 hydrocarbons selectivity of 40% with a C_2-C_4 olefins yield of 12%. These promoted catalysts displayed higher light hydrocarbons and C_2-C_4 olefins selectivity compared with iron-based catalyst which did not contain zeolites. Additionally, it was claimed that the catalysts showed a limited deactivation with time on stream.

The design strategy used by Kang *et al. (133)* for a zeolite-supported FTO catalyst was to use a bifunctional catalyst where the FT active metal transformed syngas into a primary straight hydrocarbon chain that underwent cracking on the acid zeolite to produce hydrocarbons of limited chain length. For the preparation Kang en coworkers used aqueous solutions or iron and copper nitrates and potassium carbonate to impregnate ZSM-5, mordenite, and

beta-zeolite. The catalysts were tested at 300°C, 10 bar and a H_2/CO ratio of 2. Fe-Cu-K/ZSM-5, which had the lowest amount of acidic sites, showed a light olefins selectivity of 30% and CH_4 selectivity of 20% at a high CO conversion (81%). The structure of the mordenite and beta-zeolite-supported catalyst was damaged during reaction.

Xu *et al. (134)* studied the promotion effects of K_2O and MnO on Fe/silicalite-2 for the selective production of light alkenes via syngas. The catalysts were prepared by impregnation and were tested at 20 bar, 347°C and a H_2/CO of 2. The highest C_2-C_4 olefins selectivity (70%) was obtained with a K-Fe-Mn catalyst (8.3%-9.5%-9.6%). They concluded that MnO restricted the hydrogenation of C_2H_4 and C_3H_6. They proposed that the addition of K_2O affected the CO adsorption resulting in a higher CO conversion and a higher alkene selectivity. The researchers also put forward that K_2O inhibited the disproportionation and hydrogenation of C_2H_4.

Liu *et al. (22)* performed experiments for direct syngas conversion over K-Fe-Mn/Si-2 catalysts at semi-pilot scale with the catalysts previously reported by Xu *(134,139)*. The semi-pilot plant test was performed at 300-350°C, 20 bar and a H_2/CO ratio of 2. CO conversions between 70-90% were achieved with a light olefins selectivity between 71 to 74%. Despite of the low hydrothermal stability that could be expected for zeolite supported catalysts, Liu and coworkers reported that the catalyst was stable for at least 1000 h. The K-Fe-Mn/Si-2 was regenerated after 1000 h and it displayed nearly the same properties as the fresh catalyst. From the comparison of the bench scale tests performed made by Liu *et al.*, they concluded that the direct method had a lower light olefin yield compared with the synthesis of lower olefins via dimethyl ether.

Das *et al. (135)* reported on the effect of Mn addition to silicalite-1 supported Fe and Co catalysts. The catalysts were prepared by impregnation of silicalite-1 with Fe, Co or Mn nitrate solutions. The samples were tested at 275°C, 21 bar and H_2/CO of 1. A high selectivity to lower olefins (65%) was reported for a Fe-Mn/Sil-1 catalyst (10% Fe, 5% Mn) at a low CO conversion (5%). The researchers concluded that Mn reduced iron oxide particle size and hindered carburization. They attributed the increased olefin selectivity to the presence of Fe^{3+} in the catalyst.

The effect of the Si/Al ratio of ZSM-supported catalysts on catalytic performance was studied by Kang *et al. (136)*. They synthesized the catalysts by impregnation of proton ZSM-5 with different Si/Al using Fe and Cu nitrates

and potassium carbonate. The catalysts were tested at 300°C, 10 bar and H_2/CO of 2 for 70 h. A Fe-Cu-K/zeolite with a low Si/Al ratio (Si/Al = 25) showed the highest CO conversion (81%) and the highest C_2-C_4 olefins (10%).

Other oxidic supports

Gustafson *et al. (138)* filed a patent application on palladium-promoted Fe catalysts supported on ZnO. The catalysts were prepared by impregnation of Pd and Fe nitrates. A moderate light olefin selectivity (30%) and a high methane production (45%) were achieved when the samples were tested at 300°C, 7 bar and a H_2/CO ratio of 1.

Xu and coworkers *(139)* prepared Fe-Mn catalysts by impregnation of silica, alumina, ZrO_2, TiO_2 and MgO. The researchers highlighted the importance of the selection of the support material since its properties, *e.g.*, acid-basic properties, metal-support interaction, structures of channels and micropores, have a major impact on catalytic performance. They reported that Fe-Mn catalysts synthesized on a basic supports could produce up to 70% of light olefins while maintaining a high activity (70 – 90% CO conversion) under certain reaction conditions. The highest light olefins selectivity (68%) was achieved using a Fe-Mn/MgO catalyst at 320°C, 20 bar and H_2/CO ratio of 2. Xu *et al.* ascribed the high olefins selectivity of Fe-Mn/MgO catalysts to a stronger CO adsorption originated by the basicity of the support.

Magnesium oxide was also used by Hugues *et al. (140)* for the preparation of catalysts for the selective formation of propene from syngas using $Fe_3(CO)_{12}$ as metal precursor. A high C_2-C_4 olefins selectivity was observed (58%) when testing the Fe/MgO catalyst at 176°C, 1 bar and a H_2/CO ratio of 0.5.

Barrault *et al. (141)* studied the production of lower olefins from syngas using manganese oxide-supported catalysts. The catalysts were prepared by impregnation of MnO or MnO_2 with iron nitrate, $Fe(Acac)_3$ or $Fe(Acac)_2$. A high selectivity to light olefins (59%) was obtained when using a $Fe(C_5H_7O_2)_3/MnO_2$ catalyst tested at 350°C, 1 bar and a H_2/CO ratio of 1. Their results demonstrated that an adequate Fe/Mn stoichiometry is needed for selective conversion of syngas into light olefins and that the nature of iron precursor and the preparation method have a large impact on catalytic activity and selectivity. Barrault and coworkers *(142)* also explored the use of ion-exchanged pillared laponites for the Fischer-Tropsch synthesis of lower olefins from synthesis gas.

Carbon supported catalysts

Carbonaceous materials are an interesting alternative for the preparation of supported catalysts. Carbon supports can be obtained with surface areas ranging from 150 to 1500 m^2/g, with diverse pore sizes and pore structures and their surface can be modified to tune their affinity with metal precursors *(49,159,160)*. Carbon supports are relatively inert and they can display a weak interaction with iron depending on their surface properties.

Activated *(89,90,144,146,161)*, graphitic and glassy carbons *(147)* have been used by several research groups to synthesize supported Fe catalysts for the production of lower olefins from syngas. Venter *et al. (89)* prepared Fe/C catalysts using amorphous carbon black as support and impregnating with organometallic mixed-metal carbonyl clusters (Mn, Fe, and/or K). The catalysts were tested at 275-290°C, 1 bar, and a H_2/CO ratio of 3. Under these reaction conditions, a $K[MnFe(CO)_9]$/C catalyst displayed a light olefins selectivity of 76% while no paraffins were detected. It is important to note that the researchers reported that their carbon support contained sulfur. The presence of sulfur in low concentrations could have improved the catalysts selectivity toward lower olefins as discussed previously.

Venter *et al.* reported that better catalytic performances could be achieved using carbonyl precursors instead of metal nitrates. They also mentioned that the pretreatment method has a strong influence on selectivity and activity.

In a further study, Venter and coworkers *(90)* reported on the stability of their catalytic systems. The catalysts stabilized within 24 h and the high olefin to paraffin ratio remained unchanged during long periods on stream. Activity declined about 55% compared to the initial value after 100 h and the deactivation was mainly due to carbon deposition and not to sintering. The high stabilities of the K-Mn-Fe/C catalysts were related to the high H_2/CO ratio used during reaction. The researchers claimed that these catalysts could be regenerated with reduction under H_2 at 350°C for 16 h.

Barrault *et al. (144)* filed a patent application on a Fe-Mn/AC catalysts prepared using acetyl-acetonate complexes. They reported a C_2-C_4 olefins selectivity of approximately 50% when the catalyst was tested at 250°C, 1 bar, and a H_2/CO of 1.

Activated carbons have very high surface areas and they are relatively cheap, as they are generally produced by carbonization of nutshells, wood, and other natural carbon sources. However, they usually contain traces of other elements that might act as promoters or poisons for the Fischer-Tropsch active

metals. Carbon materials with more controlled morphologies and higher purities can be synthesized in the form of carbon nanotubes (CNT) of carbon nanofibers (CNF).

Yang *et al.* (145) investigated the effect of Mn and K on the catalytic performance of FeN catalysts confined in CNT's. Yang and coworkers synthesized the FeN catalysts by introducing an iron nitrate solution into the CNT channels using ultrasonication and stirring. The nitridation process was performed using ammonia. The promoted samples were prepared using a solution containing Fe, Mn and K nitrates. The catalysts were tested at 300°C, 5 bar and a H_2/CO ratio of 1. The addition of Mn reduced CO conversion to 12% and increased light olefins selectivity to 44%. The researchers stated that addition of K did not affect activity or selectivity under the studied reaction conditions.

Schulte *et al. (143)* used CNT as support to prepare supported iron catalysts. They studied the influence of CNT surface modification on catalytic performance. Oxygen and nitrogen-functionalized CNTs were impregnated with ammonium iron citrate and tested at 340°C, 25 bar and a H_2/CO of 1. The highest light olefins selectivity (up to 92% of alkenes in the C_2-C_6 fraction) was obtained with a Fe/O-CNT which also exhibited a low methane selectivity (9%) at a CO conversion of 45%. The catalysts reported in this study exhibited a high and constant CO conversion for a period of 80 h time on stream. The catalysts supported on nitrogen-functionalized CNT's showed a slower deactivation compared with O-CNT's.

Surface-oxidized carbon nanofibers were used by Torres Galvis *et al.* to prepare Na-S-promoted iron catalysts *(55)*. The CNF supported catalyst showed a high selectivity to C_2-C_4 olefins (52%) at high CO conversion (88%) when the FTO reaction was performed at 340°C, 20 bar and a H_2/CO ratio of 1. The catalyst showed a stable activity during 64 h of reaction. In a complementary study, Torres Galvis *et al.* investigated the influence of iron (carbide) particle size on catalytic performance using CNF supported catalysts *(162)*. The researchers concluded that the surface-specific catalytic activity increases with decreasing iron particle size, which is, surprisingly, in contrast to results found for Co nanoparticles on carbon nanofibers *(163,164)*. The catalysts with the smallest iron-containing particles displayed a high catalytic activity but also exhibited a high methane selectivity. This result highlights the importance of selecting an optimum particle size for the design of active, selective and stable catalyst for the production of lower olefins from synthesis

gas. The catalysts prepared using inert supports showed a good combination of high catalytic activity with a high C_2-C_4 olefins selectivity and low methane formation as shown in Figure 12.

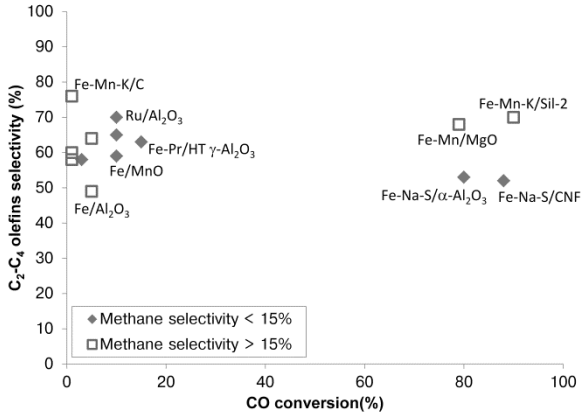

Figure 12. Supported catalysts for the FTO reaction (C_2-C_4 olefins selectivity > 50%). Catalysts with CH_4 selectivities below 15%: diamonds.

Figure 12 shows that it is possible to obtain high C_2-C_4 olefins selectivities (>50%) with different formulations of supported Fe catalysts at low CO conversions. It is possible to achieve such high selectivities even with unpromoted catalysts because under these conditions secondary hydrogenation reactions are limited. The main challenge is to maintain the high C_2-C_4 selectivity at high CO conversion levels. From Figure 12 it is shown the Fe-Mn-K/Sil-2, Fe-Mn/MgO and the Fe-Na-S catalysts prepared on inert supports displayed a high activity combined with high C_2-C_4 olefins selectivity. It is important to note that a methane selectivity of about 30% is expected when achieving a high C_2-C_4 olefins selectivity (~ 50%) according to the ASF distribution (Figure 8). From the catalysts with high CO conversion and C_2-C_4 olefins selectivity, only the Na and S-promoted catalysts showed methane selectivities below 20%.

Figure 13 displays lower olefins selectivity as a function of temperature for supported catalysts. This graph shows that high CO conversions can be achieved using high reaction temperatures (> 300°C). Under these conditions, the selectivity to shorter hydrocarbons is enhanced, increasing lower olefins selectivity but at the same time increasing methane production. The formation of carbon deposits is also favored at high reaction temperatures thus having a

negative effect on catalytic activity. Carbon lay-down can be decreased by performing the reaction in the presence of H_2-rich syngas. Fe-Mn-K/Sil-2 and Fe-Mn/MgO showed a good catalytic performance when the reaction was carried out with a H_2/CO ratio of 2 whereas the Fe-Na-S catalysts supported on CNF or α-Al_2O_3 exhibited high activity even when using syngas with a H_2/CO ratio of 1.

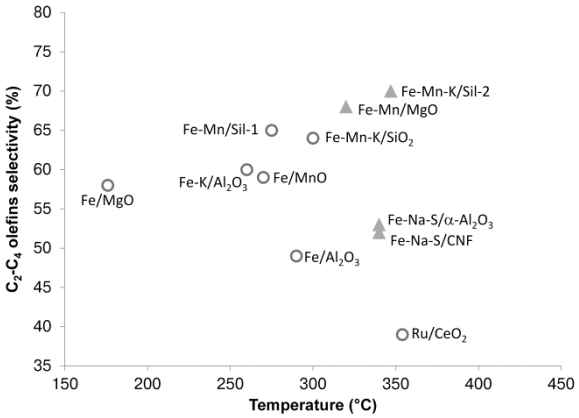

Figure 13. Selectivity to lower olefins as a function of temperature. Catalysts with light olefins selectivity higher than 35%. Catalysts with low CO conversion (< 10%): circles; Catalysts with high CO conversion (> 70%): triangles.

Non Fe-based supported catalysts

Kou *et al. (165)* reported on gamma alumina supported zirconia catalyst for the production of ethylene from syngas. The catalyst exhibited a high selectivity to ethylene (70%) when the Fischer-Tropsch reaction was performed at 357°C, 8 bar and a H_2/CO ratio of 4.

Several Co-based catalyst have been proposed for the production of light olefins from synthesis gas *(106,130,148,149,166,167)*. Feyzi *et al. (148)* prepared Co catalysts by precipitation in the presence of TiO_2. They investigated the catalytic performance under different reaction conditions and the promotion effects of Zn, K, Li, Rb or Ce. The highest light olefins selectivity (47%) was obtained for a Co/TiO_2 catalyst promoted with 6 wt% Zn and tested at 240°C and 1 bar.

Das *et al. (149)* reported on Co and Co-Mn supported catalysts prepared by impregnation of silicalite-1 with metal nitrates. A Co-Mn/sil-1 displayed a lower olefins selectivity of 33% when the reaction was performed at 275°C, 21 bar

and H_2/CO ratio of 3. The addition of Mn to Co/sil-1 catalysts increased CO conversion only when the reaction was performed at 250°C and not at higher temperatures. The modification with Mn slightly reduced the alkene selectivity which is in contrast with results reported by other research groups.
A Co-Mo-K/SiO_2 catalyst was prepared by Chen *et al. (167)* using incipient wetness impregnation of cobalt nitrate, ammonium molybdate and potassium carbonate. The catalyst was tested at 1 bar, 250-330°C and H_2/CO ratios ranging from 0.05-19. The introduction of Mo to the catalyst resulted in an improvement on the total O/P ratio (from 0.3 to 0.6), suppression of methane formation and increase of chain growth probability. High light olefins selectivity on supported Mo-containing catalysts was also reported by Murchison *(82)*.
High selectivities to light olefins have been also reported for Ru-based catalysts supported on titania *(150,151)*, alumina *(152)*, CeO_2 *(153)*, and Nb_2O_5 *(154)*. However, these high C_2-C_4 olefins selectivities have only been obtained at low CO conversions (Table 4).

Outlook

The growing interest of different countries to secure their supply of C_2-C_4 olefins will continue to drive research and development of catalysts and processes for the production of these important commodity chemicals from non-oil based feedstocks. The indirect processes, MTO and DMTO, are already industrially applied for the production of lower olefins from synthesis gas. These processes display high selectivities to ethylene and propylene and could be an attractive option for supplying the polymers industry with feedstocks. The MTO and DMTO processes require hydrogen-rich syngas as for the preceding methanol synthesis. For this reason, MTO and DMTO are suitable options using natural gas as feed. In the case of CO-rich syngas, produced by gasification of coal or biomass, an additional step for the adjustment of the H_2/CO ratio is required by means of the water gas shift reaction. Additionally, coal or biomass-based syngas contains sulfur and other contaminants that act as strong poisons for the catalysts used in the synthesis of methanol and DME. This implies that stringent, and costly, gas clean-up procedures should be used for the conditioning of CO-rich syngas intended to be used in the methanol synthesis process. Also, research is needed to improve the activity,

selectivity and stability of MTO and DMTO catalysts as most of them exhibit fast deactivation due to the formation of carbon deposits.

The FTO process is a direct route that offers feedstock flexibility. When iron-based catalysts are used, the process can be performed using CO-rich syngas directly, without any H_2/CO ratio adjustment, in view of their high water gas shift activity. Iron is more robust than other metals and can withstand some contaminants present in coal or biomass-based syngas. In fact, it is shown from this review that iron can be even more selective to light olefins in the presence of low concentrations of sulfur.

The FTO process displays lower ethylene and propylene selectivities in comparison to MTO or DMTO. However, FTO could be an attractive route to supply chemical complexes where the byproducts, *i.e.*, C_{5+} and oxygenates, could be utilized. In view of limited availability of the composition of the C_2-C_4 olefin fraction we are not able to make a detailed assessment of FTO versus MTO.

The development of catalytic processes for the conversion of CO_2 into olefins might gain importance in the future as an alternative pathway for light olefins production *(168-175)*. The environmental impact of FTO might be further reduced using CO_2 and 'solar' hydrogen as feedstock.

The FTO route becomes more feasible with every improvement on activity, selectivity and stability of the catalytic system. Iron can be presented as the metal of choice for the FTO reaction as it is inexpensive, it is highly selective toward olefins and it is possible to achieve methane selectivities below the prediction of the ASF product distribution. The design of effective iron-based catalysts for the selective production of light olefins involves several factors:

- The selection of a support that enables the formation of the active phase and its intimate contact with the chemical promoters
- The adequate choice of promoters to increase the selectivity to light olefins and minimize methane production
- The use of preparation methods that allow obtaining a homogeneous spatial distribution of iron-containing particles with narrow size distribution in the optimum size range
- The selection of optimum process conditions to maximize the catalyst life without compromising product selectivity

The application of FTO is subject to economical and technical feasibility studies and to the development of optimum catalysts and production processes. The selection of a process for the production of lower olefins depends not only on capital and operational costs but also on the feedstocks available and the product slate.

References

1. M. McCoy (ed.), *Chem. Eng. News* **89**, 55-56 (2011).
2. H. A. Wittcoff, B. G. Reuben, J. S. Plotkin, *Industrial Organic Chemicals* (John Wiley and Sons, Inc., New Jersey, 2nd ed., 2004), pp. 662.
3. Association of Petrochemicals Producers in Europe. West European Market Review 2010. http://www.petrochemistry.net.
4. Nexant Inc., *CHEMSYSTEMS PERP program "Propylene", Rep. No. PERP 06/07-3*, 2008). http://www.chemsystems.com.
5. North American olefin producers riding the shale gas wave by Tallman, M. J. and Klavers R. April 1st, 2013. http://www.hydrocarbonprocessing.com/.
6. C. P. Bowen, D. Jones, *Hydrocarb. Process.*, 71-79 (April 2008).
7. International Energy Agency (IEA)., *Energy technology transitions for industry,* (OECD/IEA, Paris, 2009). http://www.iea.org.
8. S. P. Pyl *et al.*, *Chem. Eng. J.* **176-177**, 178-187 (2011).
9. International Energy Agency (IEA)., *World Energy Outlook,* (OECD/IEA, Paris, France, 2010). http://www.iea.org.
10. International Energy Agency (IEA)., *Technology roadmap. Biofuels for transportation.* (OECD/IEA, Paris, France, 2011). http://www.iea.org.
11. M. Stöcker, *Angew. Chem. Int. Ed.* **47**, 9200-9211 (2008).
12. A. J. Ragauskas *et al.*, *Science* **311**, 484-489 (2006).
13. R. C. Brown, Ed., *Thermochemical processing of biomass: conversion into fuels, chemicals, and power* (John Wiley & Sons, Ltd., Chichester, UK, ed. 1st, 2011), pp. 350.
14. A. P. C. Faaij, *Mitig. Adapt. Strateg. Glob. Change* **11**, 343-375 (2006).
15. M. J. A. Tijmensen, A. P. C. Faaij, C. N. Hamelinck, van Hardeveld, M. R. M., *Biomass Bioenerg.* **23**, 129-152 (2002).
16. U.S. Energy Information Administration (EIA)., *Summary: U.S. crude oil, natural gas, and natural gas liquid proved reserves 2009,* (U.S. Energy Information Administration, Washington, 2010). http://www.eia.gov.
17. U.S. Energy Information Administration (EIA)., *International Energy Outlook 2011, Rep. No. DOE/EIA-0484(2011)* (U.S. Energy Information Administration, Washington, 2011). http://www.eia.gov.
18. S. Jenkins, *Chem. Eng.* **October**, 17-19 (2012).
19. P. McDonald, *Oil and Energy Trends* **38**, 10-17 (2013).

20. International Energy Agency (IEA)., *Golden rules for a golden age of gas. World energy outlook. Special report on unconventional gas.* (OECD/IEA, Paris, 2012). http://www.iea.org.
21. J. D. Hughes, *Nature* **494**, 307-308 (2013).
22. Z. Liu, C. Sun, G. Wang, Q. Wang, G. Cai, *Fuel Process. Technol.* **62**, 161-172 (2000).
23. C. Wang, Q. Wang, X. Sun, L. Xu, *Catal. Lett.* **105**, 93-101 (2005).
24. C. Wang, L. Xu, Q. Wang, *J. Nat. Gas Chem.* **12**, 10-16 (2003).
25. M. Janardanarao, *Ind. Eng. Chem. Res.* **29**, 1735-1753 (1990).
26. J. H. Lunsford, *Catal. Today* **63**, 165-174 (2000).
27. D. Chen, K. Moljord, A. Holmen, *Microporous Mesoporous Mater.* **164**, 239-250 (2012).
28. T. S. Zhao, T. Takemoto, N. Tsubaki, *Catal. Comm.* **7**, 647-650 (2006).
29. J. Čejka, A. Corma, S. Zones, Eds., *Zeolites and Catalysis. Synthesis, reactions and applications* (Wiley-VCH Verlag GmbH & Co. KGaA, Weinheim, Germany, ed. 1st, 2010), pp. 1056.
30. G. Cai *et al.*, *Appl. Catal. A* **125**, 29-38 (1995).
31. J. F. Knifton, *J. Catal.* **79**, 147-155 (1983).
32. X. Dupain, R. A. Krul, C. J. Schaverien, M. Makkee, J. A. Moulijn, *Appl. Catal. B* **63**, 277-295 (2006).
33. Y. Traa, *Chem. Commun.* **46**, 2175 (2010).
34. E. Schwab, A. Weck, J. Steiner, K. Bay, *Oil Gas Eur. Mag.* **1**, 44-47 (2010).
35. R. Snel, *Catal. Rev. Sci. Eng.* **29**, 361-445 (1987).
36. Literature survey on patents and scientific articles in the CAS database using the keywords "Fischer-Tropsch", "CO hydrogenation", and "lower olefins".
37. BP Statistical Review of World Energy June 2012. http://www.bp.com/statisticalreview.
38. A. P. Steynberg, M. E. Dry, Eds., *Fischer-Tropsch Technology (Series: Studies in surface science and catalysis No. 152)* (Elsevier, Amsterdam, 2004).
39. H. Arakawa *et al.*, *Chem. Lett.*, 1341-1342 (1986).
40. B. Denise, R. P. A. Sneeden, *Appl. Catal.* **27**, 107-116 (1986).
41. J. Y. Park *et al.*, *J. Ind. Eng. Chem.* **15**, 847-853 (2009).
42. Y. J. Lee, J. Y. Park, K. W. Jun, J. W. Bae, N. Viswanadham, *Catal. Lett.* **126**, 149-154 (2008).
43. S. Abelló, D. Montané, *ChemSusChem* **4**, 1538-1556 (2011).
44. A. de Klerk, *Fischer-Tropsch refining* (Wiley-VCH Verlag and Co., KGaA, Weinheim, Germany, 2011), pp. 638.
45. G. P. van der Laan, A. A. C. M. Beenackers, *Catal. Rev.* **41**, 255-318 (1999).
46. M. E. Dry, *Catal. Today* **71**, 227-241 (2002).
47. Q. Zhang, J. Kang, Y. Wang, *ChemCatChem* **2**, 1030-1058 (2010).
48. Q. Zhang, W. Deng, Y. Wang, *J. Energy Chem.* **22**, 27-38 (2013).

49. B. Sun, K. Xu, L. Nguyen, M. Qiao, F. Tao, *ChemCatChem* **4**, 1498 (2012).
50. E. de Smit, B. M. Weckhuysen, *Chem. Soc. Rev.* **37**, 2758 (2008).
51. E. Iglesia, *Appl. Catal. A* **161**, 59-78 (1997).
52. A. Y. Khodakov, W. Chu, P. Fongarland, *Chem. Rev.* **107**, 1692-1744 (2007).
53. N. E. Tsakoumis, M. Rønning, Ø. Borg, E. Rytter, A. Holmen, *Catal. Today* **154**, 162-182 (2010).
54. B. C. Enger, A. Holmen, *Catal. Rev. Sci. Eng.* **54**, 437-488 (2012).
55. H. M. Torres Galvis *et al.*, *Science* **335**, 835-838 (2012).
56. H. M. Torres Galvis *et al.*, *J. Catal.* **303**, 22-30 (2013).
57. M. E. Dry, Erasmus, H. B. de W., *Ann. Rev. Energy* **12**, 1-21 (1987).
58. B. Büssemeier, C. D. Frohning, B. Cornils, *Hydrocarb. Process.* **56**, 105-112 (1976).
59. B. Büssemeier, C. D. Frohning, W. Kluy, DE Patent 2518964 (1976).
60. B. Büssemeier, C. D. Frohning, G. Horn, W. Kluy, US Patent 4564642 (1986).
61. S. C. Roy *et al.*, *Appl. Catal. A* **220**, 153-164 (2001).
62. M. R. Goldwasser *et al.*, *J. Mol. Catal. A* **193**, 227-236 (2003).
63. M. Sağlam, *Ind. Eng. Chem. Res.* **28**, 150-154 (1989).
64. S. H. Kang *et al.*, *Catal. Lett.* **130**, 630-636 (2009).
65. W. Vielstich, D. Kitzelmann, GB Patent 2050859 (1981).
66. B. W. Hoffer, et al., International Patent Application No. WO2009013174 (2009).
67. F. Tihay, A. C. Roger, A. Kiennemann, G. Pourroy, *Catal. Today* **58**, 263-269 (2000).
68. F. Tihay, G. Pourroy, M. Richard-Plouet, A. C. Roger, A. Kiennemann, *Appl. Catal. A* **206**, 29-42 (2001).
69. W. L. van Dijk, J. W. Niemantsverdriet, van der Kraan, A. M., van der Baan, H. S., *Appl. Catal.* **2**, 273-288 (1982).
70. R. Crous, T. C. Bromfield, S. Booyens, International Patent Aplication No. WO2010066386 (2010).
71. H. Hadadzadeh *et al.*, *Petrol. Chem.* **50**, 78-86 (2010).
72. S. L. Gónzalez-Cortés *et al.*, *React. Kinet. Catal. Lett.* **75**, 3-12 (2002).
73. A. A. Mirzaei, R. Habibpour, E. Kashi, *Appl. Catal. A* **296**, 222-231 (2005).
74. M. Feyzi, A. Hassankhani, *J. Nat. Gas Chem.* **20**, 677-686 (2011).
75. H. Kölbel, K. D. Tillmetz, US Patent 4177203 (1979).
76. W. D. Deckwer, Y. Serpemen, M. Ralek, B. Schmidt, *Ind. Eng. Chem. Process. Des. Dev.* **21**, 222-231 (1982).
77. S. L. Soled, R. A. Fiato, GB Patent 2152072A (1985).
78. G. J. Hutchings, J. C. A. Boeyens, *J. Catal.* **100**, 507-511 (1986).
79. R. G. Copperthwaite, G. J. Hutchings, M. van der Riet, J. Woodhouse, *Ind. Eng. Chem. Res.* **26**, 869-874 (1987).

80. J. Zhang, S. Fan, T. S. Zhao, W. Li, Y. Sun, *React. Kinet. Mech. Cat.* **102**, 437-445 (2011).
81. T. Sano *et al.*, *Appl. Catal.* **19**, 247-258 (1985).
82. C. B. Murchison, D. A. Murdick, US Patent 4199522 (1980).
83. T. Arai, K. Maruya, K. Domen, T. Onishi, *J. Chem. Soc. , Chem. Commun.* **23**, 1757-1758 (1987).
84. I. Kojima, E. Miyazaki, I. Yasumori, *J. Chem. Soc. , Chem. Commun.* **12**, 573-574 (1980).
85. K. Y. Park, W. K. Seo, J. S. Lee, *Catal. Lett.* **11**, 349-356 (1991).
86. A. A. Mirzaei, M. Galavy, A. Beigbabaei, V. Eslamimanesh, *J. Iran. Chem. Soc.* **4**, 347-363 (2007).
87. J. L. Costa, A. F. Noels, A. Demonceau, A. J. Hubert, *J. Catal.* **105**, 1-9 (1987).
88. J. Yao, J. B. Kimble, US Patent 2007043127 A1 (2007).
89. J. Venter, M. Kaminsky, G. L. Geoffroy, M. A. Vannice, *J. Catal.* **103**, 450-465 (1987).
90. J. Venter, M. Kaminsky, G. L. Geoffroy, M. A. Vannice, *J. Catal.* **105**, 155-162 (1987).
91. J. R. Anderson, M. Boudart, Eds., *Catalysis: Science and Technology* (Springer-Verlag, New York, 1981).
92. M. E. Dry, G. J. Oosthuizen, *J. Catal.* **11**, 18-24 (1968).
93. Y. Yang, H. W. Xiang, Y. Y. Xu, L. Bai, Y. W. Li, *Appl. Catal. A* **266**, 181 (2004).
94. N. Lohitharn, J. G. J. Goodwin, *J. Catal.* **260**, 7 (2008).
95. J. L. Rankin, C. H. Bartholomew, *J. Catal.* **100**, 533 (1986).
96. M. C. Ribeiro *et al.*, *J. Phys. Chem. C* **114**, 7895-7903 (2010).
97. X. An *et al.*, *Catal. Comm.* **8**, 1957-1962 (2007).
98. D. S. Kalakkad, M. D. Shroff, S. D. Köhler, N. B. Jackson, A. K. Datye, *Appl. Catal. A* **133**, 335-350 (1995).
99. T. C. Bromfield, N. J. Coville, *Appl. Catal. A* **186**, 297-307 (1999).
100. T. C. Bromfield, N. J. Coville, *Appl. Surf. Sci.* **119**, 19-24 (1997).
101. B. Wu *et al.*, *Fuel* **83**, 205-212 (2004).
102. J. A. Kritzinger, *Catal. Today* **71**, 307-318 (2002).
103. R. Malessa, M. Baerns, *Ind. Eng. Chem. Res.* **27**, 279-283 (1988).
104. M. E. Cooper, J. Frost, *Appl. Catal.* **57**, L5-L8 (1990).
105. M. Blanchard, D. Vanhove, F. Petit, A. Mortreux, *J. Chem. Soc. , Chem. Commun.* **19**, 908-909 (1980).
106. K. Peters, GB Patent 833976 (1960).
107. A. A. Mirzaei, M. Faizi, R. Habibpour, *Appl. Catal. A* **306**, 98-107 (2006).
108. M. D. Shroff *et al.*, *J. Catal.* **156**, 185-207 (1995).
109. D. B. Bukur, W. P. Ma, V. Carreto-Vazquez, *Top. Catal.* **32**, 135-141 (2005).
110. B. Jager, R. Espinoza, *Catal. Today* **23**, 17-28 (1995).

111. E. de Smit *et al.*, *J. Am. Chem. Soc.* **132**, 14928-14941 (2010).
112. E. de Smit *et al.*, *Nature* **456**, 222-225 (2008).
113. I. D. Gonzalez-Jimenez *et al.*, *Angew. Chem. Int. Ed.* **51**, 11986-11990 (2012).
114. H. M. Torres Galvis *et al.*, *Catal. Today* , **DOI: 10.1016/j.cattod.2013.03.018** (2013).
115. J. Y. Park *et al.*, *J. Mol. Catal. A* **323**, 84-90 (2010).
116. V. Perrichon, H. Charcosset, J. Barrault, C. Forquy, *Appl. Catal.* **7**, 21-29 (1983).
117. Rao, K. R. P. M. *et al.*, *Top. Catal.* **2**, 71-78 (1995).
118. C. H. Zhang, H. J. Wan, Y. Yang, H. W. Xiang, Y. W. Li, *Catal. Comm.* **7**, 733-738 (2006).
119. H. Suo *et al.*, *J. Catal.* **286**, 111-123 (2012).
120. L. Bruce, G. Hope, T. W. Turney, *React. Kinet. Catal. Lett.* **20**, 175-180 (1982).
121. D. Commereuc, Y. Chauvin, *J. Chem. Soc. , Chem. Commun.* **4**, 154-155 (1980).
122. F. Stoop, K. van der Wiele, *Appl. Catal.* **23**, 35-47 (1986).
123. N. Jiang *et al.*, *Catal. Comm.* **12**, 951-954 (2011).
124. B. G. Baker, N. J. Clark, *Stud. Surf. Sci. Catal.* **31**, 455-465 (1987).
125. B. G. Baker, N. J. Clark, H. Macarthur, E. Summerville, International Patent Application No. WO8400702 (1984).
126. J. Basset, Y. Chauvin, D. Commereuc, A. Smith, A. Theolier, FR Patent 2391978 (1977).
127. J. Barrault, C. Forquy, J. C. Menezo, R. Maurel, *React. Kinet. Catal. Lett.* **15**, 153-158 (1980).
128. H. Arakawa, A. T. Bell, *Ind. Eng. Chem. Process. Des. Dev.* **22**, 97-103 (1983).
129. J. Barrault, C. Forquy, V. Perrichon, *J. Mol. Catal.* **17**, 195-202 (1982).
130. J. Barrault, C. Forquy, V. Perrichon, *Appl. Catal.* **5**, 119-125 (1983).
131. V. U. S. Rao, R. J. Gormley, US Patent 4340503 (1982).
132. J. W. Bae, S. H. Kang, Y. J. Lee, K. W. Jun, International Patent Application No. WO 2009051353 (2009).
133. S. H. Kang, J. W. Bae, P. S. S. Prasad, K. W. Jun, *Catal. Lett.* **125**, 264-270 (2008).
134. L. Xu, Q. Wang, Y. Xu, J. Huang, *Catal. Lett.* **31**, 253-266 (1995).
135. D. Das, G. Ravichandran, D. K. Chakrabarty, *Catal. Today* **36**, 285-293 (1997).
136. S. H. Kang, J. W. Bae, K. J. Woo, P. S. S. Prasad, K. W. Jun, *Fuel Process. Technol.* **91**, 399-403 (2010).
137. T. Mitsudo, H. Boku, S. Murachi, A. Ishihara, Y. Watanabe, *Chem. Lett.*, 1463-1466 (1985).
138. B. L. Gustafson, US Patent 4518714 (1985).
139. L. Xu, Q. Wang, Y. Xu, J. Huang, *Catal. Lett.* **24**, 177-185 (1994).
140. F. Hugues, B. Besson, J. M. Basset, *J. Chem. Soc. , Chem. Commun.* **15**, 719-721 (1980).

141. J. Barrault, C. Renard, *Appl. Catal.* **14**, 133-143 (1985).
142. J. Barrault *et al.*, *J. Chem. Soc. , Chem. Commun.* **21**, 1403-1404 (1988).
143. H. J. Schulte, B. Graf, W. Xia, M. Muhler, *ChemCatChem* **4**, 350-355 (2012).
144. J. Barrault, C. Renard, FR Patent 2571274 (1984).
145. Z. Yang, X. Pan, J. Wang, X. Bao, *Catal. Today* **186**, 121-127 (2012).
146. A. P. B. Sommen, F. Stoop, K. van der Wiele, *Appl. Catal.* **14**, 277-288 (1985).
147. H. J. Jung, P. L. Walker Jr., M. A. Vannice, *J. Catal.* **75**, 416-422 (1982).
148. M. Feyzi, M. M. Khodaei, J. Shahmoradi, *Fuel Process. Technol.* **93**, 90-98 (2012).
149. D. Das, G. Ravichandran, D. K. Chakrabarty, *Appl. Catal. A* **131**, 335-345 (1995).
150. M. A. Vannice, R. L. Garten, *J. Catal.* **63**, 255-260 (1980).
151. Y. Doi, H. Miyake, A. Yokota, K. Soga, *J. Catal.* **95**, 293-295 (1985).
152. T. Okuhara, K. Kobayashi, T. Kimura, M. Misono, Y. Yoneda, *J. C. S. Chem. Comm.* **21**, 1114-1115 (1981).
153. R. Pierantozzi, GB Patent 2119277 (1983).
154. M. A. Vannice, S. J. Tauster, GB Patent 2006261 (1979).
155. A. J. van Dillen, Terörde, Robert J. A. M., D. J. Lensveld, J. W. Geus, K. P. de Jong, *J. Catal.* **216**, 257-264 (2003).
156. E. B. Yeh, L. H. Schwartz, J. B. Butt, *J. Catal.* **91**, 241-253 (1985).
157. A. C. J. Koeken, H. M. Torres Galvis, T. Davidian, M. Ruitenbeek, K. P. de Jong, *Angew. Chem. Int. Ed.* **51**, 7190-7193 (2012).
158. M. L. Cubeiro *et al.*, *Appl. Catal. A* **167**, 183-193 (1998).
159. K. P. de Jong, J. W. Geus, *Catal. Rev. Sci. Eng.* **42**, 481-510 (2000).
160. H. Jüntgen, *Fuel* **65**, 1436-1446 (1986).
161. V. K. Jones, L. R. Neubauer, C. H. Bartholomew, *J. Phys. Chem.* **90**, 4832-4839 (1986).
162. H. M. Torres Galvis *et al.*, *J. Am. Chem. Soc.* **134**, 16207-16215 (2012).
163. G. L. Bezemer *et al.*, *J. Am. Chem. Soc.* **128**, 3956-3964 (2006).
164. J. P. den Breejen *et al.*, *J. Am. Chem. Soc.* **131**, 7197-7203 (2009).
165. Y. Kou, G. Q. Su, W. Z. Zhang, Y. Q. Yin, *J. Catal.* **162**, 361-364 (1996).
166. D. Fraenkel, B. C. Gates, *J. Am. Chem. Soc.* **102**, 2478-2480 (1980).
167. H. Chen, A. A. Adesina, *Appl. Catal. A* **112**, 87-103 (1994).
168. P. S. S. Prasad, J. W. Bae, K. W. Jun, K. W. Lee, *Catal. Surv. Asia* **12**, 170-183 (2008).
169. T. Riedel *et al.*, *Top. Catal.* **26**, 41-54 (2003).
170. T. Riedel *et al.*, *Appl. Catal. A* **186**, 201-213 (1999).
171. J. Wang, Z. You, Q. Zhang, W. Deng, Y. Wang, *Catal. Today ,* **DOI: 10.1016/j.cattod.2013.03.031** (2013).
172. W. Wang, S. Wang, X. Ma, J. Gong, *Chem. Soc. Rev.* **40**, 3703-3727 (2011).

173. C. Moreno-Castilla, M. Salas-Peregrin, F. J. López-Garzón, *Fuel* **74**, 830-835 (1995).
174. Y. Yao, X. Liu, D. Hildebrandt, D. Glasser, *Appl. Catal. A* **433-434**, 58-68 (2012).
175. B. Hu *et al.*, *Appl. Catal. B* **132-133**, 54-61 (2013).

Chapter 3

Supported iron nanoparticles as catalysts for sustainable production of lower olefins

Abstract

Lower olefins are key building blocks for the manufacture of plastics, cosmetics and drugs. Traditionally, olefins with 2 to 4 carbons are produced by steam cracking of crude oil derived naphtha but there is a pressing need for alternative feedstocks and processes in view of supply limitations and of environmental issues. Although the Fischer-Tropsch synthesis has long offered a means to convert coal, biomass and natural gas into hydrocarbon derivatives through the intermediacy of synthesis gas (a mixture of H_2 and CO), selectivity toward lower olefins tend to be low. Here we report on the conversion of synthesis gas to C_2 through C_4 olefins with up to 60% selectivity by carbon, using catalysts which comprise Fe promoted nanoparticles (5 to 30 nm in diameter) homogeneously dispersed on weakly interactive α-alumina or carbon nanofiber supports.

Adapted with permission from H. M. Torres Galvis, J. H. Bitter, C. B. Khare, M. Ruitenbeek, A. I. Dugulan, K. P. de Jong, *Supported iron nanoparticles as catalysts for the sustainable production of lower olefins,* Science **335**, 835-838 (2012).

Introduction

Lower olefins (C_2 to C_4) are extensively used in the chemical industry as building blocks to synthesize a wide range of products such as polymers, solvents, drugs, cosmetics and detergents. Traditionally, lower olefins have been produced by thermal or catalytic cracking of naphtha or vacuum gas oil *(1)* or from dehydrogenation of alkanes *(2,3)*, but environmental and economic factors are currently spurring exploration of alternative routes for their production.

In recent years there has been growing interest in the development of biomass as a renewable feedstock for the production of commodity compounds *(4,5)*. Pyrolyzed biomass or bio-oil can be converted catalytically to lower olefins with moderate selectivity (43%C) *(5)*, though significant amounts of other compounds such as aromatics are also produced. Schemes put forward to produce lower olefins from synthesis gas (syngas) – a mixture of H_2 and CO obtained through biomass gasification – consist of at least two conversion steps, which involve either cracking of Fischer-Tropsch (FT) derived hydrocarbons *(6)* or the Methanol to Olefins (MTO) process *(7)*. Here we consider Fischer-Tropsch to Olefins (FTO) as a direct route, without intermediate steps, to transform syngas into light olefins.

For several decades research groups have attempted to develop iron-based catalysts to direct product selectivity of the FT synthesis towards light olefins *(8,9)*. Compared to other FT catalysts such as cobalt, iron disfavors competing formation of methane, and furthermore catalyzes the water-gas shift (WGS) reaction, enabling the use of a CO-rich syngas feed without an H_2/CO ratio adjustment. Mainly unsupported (sometimes referred to as bulk) iron oxide catalysts have been investigated *(9-12)*, and in some cases exhibited high selectivities towards lower olefins (up to 70 wt%) when the iron was modified by the addition of promoters *(9)*. Despite of these promising results however the bulk iron catalysts are mechanically unstable when the reaction is performed at high temperature, which is necessary to steer product selectivity to lighter hydrocarbons. Under these conditions the undesirable Boudouard reaction, $2CO\ (g) \rightarrow C(s) + CO_2(g)$ *(13)*, leads to the deposition of carbon, which can block the active sites and induce fragmentation of the particles in bulk iron catalysts *(14)*. The poor mechanical stability of the bulk iron oxide catalysts may lead to pressure drop increase in fixed bed operation caused by the plugging of the catalyst bed or to fouling of separation equipment in a fluidized bed process.

Supported iron catalysts display enhanced dispersion of the active phase and may withstand the mechanical degradation that threatens bulk iron catalysts. Research on supported iron catalysts *(15-21)* has met with limited success, however. Barrault *et al*. *(15)* found that iron dispersed on high surface area alumina displayed much lower activity than that dispersed on low surface area alumina. This finding points to a key aspect of supported iron catalysts, that is their cumbersome activation. If highly dispersed iron oxide interacts strongly with a high surface area oxidic support, the conversion of iron oxide into the active phase (iron carbide) is impeded *(14)*. Next to alumina *(15,16),* zeolites *(18)*, aluminophosphate molecular sieves *(19)* and carbonaceous materials *(20,21)* have been explored as catalyst supports for iron-based FTO catalysts. In Appendix A, Table 1 summarizes the most relevant results reported in literature regarding the development of supported iron catalysts for the selective production of lower olefins using carbon or alumina as a support. Iron supported on activated carbon (AC) displayed a high catalytic activity but also either low selectivity to light olefins *(20)* or a high deactivation rate *(21)*. After many years of research it has been regularly observed that supported iron catalysts which are the most active are the least selective *(15)*.

To overcome the low activity and the mechanical stability problems, we explored the use of support materials weakly interactive toward iron. As a working hypothesis we posited that these inert supports would impart mechanical stability to the iron nanoparticles without inhibiting their activation. In particular, nanostructured carbon materials *(22)* such as carbon nanofibers (CNF) *(23,24)* or nanotubes (CNT) *(25)* boast high specific surface area, chemical inertness and good mechanical strength.

In addition to carbon nanofibers we explored β-silicon carbide and α-alumina as supports. For comparison, we also examined three bulk iron catalysts (one unpromoted and two promoted) and iron supported on conventional high surface area SiO_2 and γ-Al_2O_3. The supported Fe catalysts were prepared using ammonium iron citrate as precursor with a nominal iron loading of 10 wt%, whereas the bulk catalysts had an iron content higher than 30 wt% (Appendix A, Table 2). The ammonium iron citrate used in the preparation of the supported samples contained low amounts of sulfur and sodium and efficiently introduced these promoters in the catalysts (Appendix A, Table 3).

Materials and Methods

Catalyst preparation

Preparation of supported Fe catalysts. Fe supported catalysts with a nominal loading of 10 wt% Fe were prepared by multi-step incipient wetness impregnation of the selected support (2 g) with 2.7 ml of a 1.4M aqueous solution of ammonium iron citrate (90-100%, J. T. Baker). The ammonium iron citrate as purchased contained low amounts of sulfur and sodium. Different support materials were used: α-Al_2O_3 (10 m^2 g^{-1}; BASF), β-SiC (25 m^2 g^{-1}; SICAT), γ-Al_2O_3 (250 m_2 g^{-1}; BASF), SiO_2 (495 m^2 g^{-1}; Grace Davison) and CNF (150 m^2 g^{-1}). Before impregnation, the β-SiC support was calcined at 700°C under static air for 3 hours. The carbon nanofibers support was prepared and surface-oxidized as described before *(26)*. The solution was added to the support until the pore volume was completely filled. After each impregnation step, the catalysts were dried at room temperature and 60 mbar for 2 hours. 6 wt% and 25 wt% Fe/α-Al_2O_3 catalysts were prepared by impregnation of 4 g of support with 2.8 ml (1.3M) and 12.8 ml (1.4M) of aqueous solutions of ammonium iron citrate. Impregnation and drying steps were repeated until incorporation of the total volume of the solution was achieved. The dried impregnates, except for the CNF supported sample, were heated at 500°C for 2 h, at a heating rate of 10 °C min^{-1} under air flow. Impregnated CNF was heated at 355°C for 2 h, at a heating rate of 10 °C min^{-1} under nitrogen flow.

Preparation of bulk Fe catalysts. A bulk promoted iron oxide catalyst (Fe-Ti-ZnO-K_2O with a weight composition 100:25:10:4) was synthesized according to the procedure reported by Büssemeier *et al. (9)*. Additionally, two bulk (unpromoted Fe_2O_3 and Fe_2O_3/CuO/K_2O/SiO_2) catalysts were prepared by precipitation of an aqueous solution of ferric nitrate and adding a basic sodium carbonate solution as precipitating agent. 25 g of $Fe(NO_3)_3.9H_2O$ (98% A.C.S. reagent, Acros) were dissolved in 100 ml of distilled water. For the promoted catalyst, 2.9 g of $Cu(NO_3)_2.3H_2O$ (p.a. 99.5%, Merck) was added to the solution. The solution was heated to its boiling point and after that, a near boiling solution of 25 g of Na_2CO_3 (99%, Acros) in 100 ml of distilled water was slowly added while stirring vigorously. The precipitate was filtered and re-slurried in boiling water to remove residual sodium. The washing process was repeated until neutral pH was reached. The unpromoted catalyst was dried at 60°C for 6 h and then at 120°C for 24 h. Subsequently, the catalyst was calcined under air flow at 300°C for 5 h with a heating ramp of 5°C min^{-1}. For

addition of K, after precipitation the Cu-promoted catalyst was re-slurried in 200 ml of distilled water. 16 g of potassium water glass solution (K_2O: SiO_2 1:2.15, Akzo-PQ) were added to the slurry under vigorous stirring. 3 ml of HNO3 was added to precipitate SiO_2 and to lower the potassium content. After this, the catalyst was washed, dried and calcined following the same procedure as for the unpromoted catalyst.

Catalyst characterization

X-ray fluorescence measurements were carried out to determine the iron loading and the elemental composition of the catalysts on Goffin Meyvis spectro X-lab 2000. X-ray diffraction measurements were performed with a Bruker AXS D8 ADVANCE diffractometer equipped with a $CoK_{\alpha 1}$ source ($\lambda = 0.1789$ nm) in a wide angle range (from 20 to 90° in 2θ). TEM images were obtained on a Philips Tecnai-20FEG (200 kV) microscope equipped with an EDX and HAADF detector. Thermal gravimetric analysis of the spent catalysts to determine carbon lay-down was performed in a Perkin Elmer Pyris 1 TGA under oxygen flow (10 ml min^{-1}). Temperature was increased from 30°C to 600°C with a heating ramp of 5 °C min^{-1}. After reaching 600°C, the samples remained at that temperature for 1 hour. Transmission 57Fe Mossbauer spectra were collected at room temperature with a conventional constant acceleration spectrometer using a 57Co (Rh) source. Velocity calibration was carried out using an α-Fe foil. The Mössbauer parameters were determined by fitting the spectra with calculated subspectra consisting of Lorentzian-shaped lines, using the Mosswin 3.0i program.

Catalytic tests

Low pressure testing. Fischer-Tropsch synthesis was performed at 1 bar and 350°C in a plug flow reactor (H_2/CO ratio of 1). 20 mg of the catalyst (particle size = 0.2-0.4 mm) were diluted with 200 mg of SiC (particle size = 0.2 mm) to achieve isothermal plug-flow conditions and reduced in situ in H_2/Ar (33% v/v; 60 ml min^{-1}) at 350°C for 2 h (Heating ramp: 5 °C min^{-1}). Gas chromatography was used to determine the selectivity for hydrocarbons up to C_{16}. Catalytic activities and product selectivities were determined uptill 15 h of reaction at low CO conversions (0.5-1%). CO_2 selectivity was not measured. Product selectivity has been calculated as equivalent amount of carbon atoms in a product with respect to the total carbon atoms present in the

hydrocarbons produced. The selectivity to oxygenates was below 1%C and has been excluded from the reported product selectivities.

Medium pressure testing. The Fischer-Tropsch reaction was carried out at 20 bar and 340°C in a plug flow reactor. 2 ml of catalyst (particle size = 0.2-0.4 mm) were diluted with 10 ml of SiC (particle size = 0.2-0.4 mm) and reduced in situ under H_2 flow (22 ml min^{-1}) at 350°C for 2 h. After reduction, temperature was lowered to 290°C and the feed flow was switched to a syngas/internal standard mixture (H_2/CO/He: 45/45/10%v/v, GHSV = 1500 h^{-1}). Temperature was raised to 340°C (Heating ramp: 10 °C h^{-1}). Catalytic activities and product selectivities were determined up to 64 h of reaction. Product selectivity was determined by gas chromatography analysis of the products up to C_{10}. Analysis of the liquid product confirmed the production of hydrocarbons, mainly in the range of C_8 to C_{15}. Only trace amounts (< 1%C) of alcohols (ethanol) were observed.

Results and Discussion

The use of ammonium iron citrate as the metal precursor provides a homogeneous distribution of the iron nanoparticles on the support, in contrast to extensive clustering that is observed when using iron nitrate *(27)*. Fe nanoparticle aggregation could lead to low catalytic activity and high methane selectivity as observed when using bulk iron catalysts. Transmission electron microscopy (TEM) was used to determine the size of the iron oxide particles and their distribution on the support.

Figure 1A shows a representative TEM micrograph of the calcined Fe/α-Al_2O_3, which exhibited a homogeneous distribution of iron oxide particles. The Fe_2O_3 particle size distribution (Appendix A, Figure 1) was 14 ± 5 nm on this support, and 5 ± 1 nm on CNF. The bulk promoted catalyst (Fe-Ti-Zn-K) consisted of large Fe_2O_3 particles (Average size: 400 nm), which formed aggregates resembling grape bunches (Figure 1B).

The volume averaged Fe_2O_3 crystallite size of the Fe catalyst precursors was calculated with the Scherrer equation using the parameters obtained by X-ray diffraction (XRD) analysis (Appendix A, Figure 2 and Table 2). Fe/SiO_2, Fe/γ-Al_2O_3 and Fe/β-SiC did not show the characteristic diffraction lines from iron oxide, indicating that the Fe_2O_3 was amorphous or that the crystallites were smaller than 4 nm (Appendix A, Figure 2).

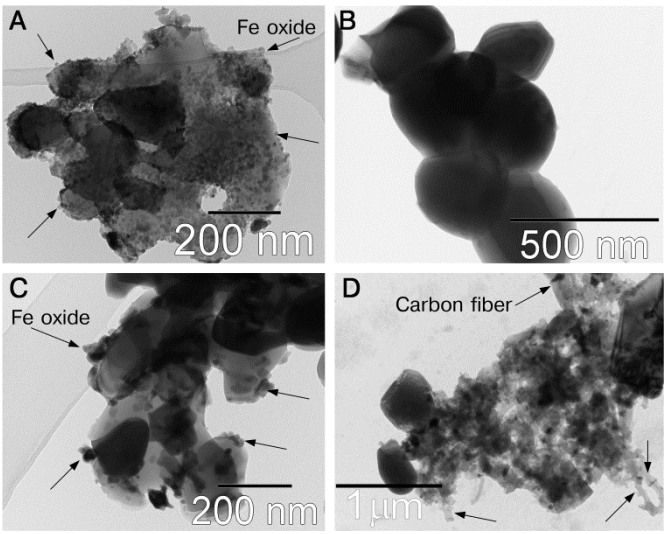

Figure 1. TEM images of fresh and spent Fe catalysts. The images from the fresh Fe/α-Al_2O_3 catalysts (**A**) show a homogeneous distribution of iron oxide nanoparticles on the support, whereas the bulk Fe-Ti-Zn-K catalyst (**B**) is mainly composed of aggregates of iron oxide crystals. In images of the spent catalysts after 64 h of reaction at 340°C, 20 bar and a H_2/CO ratio of 1, the Fe/α-Al_2O_3 (**C**) showed sintering of Fe particles after reaction; the bulk spent catalyst (**D**) fragmented and manifested carbon fiber growth (indicated by arrows).

The fresh catalysts were also analyzed by Mössbauer spectroscopy to determine the composition of the iron phase (Appendix A, Tables 4 and 5). Iron was present in the form of hematite (α-Fe_2O_3) in all samples. A superparamagnetic (SPM) iron oxide phase (α-Fe_2O_3 SPM) was measured in Fe_2O_3 particles smaller than 13.5 nm (Appendix A, supporting text accompanying Table 4). Iron was highly dispersed on CNF, γ-Al_2O_3 and SiO_2, as evidenced by the presence of SPM nanoparticles exclusively. The iron oxide particles on α-Al_2O_3 and β-SiC had a broader size distribution, whereas the bulk Fe-Ti-Zn-K catalyst was primarily composed of large Fe_2O_3 particles.

The supported and bulk Fe catalysts were tested in the Fischer-Tropsch reaction at 1 bar and 350°C at low CO conversion (0.5 to 1%) to restrict secondary hydrogenation of olefins (Table 1 and Appendix A, Figure 3).

Table 1. Product selectivity and catalytic activity at 1 bar. Catalytic tests performed at 350°C and H_2/CO ratio of 1; results after 15 h on stream (CO conversion: 0.5 - 1.0%). The product mixture that was analyzed consisted of C_1 to C_{16} hydrocarbons. Iron time yield (FTY): moles of CO converted to hydrocarbons per g of Fe per second. %C is defined as carbon atoms in a product with respect to the total number of C atoms in the hydrocarbon mixture. CO_2 was not measured.

Sample	FTY	Selectivity (%C)			
	(10^{-6} $mol_{CO}/g_{Fe}.s$)	CH_4	C_2-C_4 olefins	C_2-C_4 paraffins	C_{5+}
Fe/CNF	1.41	23	61	4	12
Fe/α-Al_2O_3 (12 wt% Fe)	0.65	22	61	4	13
Fe/β-SiC	6.52	31	58	4	7
Fe/SiO_2	0.14	38	56	5	1
Fe/γ-Al_2O_3	0.07	54	44	2	0
Fe-Ti-Zn-K	0.13	83	16	1	0
Fe-Cu-K-SiO_2	0.20	43	46	2	9
Bulk Fe	0.08	76	21	2	1

Catalytic activity is expressed as iron time yield (FTY), *i.e.* the number of CO moles converted to hydrocarbons per gram of iron per second. A high initial activity was observed for Fe/β-SiC and Fe/CNF. The activity of the Fe/CNF decreased continuously during the 15 h of reaction; the activity of the Fe/β-SiC catalyst increased during the first 5 hours of reaction, then decreased slowly afterwards (Appendix A, Figure 3A). The Fe/α-Al_2O_3 exhibited a lower catalytic activity than Fe/CNF and Fe/β-SiC; however, it showed remarkable stability, as the activity remained constant over 15 hours. Fe/γ-Al_2O_3 and Fe/SiO_2 displayed a low catalytic activity, comparable to the bulk Fe catalysts (Appendix A, Figure 3B). The Fe-Cu-K-SiO_2 catalysts showed an initial activity approximately 4 times higher than the Fe-Ti-Zn-K catalyst. Nevertheless, the iron time yield decreased rapidly to achieve comparable values after 15 h of reaction.

One of the most important requirements for an FTO catalyst is to obtain the maximum production of the lower olefins fraction while limiting methane selectivity to the lowest level possible. Fe/CNF and Fe/α-Al_2O_3, exhibited high selectivity towards lower olefins (~ 60 %C) while directing comparatively little carbon to methane (< 25 %C) (Table 1). Fe/β-SiC and Fe/SiO_2 also showed high selectivity to C_2 through C_4 olefins but the CH_4 product fraction was higher than 30 %C. Fe/γ-Al_2O_3 and the bulk catalysts displayed a high selectivity to methane (> 40 %C) which is not desired for their application in the FTO process.

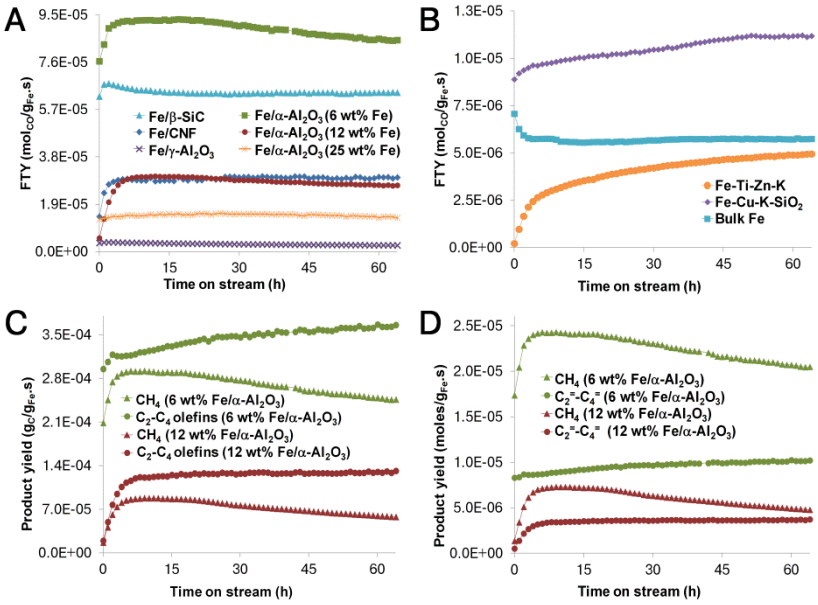

Figure 2. Catalytic performance of iron catalysts for the Fischer-Tropsch to Olefins process at 20 bar. Catalytic tests were carried out at T = 340°C, P = 20 bar, H_2/CO ratio of 1. Iron time yield is plotted above as a function of time for (**A**) Fe supported catalysts and (**B**) bulk Fe catalysts. Methane and lower olefins yields are plotted below as a function of time for (**C**) Fe supported catalysts and (**D**) bulk Fe catalysts. The product yields were obtained at CO conversion levels between 70 and 80%.

Additional tests were carried out at 20 bar, 340°C and an H_2/CO ratio of 1 to observe the performance of supported and bulk Fe catalysts under industrially relevant conditions (Figure 2). In view of the promising results obtained at 1 bar, we prepared and tested additional α-Al_2O_3 supported catalysts with different iron loadings (6 and 25 wt% Fe) to study the effect of iron content on catalytic performance. Most of the catalysts showed an initial increase in activity, except for the unpromoted bulk Fe (Figure 2B) which exhibited a decrease in activity during the first 10 h of reaction before reaching stability. After an initial activation period, Fe/β-SiC, Fe/CNF, 25 wt% Fe/α-Al_2O_3 and Fe/γ-Al_2O_3 showed a stable catalytic activity for 60 h. A slight decrease in activity during reaction was observed for the 6 wt% and 12 wt% Fe/α-Al_2O_3 catalysts mainly due to a continuous drop in CH_4 production (Figure 2C). The stability maintained during 60 hours fully complies with the requirements for the application of these catalysts in fluidized bed reactors. In view of their

favorable heat transfer characteristics, it is expected that these reactors will be preferred in industrial application of the exothermic FTO process.

Table 2 summarizes the activities and product selectivities measured after 64 h of reaction at 20 bar. The CO_2 selectivity for all the samples was approximately 40% on the basis of CO converted except for Fe/γ-Al_2O_3 (Appendix A, Table 6). Under the selected reaction conditions, most of the catalysts had comparable CO conversion levels (77 to 81%, Appendix A, Table 6).

Table 2. Catalytic performance at 20 bar. Catalytic tests performed at 340°C and H_2/CO ratio of 1; results after 64 h on stream. The product mixture that was analyzed consisted of C_1 to C_{10} hydrocarbons. FTY and selectivity defined as in Table 1. The selectivities were calculated on hydrocarbons produced*.

Sample	FTY (10^{-5} $mol_{CO}/g_{Fe}.s$)	Selectivity (%C)				
		CH_4	C_2-C_4 olefins	C_2-C_4 paraffins	C_{5+}	Oxygenates
Fe/CNF	2.98	13	52	12	18	5
Fe/α-Al_2O_3 (6 wt% Fe)	8.48	24	35	21	10	10
Fe/α-Al_2O_3 (12 wt% Fe)	2.66	17	39	19	14	11
Fe/α-Al_2O_3 (25 wt% Fe)	1.35	11	53	6	21	9
Fe/β-SiC	6.38	35	19	39	4	3
Fe/γ-Al_2O_3	0.25	49	33	11	1	6
Fe-Ti-Zn-K	0.49	24	28	29	10	9
Fe-Cu-K-SiO_2	1.12	26	36	12	18	8
Bulk Fe	0.57	30	32	18	14	6

*CO conversions and CO_2 selectivities are reported in Appendix A, Table 6

However, the Fe/γ-Al_2O_3 catalyst only achieved a CO conversion of 10%. The promoted catalysts prepared using supports with low interaction with iron showed high catalytic activities combined with high selectivities to the desired products. Fe/CNF and 25 wt% Fe/α-Al_2O_3 exhibited high selectivities towards C_2 through C_4 olefins (> 50%C) while yielding a methane product fraction lower than 15 %C. The Fe-Cu-K-SiO_2 catalyst showed a catalytic activity comparable to the 25 wt% Fe/α-Al_2O_3; however, only moderate selectivities towards lower olefins were obtained.

The Anderson-Schulz-Flory model (Equation 6, Chapter 2) that is used to predict the product distribution indicates that the maximum selectivity achievable for the C_2-C_4 fraction, including olefins and paraffins, is approximately 50 wt%, at a chain growth probability (α) between 0.4 to 0.5,

as shown in Figure 8 of Chapter 2. This model predicts that methane selectivity is about 30 wt% when this maximum C_2-C_4 selectivity is reached. Anderson-Schulz-Flory (ASF) plots (Figures 3 and Appendix A, Figure 4) demonstrate that the catalysts prepared using inert supports provide us with α-values of ~0.4 close to the optimal value for maximum lower olefins production. Moreover, the plots in Figure 3 revealed lower methane selectivities compared with the values predicted from the ASF model. This can be rationalized from the simplified 'surface carbide' or 'alkyl' mechanism (Figure 7, Chapter 2) which is widely accepted for the Fischer-Tropsch synthesis *(13)*.

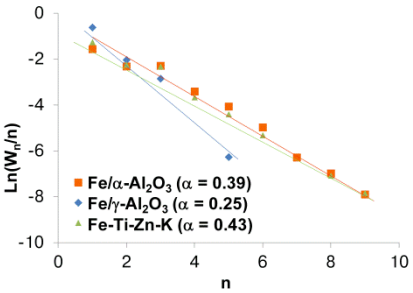

Figure 3. Comparison of ASF plots for supported and bulk catalysts. The ASF plots are based on the product distribution obtained when performing the Fischer-Tropsch reaction at 20 bar, 340°C and H_2/CO ratio of 1 after 64 h time on stream. Fe/α-Al_2O_3 has an iron loading of 12 wt%; n is the number of carbon atoms in a product and W_n is the weight fraction of the product with carbon number equal to n.

In this model, following CO dissociation and carbon hydrogenation, a CH_3 group adsorbed on the catalyst surface is proposed to act as chain initiator. The carbon chain grows by the addition of methylene monomer units (CH_2) to the adsorbed alkyl species. The chain growth is terminated by β-hydride abstraction to form α-olefins or by hydrogenation to produce paraffins. Negative deviations from the ASF prediction for methane selectivity can be expected when using iron catalysts modified with promoters which limit the hydrogenation reactions *(8)* thus favoring chain growth and the termination step via β-hydride abstraction that cannot give rise to CH_4 production. The suppression of the methanation reaction induced by the promoters was only observed when using CNF or α-Al_2O_3 since these 'inert' supports are thought to favor the proximity between iron and promoters (Na + S) in contrast to reactive supports such as γ-Al_2O_3 which lead to more methane (Figure 3). In

the case of the bulk catalysts, CH_4 selectivities coincided with the values predicted by the ASF model or were slightly above.

Mössbauer spectroscopy of the spent catalysts after reaction at 1 bar (Appendix A, Table 5) showed that the nature of the iron phases varied when using different support materials. Although some of the iron carbides may be oxidized after exposure to air, Fe_xC_y was detected on the samples with moderate to high catalytic activity. In contrast, the samples with the lowest catalytic activity, Fe/SiO_2 and $Fe/\gamma\text{-}Al_2O_3$, did not contain any carbides. A strong metal-support interaction clearly inhibits the formation of catalytically active iron carbides as observed for conventional high surface area support materials. Please note that in the size range of iron particles dispersed on inert supports (7-20 nm) particle size effects seem to be minimal.

TEM performed on spent catalysts revealed size increase of the iron nanoparticles in the supported samples. The particle size distributions of the fresh and spent $Fe/\alpha\text{-}Al_2O_3$ and Fe/CNF are shown in Appendix A, Figure 1. For Fe/CNF, changes in the catalytic activity were only observed during the first 4 hours of reaction, suggesting that the changes in the catalyst structure took place during catalyst activation and initial usage. In the case of $Fe/\alpha\text{-}Al_2O_3$, the average iron nanoparticle size increased from 14 ± 5 nm to 17 ± 5 nm (Figure 1C). The promoted bulk iron oxide showed extensive particle fragmentation and carbon filament growth, which brings about the poor mechanical stability of this catalyst (Figure 1D).

The spent catalysts were characterized with thermogravimetric analysis (TGA) to determine the extent of carbon lay-down. Carbon burn-off experiments were performed for all the samples, except for the Fe/CNF catalyst. Although extensive carbon deposition on the samples after reaction with CO-rich syngas and high temperatures could be expected, most of the samples exhibited low solid carbon formation. After 64 h of reaction at 340°C and 20 bar, the levels of carbon lay-down measured on the spent catalysts were lower than 10 wt%. In contrast, $Fe/\alpha\text{-}Al_2O_3$ (25 wt% Fe) and $Fe\text{-}Cu\text{-}K\text{-}SiO_2$ exhibited a higher extent of coke formation (23 wt% and 40 wt%, respectively).

Conclusion

The Fischer-Tropsch to Olefins (FTO) process arises as a strong alternative route for the sustainable production of lower olefins from biomass-derived synthesis gas. The industrial potential of this process is greatly enhanced by the reported development of active, selective and mechanically stable catalysts

that consist of promoted iron nanoparticles dispersed on weakly interactive supports. Further suppression of methane production, maximization of the C_2-C_4 olefins fraction and reduction of carbon lay-down by addition of promoters and by optimization of physical properties (*e.g.*, Fe particle size, distribution of Fe nanoparticles on the support) will allow us to further understand and develop the performance of these catalysts.

Supporting information

Results of XRD analysis, particle size distribution histograms, Anderson-Schulz-Flory plots, catalytic activity as a function of time for samples tested at 1 bar and Mössbauer spectroscopy results are provided in Appendix A.

Acknowledgements

M. van de Vijver, Dr. C. B. Khare and Dr. M. Ruitenbeek are thanked for the catalytic tests at 20 bar performed at Dow Benelux B.V. in Terneuzen. Dr. A. I. Dugulan is thanked for the Mössbauer spectroscopy measurements performed at the Fundamentals Aspects of Materials and Energy Group at the Technical University of Delft. Prof. Dr. Ir. E. J. M. Hensen (Technical University of Eindhoven) is thanked for his contribution in the discussion of the Mössbauer spectroscopy results. C. van der Spek is thanked for the TEM images.

References

1. A. Corma, F. V. Melo, L. Sauvanaud, F. Ortega, *Catal. Today* **107-108**, 699-706 (2005).
2. R. Diercks *et al.*, *Chem. Eng. Technol.* **31**, 631-637 (2008).
3. S. Wang, Z. H. Zhu, *Energy Fuels* **18**, 1126-1139 (2004).
4. E. L. Kunkes *et al.*, *Science* **322**, 417-421 (2008).
5. T. P. Vispute, H. Zhang, A. Sanna, R. Xiao, G. W. Huber, *Science* **330**, 1222-1227 (2010).
6. X. Dupain, R. A. Krul, C. J. Schaverien, M. Makkee, J. A. Moulijn, *Appl. Catal. B* **63**, 277-295 (2006).
7. G. A. Olah, *Angew. Chem. Int. Ed.* **44**, 2636-2639 (2005).
8. C. Wang, L. Xu, Q. Wang, *J. Nat. Gas Chem.* **12**, 10-16 (2003).
9. B. Büssemeier, C. D. Frohning, G. Horn, W. Kluy, US Patent 4564642 (1986).
10. B. H. Davis, *Catal. Today* **84**, 83-98 (2003).
11. S. Soled, E. Iglesia, *Catal. Lett.* **7**, 271-280 (1990).
12. Y. Jin, A. K. Datye, *J. Catal.* **196**, 8-17 (2000).

13. A. P. Steynberg, M. E. Dry, Eds., *Fischer-Tropsch Technology (Series: Studies in surface science and catalysis No. 152)* (Elsevier, Amsterdam, 2004).
14. M. D. Shroff *et al.*, *J. Catal.* **156**, 185-207 (1995).
15. J. Barrault, C. Forquy, J. C. Menezo, R. Maurel, *React. Kinet. Catal. Lett.* **15**, 153-158 (1980).
16. B. G. Baker, N. J. Clark, H. MacArthur, E. Summerville, US Patent 4610975 (1986).
17. D. B. Bukur *et al.*, *Ind. Eng. Chem. Res.* **29**, 1588-1599 (1990).
18. L. Xu, Q. Wang, Y. Xu, J. Huang, *Catal. Lett.* **31**, 253-266 (1995).
19. M. L. Cubeiro *et al.*, *Appl. Catal. A* **167**, 183-193 (1998).
20. V. K. Jones, L. R. Neubauer, C. H. Bartholomew, *J. Phys. Chem.* **90**, 4832-4839 (1986).
21. A. P. B. Sommen, F. Stoop, K. van der Wiele, *Appl. Catal.* **14**, 277-288 (1985).
22. K. P. de Jong, *Oil Gas Sci. Technol.* **61**, 527-534 (2006).
23. K. P. de Jong, J. W. Geus, *Catal. Rev. Sci. Eng.* **42**, 481-510 (2000).
24. E. van Steen, F. F. Prinsloo, *Catal. Today* **71**, 327-334 (2002).
25. W. Chen, Z. Fan, X. Pan, X. Bao, *J. Am. Chem. Soc.* **130**, 9414-9419 (2008).
26. G. L. Bezemer *et al.*, *J. Am. Chem. Soc.* **128**, 3956-3964 (2006).
27. A. J. van Dillen, Terörde, Robert J. A. M., D. J. Lensveld, J. W. Geus, K. P. de Jong, *J. Catal.* **216**, 257-264 (2003).

Chapter 4

Iron particle size effects for direct production of lower olefins from synthesis gas

Abstract

The Fischer-Tropsch synthesis of lower olefins (FTO) is an alternative process for the production of key chemical building blocks from non-petroleum-based sources such as natural gas, coal or biomass. The influence of the iron carbide particle size of promoted and unpromoted carbon nanofiber supported catalysts on the conversion of synthesis gas has been investigated at 340-350°C, H_2/CO = 1 and pressures of 1 and 20 bar. The surface-specific activity (apparent TOF) based on initial activity of unpromoted catalysts increased 6 – 8 fold when the average iron carbide size decreased from 7 to 2 nm while methane and lower olefins selectivity were not affected. The same decrease in particle size for catalysts promoted by Na plus S resulted at 20 bar in a two fold increase of the apparent TOF based on initial activity which was mainly caused by a higher yield of methane for the smallest particles. Presumably, methane formation takes place at highly active low coordination sites residing at corners and edges, which are more abundant on small iron carbide particles. Lower olefins are produced at promoted (stepped) terrace sites that are available and active, quite independent of size. These results demonstrate that the iron carbide particle size plays a crucial role in the design of active and selective FTO catalysts.

Adapted with permission from H. M. Torres Galvis, J. H. Bitter, T. Davidian, M. Ruitenbeek, A. I. Dugulan, K. P. de Jong, *Iron particle size effects for direct production of lower olefins from synthesis gas,* J. Am. Chem. Soc. **134**, 16207-16215 (2012).

Introduction

Lower olefins (C_2-C_4) are the key building blocks of the chemical industry. These short hydrocarbons are traditionally produced by steam cracking of naphtha or as byproducts of oil refining processes. The strategic determination of several countries to decrease their dependence on imported crude oil, the rapid depletion of known oil sources and the pressing necessity to minimize the carbon footprint have directed the research efforts into the development of alternative feedstocks and processes to produce chemicals.

The Fischer-Tropsch synthesis has long been known as an alternative process to produce long-chain hydrocarbons for their use in transportation fuels. In the Fischer-Tropsch reaction, synthesis gas produced from natural gas reforming or gasification of coal or biomass is transformed in the presence of cobalt, ruthenium or iron catalysts. The product distribution is highly dependent on the process conditions and the type of catalyst used.

An alternative process to produce lower olefins from synthesis gas is the so called FTO or Fischer-Tropsch to Olefins process. This reaction is carried out at more elevated temperatures (> 300°C) to shift selectivity towards short-chain hydrocarbons *(1-3)*. A catalyst for the selective production of C_2-C_4 olefins from synthesis gas that has been previously reported consists of iron nanoparticles dispersed on an inert support material *(1,2)*.

The Fischer-Tropsch reaction is recognized as a structure sensitive reaction *(4,5)* which means that the catalytic performance is strongly related to the particle size of the metal or active phase. The effect of metal particle size has been extensively studied for cobalt *(6-10)* and ruthenium *(11-14)*. However, in the case of iron, the number of research studies concerning the effect of particle size is limited since iron catalysts used in the Fischer-Tropsch synthesis are often unsupported or bulk catalysts.

Park *et al. (15)* studied the effect of Fe particle size for unpromoted δ-Al_2O_3-supported catalysts. These catalysts showed an increase of methane selectivity with a decrease of Fe crystallite size. The Turnover frequency (TOF) of Fe/δ-Al_2O_3 increased with particle size towards a maximum for catalysts with average Fe crystallite size of 6 nm and larger.

The effect of particle size of the active phase on catalytic performance might be obscured by the influence of strong metal support interactions. It is well known that iron forms mixed oxides when supported on alumina or silica *(16)*. These aluminates or silicates are difficult to reduce and the formation of the active iron carbide phase is hindered. In order to study the intrinsic particle size

effect and to limit support effects, it is necessary to use a carrier material with limited interaction towards iron such as carbon nanofibers *(1,2,6,7)*.

During the eighties, studies concerning the effect of Fe crystallite size were performed on unpromoted carbon-supported *(17,18)* and γ-Al_2O_3 supported catalysts *(19)*. Jung *et al. (17)* reported that, under the conditions used (1 bar, 275°C and H_2/CO = 3), smaller Fe particle sizes (< 1.6 nm) lead to lower turnover frequencies for CO hydrogenation, lower methane selectivities and higher olefin to paraffin (O/P) ratios. In a subsequent study, Jones *et al. (18)* found similar trends for methane selectivity and TOF with iron (carbide) particle size. However, they observed higher O/P ratios for catalysts with larger Fe particles. The discrepancy in the results was attributed to the different testing conditions used in the study of Jones *et al.* (1 bar, 200°C and H_2/CO = 2). In both studies it was stated that carbon-supported catalysts are more selective to olefins in comparison with samples prepared with γ-Al_2O_3 as support.

An interesting study related to the effect of iron particle size on catalytic performance using supported and K-promoted catalysts was carried out by Barkhuizen *et al. (12)*. The Fe particles were prepared by the reverse micelle technique and were dispersed on activated carbon or γ-Al_2O_3. The Fischer-Tropsch reaction was carried out at 270°C, 30 bar and a H_2/CO = 2. For particles with average sizes smaller than 10 nm a decrease in particle size led to a decrease in surface-specific activity and chain growth probability and higher methane selectivity. The lower activity of smaller Fe particles was attributed to preferential coverage with carbon layers or to a lower density of specific sites for chain growth during the Fischer-Tropsch reaction. However, for this particular study it was difficult to discern between particle size and promoter effects.

It is noted that iron carbide is recognized as the active phase for the Fischer-Tropsch reaction and not iron in its metallic state *(18,20-23)*. Density Functional Theory (DFT) calculations have shown that metallic iron and iron carbide have distinct catalytic behaviors as they display different CO dissociation barriers and binding strengths for C and O atoms *(24-26)*.

The research studies concerning the Fe particle size effect for supported catalysts have been performed at relatively low temperature (~ 250°C) to investigate catalysts dedicated to the production of transportation fuels and not the high temperatures (~ 350°C) required for the synthesis of lower olefins.

In this study, we focused on the influence of Fe carbide particle size on catalytic performance at elevated temperatures (340-350°C). Carbon nanofibers (CNF) supported catalysts with different iron oxide particle sizes were synthesized and tested under FTO conditions to analyze the carbide particle size effect on activity and C_2-C_4 olefins and methane selectivity. Here we have studied both promoted and unpromoted systems to decouple size effects from the influence of promoters.

Experimental methods

Preparation of the CNF support

A 5 wt% Ni/SiO_2 catalyst was prepared by homogenous deposition precipitation as described elsewhere *(27)*. 4 g of the calcined nickel catalyst, sieve fraction 150-212 μm, was placed in a tubular oven and reduced *in situ* under the flow of a H_2 (80 ml min^{-1}) and N_2 (320 ml min^{-1}) mixture at a pressure of 2.8 bar and 700°C for 2 h (ramp 5°C min^{-1}). After reduction, the flow was switched to a mixture of CO (80 ml min^{-1}), H_2 (28 ml min^{-1}) and N_2 (292 ml min^{-1}) at a pressure of 3 bar and the oven temperature was decreased to 550°C. The carbon nanofibers were grown for 24 h. After growth the product was refluxed in 200 ml of 1 M aqueous solution of KOH for 2 h to remove the silica support. After the basic treatment, the fibers were washed until neutral pH with demineralized water. Subsequently, the fibers were subjected to a treatment by refluxing in concentrated HNO_3 for 2 h to remove nickel and to introduce oxygen-containing groups on the surface of the fibers. After the acid treatment the fibers were washed with demineralized water until neutral pH and dried overnight under static air at 120°C.

Catalyst preparation and characterization

Preparation of unpromoted supported catalysts (Impregnation). Five catalysts with different iron loadings (1, 2, 5, 10 and 20 wt% Fe) were pre-pared by incipient wetness impregnation of aqueous solutions of ammonium iron citrate (Fluka, *purum* p.a., 14.5-16 wt% Fe) on oxidized CNF (150 m^2 g^{-1}, pore volume 0.5 ml g^{-1}). In the case of the 1 and 2 wt% Fe catalysts, the pore volume of the support was filled with the total volume of the solution in a single step. For the other samples it was necessary to carry out successive impregnations. Between impregnation steps the samples were dried under static air at 120°C for 1 h. After total usage of the solution the samples were dried overnight under static air at 120°C. In a subsequent step, the

impregnated and dried samples were heat treated under nitrogen in a plug flow reactor at 500°C for 2 h (5°C min^{-1}; 150 ml min^{-1} for 150 mg of precursor loaded catalyst). The samples were cooled down to room temperature and were passivated by oxidation with diluted oxygen. The oxygen concentration was increased stepwise (2% v/v increase every 30 min) until reaching 20% v/v. The number in the sample code indicates the nominal iron loading. IM means that the sample was prepared by impregnation and did not contain promoters.

Preparation of unpromoted supported catalysts (colloidal synthesis). Three catalysts with different iron oxide particle sizes were prepared by using a colloidal synthesis based on the thermal decomposition of iron oleate. The iron complex was prepared according to the procedure described by Bronstein *et al. (28)*. 1.08 g of iron oleate were mixed with 1.24 ml of oleic acid, 13 ml of the solvent (hexadecene, octadecene or docosane, depending on the desired particle size) and 2 g of surface-oxidized carbon nanofibers (150 m^2 g^{-1}) to achieve a nominal iron loading of 10 wt%. The mixture was heated up to the boiling temperature of the solvent (275°C, 315°C, 370°C, respectively) with a heating ramp of 3.3°C min^{-1} and was kept at the final temperature for 30 min. After cooling down to room temperature, the supported catalysts were washed three times with a mixture of hexane and acetone (1:4 volumetric ratio). The solids were separated by filtration and dried under vacuum at 40°C in a rotary evaporator for 1 h. The dried catalysts were heat treated under nitrogen flow at 350°C for 2 h (ramp 10°C min^{-1}, 150 ml min^{-1} for 150 mg of precursor loaded catalyst). The number in the sample codes indicates the nominal iron loading. The letters provide information about the preparation method: CH: colloidal hexadecene; CO: colloidal octadecene; CD: colloidal docosane.

Preparation of promoted supported catalysts. Five catalysts with different iron loadings (1, 2, 5, 10 and 20 wt% Fe) were pre-pared as described above by incipient wetness impregnations of aqueous solutions of ammonium iron citrate (J. T. Baker, 14.5-16 wt% Fe, Na, S: ~ 750 mg kg^{-1}) on oxidized CNF. This iron precursor contained traces of sodium and sulfur which are suitable promoters for FTO *(1,29,30)*. The preparation procedure was as described for the unpromoted catalysts synthesized with the impregnation technique. The sample code is similar as previously explained for unpromoted samples prepared by impregnation. In order to differentiate between unpromoted and

promoted samples, a letter P was added to the sample code of promoted catalysts.

Fresh and spent catalysts characterization. Iron loadings of samples prepared by colloidal synthesis were measured with X-ray fluorescence (XRF) on a Goffin Meyvis Spectro X-lab 2000 machine. The average crystallite size of the iron oxide particles was determined by analysis of the line broadening in the X-ray diffraction (XRD) patterns recorded at room temperature. The measurements were performed with a Bruker AXS D8 Advance diffractometer equipped with a $Co_{K\alpha,1}$ source ($\lambda = 0.178897$ nm) from 25° to 80° in 2θ. The distribution of iron oxide on the support and the particle size distribution were obtained by the analysis of Transmission Electron Microscopy (TEM) micrographs. The images were acquired on a Philips Tecnai-20 FEG (200 kV) microscope equipped with an EDX and HAADF detector. The composition of the Fe phase before reaction, after reduction and after FTO reaction was determined *in situ* with Transmission ^{57}Fe Mössbauer Spectroscopy. The spectra were collected at room temperature with a conventional constant acceleration spectrometer using a ^{57}Co (Rh) source. Velocity calibration was carried out using an α-Fe foil. The Mössbauer parameters were estimated by fitting the spectra using the Mosswin 3.0i program.

Catalytic tests

Low pressure testing. The Fischer-Tropsch synthesis was performed at 1 bar and 250°C or 350°C using a mixture of H_2 and CO (1/1 v/v). H_2 (99,999%) , CO (99%) and Ar (99,999%) were supplied by Linde Gas and used without further purification. 20 mg of the catalyst (particle size 0.2 – 0.4 mm, ρ = 0.55 g ml^{-1}) were diluted with 200 mg of SiC (particle size 0.2 mm) and placed in a plug flow reactor. The reaction was carried out at low CO conversions (< 1%) to ensure differential operation. When the Fischer-Tropsch reaction was performed at 250°C the catalysts were reduced *in situ*, prior to reaction, using a mixture of H_2 and Ar (33% v/v H_2; 60 ml min^{-1}) at 350°C for 2 h (ramp 5°C min^{-1}). In the case that the reaction was carried out at 350°C, the catalysts were heated up under Ar flow until reaction temperature (ramp 5°C min^{-1}). Subsequently, the flow was switched to the H_2/CO mixture (6 ml min^{-1}). The effect of pretreatment on catalytic performance (reduction under H_2 or direct activation under syngas) was negligible for samples tested at 350°C and 1 bar. The product selectivity to hydrocarbons up to C_{16} was determined with

gas chromatography using a Varian CP3800 analyzer equipped with an FID detector (Column CP Sil 5 CB). The GC was calibrated with a gas mixture of known composition. The calibration for low concentrations was performed by dilution of the calibration mixture to ensure the reliability of the data at low CO conversions. CO_2 selectivity was not measured. The product selectivity was calculated on a carbon atom basis: (moles of product Y) x (carbon atoms in product Y)/(total carbon atoms in hydrocarbons produced). The catalytic activities expressed as moles of CO converted to hydrocarbons per gram of iron per second (FTY) or per mol of surface sites per second (TOF) were determined after 1 h and 15 h of reaction. Apparent TOF was calculated using the density of Fe_5C_2 (ρ = 7.57 g ml^{-1}) and assuming 14 Fe atoms nm^{-2}. It has been assumed that the iron-containing particles consist fully of iron carbide at their surfaces. The selectivity to oxygenates was below 1 $\%C_{at}$ and therefore excluded.

Medium pressure testing. The Fischer-Tropsch synthesis was carried out in a plug flow reactor at 20 bar and 340°C using a mixture of H_2 and CO (1/1 v/v) with a space velocity of 3000 h^{-1}. CO (99,9%), H_2 (99.95%), N_2 (99.996%), He (99.9992%) supplied by Praxair were used and further purified for sulfur and carbonyls with a Vici Metronics T400-2 trap. 100 μl of catalyst (particle size 0.2 – 0.4 mm, ρ = 0.55 g ml^{-1}) were diluted with SiC (particle size 0.2 – 0.4 mm) to complete a volume of 200 μl. The catalysts were reduced in H_2 at 350°C for 2 h prior to reaction. The initial CO conversion was in the range of 23 to 89% for the promoted catalysts. The product selectivity to hydrocarbons up to C_9 was determined with online gas chromatography and was calculated on a carbon atom basis. The analysis of the gases was performed using a Siemens Maxum II analyzer for parallel chromatography equipped with Restek CHR-PAW, Agilent GS-GasPro, Restek MXT1 columns. The catalytic activities and selectivities reported here were determined at the start of the Fischer-Tropsch reaction (1 h). The liquid products were collected in a hot trap and the composition of the cumulative liquid was analyzed offline with GC x GC on an Agilent 7890 machine equipped with Agilent DB-17 and CP-Sil5 columns. The analysis confirmed the production of hydrocarbons in the range of C_8 to C_{15}. Trace amounts of alcohols, mainly ethanol, were observed. CO_2 selectivities were determined too. A blank experiment in which heat treated CNF (heat treatment at 750°C to expose encapsulated nickel particles) were tested under FTO conditions showed negligible activity for methanation thus contributions

on activity and selectivity by methane formation due to the presence of possible nickel traces in the CNF support were ruled out.

Results and discussion

The analysis of TEM images of unpromoted catalysts pre-pared by the incipient wetness impregnation (IWI) method demonstrated that different iron oxide particle sizes were obtained at different iron loadings. Nominal or apparent iron carbide (χ-Fe_5C_2) particle sizes were calculated from the average Fe_2O_3 particle sizes determined with TEM analysis. Here we report our results in relation to iron carbide sizes instead of referring to metallic Fe since Hägg carbide, Fe_5C_2, has being suggested to be the active phase during the Fischer-Tropsch reaction *(21,24,31)*. The estimated carbide sizes are smaller than measured Fe_2O_3 sizes and similar to calculated Fe sizes in view of density differences (Table 1).

Table 1. Properties of unpromoted CNF-supported iron catalysts

Sample	Preparation	Fe loading (wt%)	Fe_2O_3 crystallite size; XRD (nm)	Fe_2O_3 particle size (nm)[c]	Fe_5C_2 particle size (nm)[d]	Fe particle size (nm)[d]
1IM	Impregnation	1[a]	–	2.6	2.1	2.0
2IM	Impregnation	2[a]	–	2.5	2.0	1.9
5IM	Impregnation	5[a]	–	4.0	3.2	3.1
10IM	Impregnation	10[a]	7	5.5	4.4	4.3
20IM	Impregnation	20[a]	10	8.6	6.9	6.7
10CH	Colloidal	8[b]	7	8.1	6.5	6.3
10CO	Colloidal	8[b]	11	14.2	11.5	11.0
10CD	Colloidal	12[b]	17	16.9	13.6	13.1

[a] Nominal iron loading

[b] Iron loading measured with XRF

[c] Number average determined by TEM analysis

[d] Calculated from TEM data of Fe_2O_3

In the case of the samples synthesized with the IWI technique iron carbide particle size increased as a function of iron loading (Table 1 and Appendix B, Figure 1). The Fe_2O_3 particle sizes reported in Table 1 and Appendix B, Figure 1 correspond to unpromoted catalysts. TEM analysis of selected promoted samples demonstrated that average iron oxide particle sizes were identical for unpromoted and promoted catalysts prepared by the IWI preparation method.

Figure 1 shows that particle size distribution for the 2 and 5 wt% Fe samples prepared by impregnation is narrow.

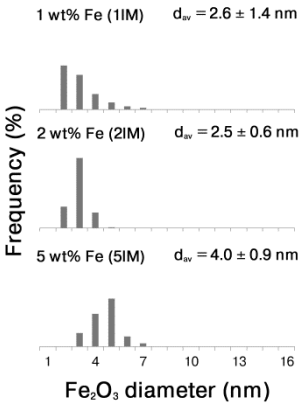

Figure 1. Particle size distribution of iron oxide from TEM analysis of unpromoted catalysts prepared by incipient wetness impregnation revealed narrow size distributions of Fe_2O_3 particles for the 2 wt% Fe/CNF and 5 wt% Fe/CNF samples.

The standard deviation from the average diameter was approximately 23%. Broader distributions were observed for the 1 wt% Fe catalyst and samples with higher iron loadings (Appendix B, Figure 2). TEM analysis of catalysts prepared by colloidal synthesis showed that these samples had a relatively narrow size distribution. A typical TEM image of a catalyst (10CO) prepared using octadecene as solvent is shown in Figure 2. The histograms from the particle size distribution analysis of catalysts prepared with colloidal synthesis are included in Appendix B, Figure 2.

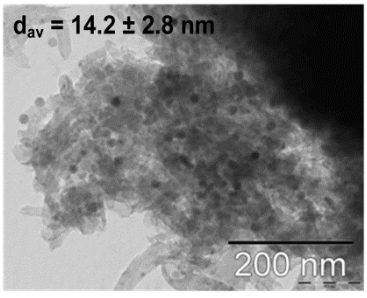

Figure 2. TEM image of a catalyst (10CO) prepared by colloidal synthesis. The Fe_2O_3 particles were homogeneously dispersed on the carbon nanofibers and had a narrow size distribution when the samples were prepared by thermal decomposition of iron oleate in octadecene.

Analysis of diffraction patterns measured with XRD showed that Fe_2O_3 line broadening was only observable on samples with crystallite sizes larger than 4 nm due to technique and equipment limitations (Table 1). The Fe_2O_3 crystallite sizes measured with XRD analysis are in close agreement with the particle sizes determined with TEM. The iron loadings, number-average Fe oxide sizes and the calculated carbide sizes are displayed in Table 1.

Promoted and unpromoted Fe/CNF catalysts were tested at 250°C and 350°C for the Fischer-Tropsch reaction to determine (1 bar, H_2/CO = 1 v/v) the effect of iron carbide particle size at 250°C and 350°C. The catalysts were tested under low CO conversion (< 1%) to ensure differential operation. Most of the samples showed deactivation probably caused by carbon deposition under low pressure and low H_2/CO ratio conditions. Deactivation due to carbon deposition during the FTO reaction at low H_2/CO ratios was previously observed by Sommen *et al. (32)* for Fe/AC and by Koeken *et al. (33)* for Fe/α-Al_2O_3 catalysts. The catalytic activity as a function of time on stream for promoted and unpromoted samples at 250°C and 350°C conditions are included in Appendix B, Figure 3. The catalytic results at 1 bar of unpromoted and promoted samples showed that the catalytic activity per gram of iron (iron time yield, FTY) increased with the decrease of Fe_5C_2 particle size regardless of reaction temperature (Figure 3, 350°C and Appendix B, Figure 4, 250°C). This effect was most pronounced for iron carbide particles smaller than 4 nm.

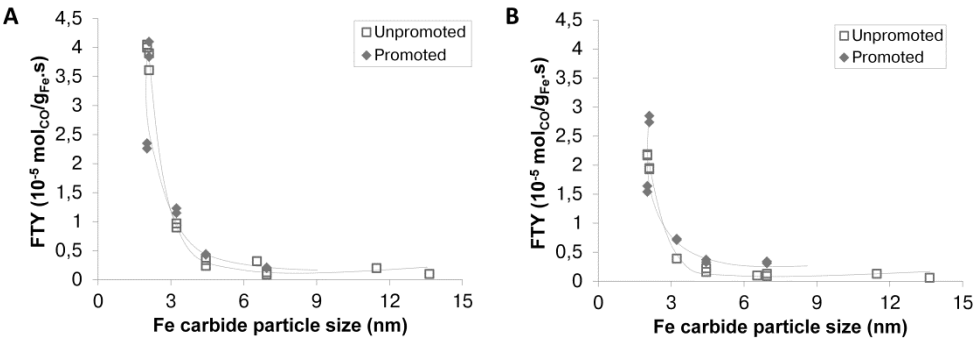

Figure 3. Iron time yield (FTY) as a function of particle size. The iron-normalized activity of Fe/CNF catalysts (unpromoted □); promoted ◆) decreased with an increase in iron particle size. A: TOS = 1 h; B: TOS = 15 h. The reaction was performed at 350°C, 1 bar and H_2/CO = 1 v/v.

Figure 3A shows FTY determined after 1 h of reaction while Figure 3B displays the catalytic activities after 15 h of reaction. From these plots it is observed

that the increase of catalytic activity with the decrease of particle size was maintained after 15 h of reaction despite of more severe deactivation for smaller particles (Appendix B, Figure 3). TEM analysis of selected samples evidenced that after reaction at 1 bar the iron-containing particles experienced limited levels of sintering (Appendix B, Table 1).

Our results on catalytic activity show an opposite trend compared to the results reported by other research groups for iron catalysts supported on activated carbon or δ and γ-Al_2O_3. In these studies the effect of metal-support interactions might have masked the influence of Fe particle size, even in the case of activated carbon *(18)*. A comparative experiment evidenced that a promoted Fe/AC catalyst (Appendix B, Table 2) prepared by impregnation of ammonium iron citrate had an FTY five times lower compared to a promoted Fe/CNF catalyst with a similar Fe particle size. Mössbauer spectroscopy suggested that the Fe/AC catalyst had a lower degree of carbidization and a concomitant higher amount of Fe (II) oxide.

The higher FTY observed for catalysts with smaller Fe_5C_2 particle sizes might be attributed to a lower extent of carbon deposition and thereby deactivation. However, activity trends are similar for short and longer times on stream (Figure 3).

Additional characterization experiments using *in situ* Mössbauer spectroscopy (1 bar, 350°C, H_2/CO ratio of 1 v/v, TOS = 15 h) indicated that catalysts with different iron carbide particle sizes before reaction (2.0 and 4.4 nm, respectively) exhibited different degrees of carbidization (Appendix B, Table 3). The higher activity of 10IMP compared with 10IM could be ascribed to higher total carbidic content (Fe_xC (SPM) plus Fe_5C_2). However, samples with similar total carbide contents exhibited different catalytic performance (comparison between 2IM and 10IM or between 2IMP and 10IMP). This result suggests that two iron-containing particles having approximately the same composition but different sizes displayed a dissimilar catalytic behavior probably because of differences in the nature and number of active sites.

The results of the catalytic tests of unpromoted and promoted catalysts under FTO conditions (350°C) are further summarized in Table 2. We have assumed that the active particles fully consist of iron carbide at their surface as suggested by HR-TEM studies of Datye and co-workers *(21)*. Nevertheless, it is acknowledged that iron oxide might be present on the surface of the Fe-containing particles in case of carbide reoxidation, as observed in previous studies at high CO conversions *(34)*. This assumption implies that the

calculated TOF values have to be considered as lower limits and will be referred to as 'apparent TOF' in the text and figures. The apparent TOF data presented in Table 2 correspond to initial activities (after 1 h of reaction). Methane and C_2-C_4 olefins selectivities are also plotted as a function of Fe_5C_2 size in Figure 4.

Table 2. Catalytic activity and product selectivity under FTO conditions of promoted and unpromoted Fe/CNF (1 bar, 350°C, H_2/CO = 1, TOS = 15 h) of Fe/CNF catalysts

Sample	FTY (10^{-5} $mol_{CO}/g_{Fe}.s$)	Apparent TOF[a] x 10^3 (s^{-1})	Product selectivity (%C_{at}, CO_2-free)			
			CH_4	C_2-C_4 olefins	C_2-C_4 paraffins	C_{5+}
1IM	1.93	10.9	40	49	5	6
2IM	2.19	11.9	45	46	3	6
5IM	0.39	3.4	36	50	3	11
10IM	0.16	1.9	34	51	3	12
20IM	0.09	1.7	36	49	3	12
10CH	0.10	1.5	38	54	3	5
10CO	0.13	3.1	37	50	2	11
10CD	0.06	2.2	48	47	2	3
1IMP	2.74	15.5	41	49	4	6
2IMP	1.64	8.9	37	51	5	7
5IMP	0.73	6.3	33	52	7	8
10IMP	0.37	4.4	28	57	5	10
20IMP	0.31	5.2	20	65	2	13
2IMDP[b]	2.68	14.6	36	52	6	6

[a] Apparent turnover frequency: moles of CO converted to hydrocarbons per mol of surface Fe_5C_2 per second.

[b] Sample prepared with an additional amount of Na and S

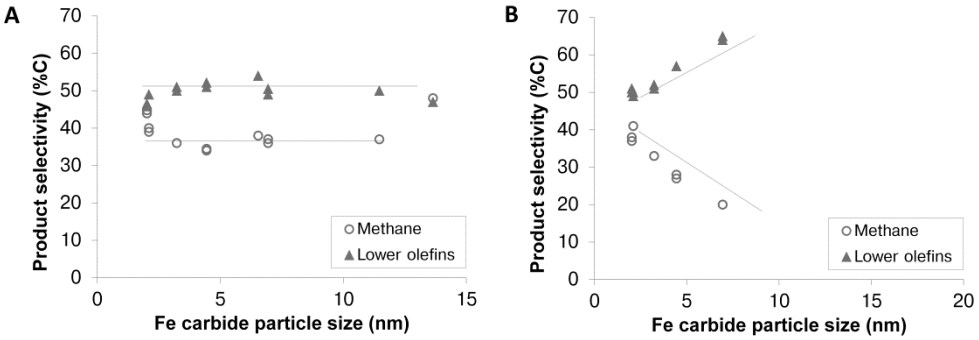

Figure 4. Product selectivity as a function of particle size. Selectivity towards methane and lower olefins of Fe/CNF catalysts, (A) unpromoted and (B) promoted; Product selectivity: C_2-C_4 olefins (▲) and methane (○) (Reaction conditions: 1 bar, 350°C, H_2/CO = 1, TOS: 15 h).

The effect of iron carbide size on product selectivity was almost nil for unpromoted catalysts, although some scatter was apparent for the smallest and largest sizes (Figure 4A). These catalysts exhibited a fairly high selectivity toward lower olefins (~ 50 $\%C_{at}$) in combination with a high methane production (~ 40 $\%C_{at}$). The samples with the lowest methane selectivity displayed slightly lower C_2-C_4 olefins selectivities (~ 47%).

In contrast to the behavior observed for unpromoted catalyst, the product selectivities of promoted Fe/CNF samples exhibited a clear effect of iron carbide particle size (Figure 4B). Lower olefins selectivity increased from 50 $\%C_{at}$ to 65 $\%C_{at}$ while CH_4 selectivity showed an opposite trend decreasing from 40 $\%C_{at}$ to 20 $\%C_{at}$ when Fe_5C_2 size increased from 2 to 7 nm.

The Anderson-Schulz-Flory (ASF) plots for the promoted catalysts are shown in Appendix B, Figure 5. For these samples it was observed that chain growth probability (α) increased with particle size. The samples with the smallest iron carbide sizes (1IMP, 2IMP) followed the ASF product distribution while larger particles (5IMP, 10IMP) showed methane selectivities below the values predicted by the model.

This remarkable selectivity response for promoted catalysts cannot be attributed to an intrinsic particle size effect of iron carbide since the results of the unpromoted catalysts confirmed that the influence of iron carbide size on product selectivity was minimal (Figure 4A). The increase of lower olefins selectivity and the decrease of CH_4 production with the increase of Fe_5C_2 particle size might be ascribed to higher coverages of promoters on the active surface for larger sizes.

The fact that unpromoted and promoted catalysts with small Fe_5C_2 sizes (~ 2 nm) exhibited similar product selectivities possibly confirms this explanation. An additional experiment was performed introducing additional Na and S during the synthesis of the catalyst 2IMDP to achieve a double amount of promoters compared with sample 2IMP. Results of the catalytic test of sample 2IMDP (Table 2) indicated that the addition of extra amounts of promoters did not affect product selectivity although it gave rise to an enhanced catalytic activity. This result might suggest that small iron carbide particles have a large number of sites for CH_4 formation that might be difficult to affect with sodium/sulfur.

Promoted and unpromoted catalysts prepared by impregnation were tested under FTO conditions at medium pressure (20 bar) to assess the effect of iron carbide particle size on catalytic performance at industrially relevant conditions. The results summarized in Table 3 were measured after 1 h time on stream

after which limited sintering as well as limited coke lay-down *(33)* is expected. In the case of unpromoted catalysts, a decrease in FTY and apparent TOF was observed with an increase in iron carbide particle size, similarly to the behavior observed when the reaction was performed at 1 bar. The C_2-C_4 olefins selectivity for these catalysts was low (< 20 %C_{at}) and accompanied by high methane production (> 30 %C_{at}) (Table 3).

Table 3. Catalytic performance of promoted and unpromoted Fe/CNF under FTO conditions (20 bar, 340°C and H_2/CO = 1, TOS = 1 h)

Sample	CO conv. (%)	CO_2 (% CO conv.)	FTY (10^{-4} $mol_{CO}/g_{Fe}.s$)	Apparent TOFx10 (s^{-1})	Product selectivity (%C_{at}, CO_2-free)				
					CH_4	C_2-C_4 olef.	C_2-C_4 par.	C_{5+}	Oxyg.
1IM	10	35	1.42	0.8	57	6	34	2	2
2IM	9	32	0.38	0.2	34	13	46	7	0
5IM	11	46	0.20	0.2	27	17	45	12	0
10IM	11	46	0.13	0.2	59	4	34	0	3
20IM	10	42	0.06	0.1	43	21	32	0	3
1IMP	12	38	1.98	1.1	50	6	34	1	9
2IMP	30	46	1.82	1.0	40	12	41	1	5
5IMP	82	49	1.02	0.9	13	46	32	6	3
10IMP	86	47	0.55	0.7	8	52	7	28	5
20IMP	87	42	0.32	0.6	10	37	23	28	2

The activity per gram of iron (FTY) and apparent turnover frequency for promoted catalysts also decreased with an in-crease of Fe_5C_2 particle size as shown in Table 3. The activity of the promoted catalysts was almost five times higher than for unpromoted catalysts with the same iron carbide sizes, with the exception of sample 1IMP. A similar trend for the catalytic activity as a function of the Fe_5C_2 particle size is observed when performing the FTO reaction under low (Figure 3) and medium pressures (Figure 5) although at the latter condition FTYs were five to fifteen times higher.

For the promoted catalysts also at 20 bar lower olefins selectivity increased with the increase of iron carbide size albeit that for the sample with the largest particle size (~ 7 nm) a somewhat lower selectivity was observed (Figure 5B). From the results of the catalytic tests it is apparent that C_{5+} selectivity also increased when particle size increased (Table 3). A different behavior at 20 bar was also observed for methane where selectivity was high for small particle

sizes (~ 2 nm) but it did not decrease any further with the increase of Fe_5C_2 size setting a limit around 10 $\%C_{at}$ (Figure 5B).

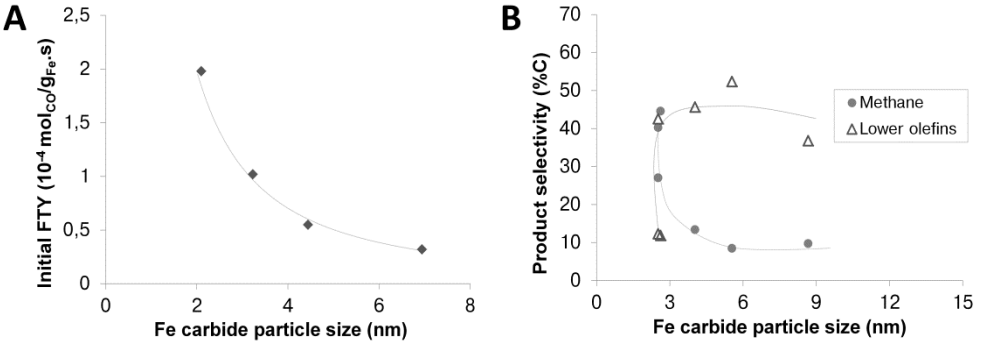

Figure 5. Catalytic performance of promoted catalysts at medium pressure (340°C, 20 bar and H_2/CO = 1). (A) The catalytic activity per gram of iron (FTY) of promoted Fe/CNF catalysts. (B) Product selectivity: Methane (●) and C_2-C_4 olefins (△) selectivities show an opposite trend with the increase of iron particle size.

Analysis of TEM images of spent samples indicated that iron containing particles had sintered during reaction at 20 bar. Figure 6 shows micrographs of two spent promoted Fe/CNF catalysts and their respective particle size distribution. The average carbide size for the spent catalyst 5IMP was 11.1 ± 6.4 nm while for the catalyst 20IMP the average size after reaction was 13.5 ± 9.5 nm.

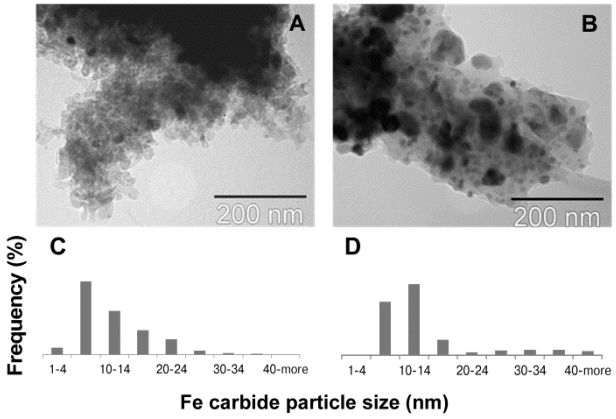

Figure 6. TEM of spent promoted samples after FTO at 340°C, 20 bar and H_2/CO = 1, TOS = 40 h. (A) Sample 5IMP with average particle size of 3 nm before reaction and (B) Sample 20IMP with particle size of 7 nm before reaction. Histograms of the iron carbide sizes after reaction: (C) sample 5IMP and (D) sample 20IMP.

From these results it is observed that a sample with a small initial particle size suffered a higher extent of sintering compared to a sample with a larger size.
Activity plots as a function of time on stream (Appendix B, Figure B6) indicated that catalyst with smaller carbide sizes indeed deactivated faster than samples with larger Fe_5C_2 sizes.
Due to the carbonaceous nature of the support it is difficult to distinguish the carbon deposited during reaction. For this reason, in future work we propose to perform *in situ* carbon lay-down measurements. Tentatively, for the catalysts with small particle sizes the fast deactivation is attributed to loss in active surface area caused by sintering rather than carbon lay-down.

General discussion and conclusions

Carbon nanofiber supported iron (carbide) particles in the range from 2 to 17 nm have been synthesized. For promoted and unpromoted catalysts at low pressure (1 bar) and medium pressure (20 bar) the initial surface specific activities (apparent TOF) for total hydrocarbons produced increased with decreasing particle size. For example, the apparent TOF of the CO conversion to hydrocarbons (340°C, 20 bar) of promoted catalysts increased from 0.06 s^{-1} to 0.11 $s^{-1}$when the iron carbide particle size decreased from 7 to 2 nm (Figure 7).

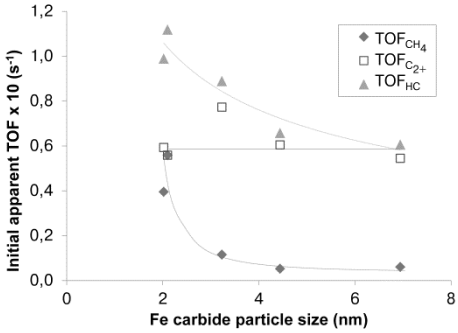

Figure 7. Apparent turnover frequencies (TOF) as a function of iron carbide size (TOS = 1h). TOF_{HC} and TOF_{C2+} correspond to the CO conversion to hydrocarbons and conversion to C_{2+} hydrocarbons, respectively. The reaction was performed at 340°C, 20 bar and a H_2/CO ratio of 1 (v/v) on promoted catalysts.

Although we realize that the TOF values of our catalysts cannot be calculated with the same accuracy as for metal catalysts (no direct way of measuring the number of active sites is available), the difference of apparent TOF values are quite large and trends are meaningful in our opinion. The apparent TOF data

discussed here correspond to initial activities. It is important to realize that the effect of particle size on specific surface activity is different when the surfaces are relatively clean (initial state) from those after the reaction has proceeded for longer times and the iron-containing particles have sintered or have been covered with amorphous or graphitic carbon (steady state). Values of apparent TOF at steady state for selected samples are shown in Appendix B, Table 4After 40 h of reaction the apparent TOF trend changed, increasing through a maximum (sample 5IMP) with decreasing the average carbide size. The apparent TOF based on initial activities are crucial to understand the fundamental surface processes and they can more easily be related to theoretical studies on clean surfaces. The values of TOF at steady state are useful to understand the processes occurring at the surface of a working catalyst and the corresponding deactivation mechanisms.

The trend observed with Fe is in stark contrast with previous results for Co as well as Ru. For these metals TOF dropped significantly below a certain critical particle size. For cobalt this has been assigned to combined effects of poisoning of low coordination sites at corners and edges by strongly bonded CO and a lower fraction of active step edge sites at terraces of particles smaller than 6 nm *(7)*. Clearly, iron carbide nanoparticles display vastly different size effects and it should be realized that the nature of chemical bonding in metal carbide is different from a metal. Here we put forward that corners and edges of iron carbide nanoparticles display high activity in particular to produce methane while terraces of the particles are not much affected by size. This proposal is based on the analysis of apparent TOF for different product fractions (Figure 7). The TOF for the production of C_{2+} hydrocarbons is independent of size whereas the TOF for methane formation increases sharply for particles smaller than 4 nm.

Based on DFT calculations Cheng *et al. (24)* have proposed a volcano-plot for M-C bond strength versus FT activity for Co and Fe. They have linked the higher activity of Fe carbide over Fe metal to weaker Fe-C bond strength of the carbide phase. From their plot it is suggested that further weakening of the Fe-C bond in iron carbide would further enhance activity. Our particle size effect suggests even weaker Fe-C bonds at corners and edges of iron carbide nanoparticles thereby enhancing overall TOF albeit mainly by enhanced methane formation.

The concept of the Fe-C bond strength also gives further insight into activity differences between Na plus S promoted and unpromoted catalysts. For

promoted catalysts the higher TOF is tentatively explained by sulfur that weakens Fe-C bonds thereby enhancing FT activity. Please note that addition of extra Na + S promoters did not affect selectivity but enhanced activity further (2IMP versus 2IMDP, Table 2).

Selectivity differences between catalysts should be considered with care in case of large conversion differences between catalysts (20 bar, Table 3) in view of possible different extents of secondary reactions. Since the experiments at 1 bar have all been carried out at low CO conversion levels (< 1%) we may use these data with more confidence. From the selectivity data obtained at 1 bar and summarized in Figure 4A it appears that for unpromoted catalysts methane selectivity as well as C_2-C_4 olefins selectivity are both high and independent of particle size. It is put forward that for unpromoted iron carbide low coordination sites at corners and edges and sites at terraces are similar in terms of selectivity but not in terms of activity since the former are more active and give rise to the particle size effect on apparent TOF discussed above. Figure 4B shows for promoted catalysts significant effects of iron carbide particle size on selectivity. For the smallest promoted particles of 2 nm the selectivities are very similar to those of unpromoted particles, whereas olefin selectivities increase and methane selectivity decrease for larger particles. Sulfur (possibly anchored by sodium) on the surface of larger iron carbide particles suppresses methane selectivity and enhances lower olefins selectivity to a large extent. The promoters are not effective with small particles, tentatively explained that only terraces of nanoparticles are affected and not corners and edges. Since corners and edges dominate activity for the smallest particles, selectivities of promoted and unpromoted particles converge (Figs. 4A and 4B).

The medium pressure results summarized in Figure 7 nicely display the overall effects of activity and selectivity. In view of the similar results obtained at 1 bar we can also quantitatively interpret the trends for these results. Large particles are effectively promoted by Na plus S thus displaying low methane selectivities that are below predictions from Anderson-Schulz-Flory distribution as discussed in reference 1 and confirmed in Appendix B, Figure B5. Sulfur might be effective in lowering hydrogen coverage on iron carbide thereby suppressing chain termination by hydrogenation and thus methane formation. From figure 7 it appears that for short time on stream TOF for methane increased for promoted catalysts much more strongly (~ factor of 10) than the overall TOF (~ factor of 2). Also note from Table 2 (1 bar) and Table 3

(20 bar) that TOF enhancements with decreasing particle sizes are much larger for unpromoted catalysts than for promoted catalysts. We propose that sulfur/sodium enhance activity and selectivity of terraces independent of size. Methane production on low coordination sites may be further enhanced by the promoters without boosting olefin selectivity for the smallest particle sizes.
In summary we report very significant particle size (2 – 17 nm) effects for supported iron carbide catalysts used for the direct production of lower olefins from synthesis gas. Smaller iron carbide particles display higher surface specific activities mainly due to higher methane production. It appears that the particle size effects of Fe under the studied reaction conditions deviate from those reported earlier for Co *(6-10)* and Ru *(11-14)* and Fe *(12,17,18)* under low temperature Fischer-Tropsch conditions. Future studies are advocated involving surface coverages *(7)*, carbon lay-down *(33)*, and chemical bonding *(21,24-26)* as a function of iron carbide particle size.

Supporting information

Average carbide sizes and particle size distributions, catalytic data at 250°C, activity as a function of time, Anderson-Schulz-Flory plots, and *in situ* Mössbauer parameters are provided in Appendix B.

Acknowledgements

G. Bonte, Dr. A. Chojecki, Dr. A. C. J. Koeken, Dr. T. Davidian, and Dr. M. Ruitenbeek are thanked for the catalytic tests at 20 bar performed at Dow Benelux B.V. in Terneuzen. Dr. A. I. Dugulan is thanked for the Mössbauer spectroscopy measurements performed at the Fundamentals Aspects of Materials and Energy Group at the Technical University of Delft. Prof. Dr. Ir. E. J. M. Hensen (Technical University of Eindhoven) is thanked for his contribution in the discussion of the Mössbauer spectroscopy results. C. van der Spek and J. D. Meeldijk are thanked for the TEM images.

References

1. H. M. Torres Galvis *et al.*, *Science* **335**, 835-838 (2012).
2. H. J. Schulte, B. Graf, W. Xia, M. Muhler, *ChemCatChem* **4**, 350-355 (2012).
3. E. Schwab, A. Weck, J. Steiner, K. Bay, *Oil Gas Eur. Mag.* **1**, 44-47 (2010).
4. M. Boudart, A. McDonald, *J. Phys. Chem.* **88**, 2185-2195 (1984).
5. R. A. van Santen, *Acc. Chem. Res.* **42**, 57-66 (2009).
6. G. L. Bezemer *et al.*, *J. Am. Chem. Soc.* **128**, 3956-3964 (2006).
7. J. P. den Breejen *et al.*, *J. Am. Chem. Soc.* **131**, 7197-7203 (2009).

8. G. Prieto, A. Martínez, P. Concepción, R. Moreno-Tost, *J. Catal.* **266**, 129-144 (2009).
9. Ø. Borg *et al.*, *J. Catal.* **259**, 161-164 (2008).
10. W. Ma *et al.*, *Fuel* **90**, 756-765 (2011).
11. E. Iglesia, S. L. Soled, R. A. Fiato, *J. Catal.* **137**, 212-224 (1992).
12. D. Barkhuizen *et al.*, *Pure Appl. Chem.* **78**, 1759-1769 (2006).
13. J. Kang, S. Zhang, Q. Zhang, Y. Wang, *Angew. Chem. Int. Ed.* **48**, 2565-2568 (2009).
14. C. S. Kellner, A. T. Bell, *J. Catal.* **75**, 251-261 (1982).
15. J. Y. Park *et al.*, *J. Mol. Catal. A* **323**, 84-90 (2010).
16. A. F. H. Wielers, A. J. H. M. Kock, C. E. C. A. Hop, J. W. Geus, van der Kraan, A. M., *J. Catal.* **117**, 1-18 (1989).
17. H. J. Jung, P. L. Walker Jr., M. A. Vannice, *J. Catal.* **75**, 416-422 (1982).
18. V. K. Jones, L. R. Neubauer, C. H. Bartholomew, *J. Phys. Chem.* **90**, 4832-4839 (1986).
19. M. Rameswaran, C. H. Bartholomew, *J. Catal.* **117**, 218-236 (1989).
20. S. Li, W. Ding, G. D. Meitzner, E. Iglesia, *J. Phys. Chem. B* **106**, 85-91 (2002).
21. M. D. Shroff *et al.*, *J. Catal.* **156**, 185-207 (1995).
22. E. de Smit *et al.*, *J. Am. Chem. Soc.* **132**, 14928-14941 (2010).
23. E. de Smit *et al.*, *Nature* **456**, 222-225 (2008).
24. J. Cheng *et al.*, *J. Phys. Chem.* **114**, 1085-1093 (2010).
25. J. M. Gracia, F. F. Prinsloo, J. W. Niemantsverdriet, *Catal. Lett.* **133**, 257-261 (2009).
26. D. B. Cao, F. Q. Zhang, Y. W. Li, H. Jiao, *J. Phys. Chem. B* **108**, 9094-9104 (2004).
27. van der Lee, M. K., A. J. van Dillen, J. W. Geus, K. P. de Jong, J. H. Bitter, *Carbon* **44**, 629-637 (2006).
28. L. M. Bronstein *et al.*, *Chem. Mater.* **19**, 3624-3632 (2007).
29. T. C. Bromfield, N. J. Coville, *Appl. Catal. A* **186**, 297-307 (1999).
30. R. Crous, T. C. Bromfield, S. Booyens, International Patent Aplication No. WO2010066386 (2010).
31. M. Luo, H. Hamdeh, B. H. Davis, *Catal. Today* **140**, 127-134 (2009).
32. A. P. B. Sommen, F. Stoop, K. van der Wiele, *Appl. Catal.* **14**, 277-288 (1985).
33. A. C. J. Koeken, H. M. Torres Galvis, T. Davidian, M. Ruitenbeek, K. P. de Jong, *Angew. Chem. Int. Ed.* **51**, 7190-7193 (2012).
34. S. L. Soled, E. Iglesia, R. A. Fiato, *Catal. Lett.* **7**, 271-280 (1990).

Chapter 5

Effects of sodium and sulfur on catalytic performance of supported iron catalysts for the Fischer-Tropsch synthesis of lower olefins

Abstract

The Fischer-Tropsch synthesis of lower olefins (FTO) is an alternative process for the production of major chemical building blocks from natural gas, coal or biomass-derived synthesis gas. The addition of low concentrations of sulfur plus sodium to Fe/α-Al_2O_3 resulted in catalysts with high C_2-C_4 olefins selectivity ($\sim$ 50 %C), enhanced catalytic activity and decreased methane production ($<$ 20 %C) when the reaction was carried out at 340°C, 20 bar and H_2/CO = 1. Sodium reduced methane selectivity by increasing the chain growth probability while sulfur probably reduced the hydrogen coverage of the catalyst resulting in even lower methane selectivities and higher olefin content of the products. The addition of extra sodium resulted in a detrimental effect on catalytic activity while favoring the formation of carbon deposits. Our results show that the nature and concentration of the promoters play a key role in the design of FTO catalysts with optimum catalytic performance.

Adapted with permission from H. M. Torres Galvis, A. C. J. Koeken, J. H. Bitter, T. Davidian, M. Ruitenbeek, A. I. Dugulan, K. P. de Jong, *Effects of sodium and sulfur on catalytic performance of supported iron catalysts for the Fischer-Tropsch synthesis of lower olefins,* J. Catal. **303,** 22-30 (2013).

Introduction

Lower olefins (C_2 to C_4), which are key building blocks of the chemical industry, are traditionally produced from naphtha cracking or fluid catalytic cracking (FCC). High prices of oil and the interest of many countries on reducing their dependence on imported oil have urged research efforts to the development of new processes to produce oil-derived chemicals from alternative sources such as natural gas, coal or biomass. The interest on these processes is not new and was already an important matter of study after the first oil crisis in the 1970's. During that period many researchers investigated the use of Fe-based catalysts for the direct production of lower olefins from synthesis gas (syngas).

For this reaction, Iron is the metal of choice not only for its low price and high availability but also for its catalytic properties since the Fischer-Tropsch-to-Olefins reaction (FTO) is carried out at high temperatures *(1)*. Compared to cobalt, iron has a low methanation activity even when the reaction is performed at temperatures higher than 300°C, which is necessary to drive product selectivity towards shorter hydrocarbon chains. Additional advantages of iron over cobalt based catalysts include a higher resistance to contaminants present in syngas, a higher selectivity to olefins and a higher water gas shift (WGS) activity allowing for the use of CO-rich syngas. Therefore iron catalysts are especially suitable for the conversion of syngas derived from coal or biomass which contains more contaminants and is rich in CO. Additionally, the products obtained with iron catalysts have a higher olefinic content compared to Co.

Many different elements have been investigated as possible promoters to improve the C_2 - C_4 olefins selectivity such as potassium *(2,3)*, sodium *(4,5)*, manganese *(6)*, titanium *(7)*, zinc *(8)* and vanadium *(9)*. Sodium has been proposed as an effective promoter to decrease methane selectivity *(5,10,11)*, to favor chain growth propagation *(5)* and to increase the olefin-to-paraffin ratio of the products *(4,11)*. It has been reported that sodium, as well as potassium, increase iron carbidization *(4,5)* and WGS activity *(12)*. Ribeiro *et al. (4)* have suggested that the addition of alkali promoters decreases the C-O bond strength resulting in an increase of the coverage of dissociatively adsorbed CO, which could explain the higher levels of carbidization. Additionally, the high CO coverage could inhibit olefin re-adsorption thus decreasing the olefin hydrogenation rates. The high coverage of the surface C

species also might increase the chain growth probability and the conversion rates *(10)*.

Studies have shown that these beneficial effects are only obtained at low concentrations of sodium. After achieving an optimum loading, further addition of the promoter has a detrimental effect inhibiting reduction and carbidization, decreasing the CO conversion and shifting the product selectivity to shorter hydrocarbons *(4,13)*. Similar effects have been reported for potassium *(14)*. Ngantsoue-Hoc *et al. (12)* have shown that not only the promoter loading defines its effectiveness but also the reaction conditions and CO conversion levels.

Studies on sulfur as a promoter are limited as this element has been considered as a poison for Fischer-Tropsch catalysts. However, Bromfield and other researchers have shown that for iron low concentrations of sulfur may act as a promoter that improves activity, decreases methane selectivity *(15-17)*, increases the chain growth probability, and enhances olefin selectivity, reduction and carbidization *(18,19)*. These positive effects of the addition of low amounts of sulfur have been observed by co-feeding low amounts of H_2S during the reaction and by direct addition of sulfur during catalyst preparation. The promoter effect for sulfur is also highly dependent on promoter concentration, catalyst pretreatment and reaction conditions *(20)*.

Research on the development of selective catalysts for the production of lower olefins has been mainly focused on bulk or unsupported catalysts with low cost and simple synthesis. These precipitated or fused catalysts can be modified by addition of promoters to increase the selectivity to lower olefins and to decrease methane production. Although catalysts with high selectivity to C_2-C_4 olefins and to short-chain hydrocarbons ($\alpha \sim 0.4$-0.6) have been reported *(21)*, their industrial use has not materialized because of their low mechanical stability *(22,23)* under high temperatures and low H_2/CO ratios.

Recently, Schulte *et al*. *(24)* have reported high selectivities to lower olefins in combination with high activity and low methane production when using iron supported on nitrogen and oxygen functionalized-carbon nanotubes (N-CNT, O-CNT) under the Fischer-Tropsch reaction at 340°C, 25 bar and a H_2/CO ratio of 1.8. Their results underline the importance of the weakly interactive nature of the support to achieve a high catalytic activity.

Most recently a breakthrough in the selective production of lower olefins from synthesis has been reported *(23,25)*. Sodium and sulfur promoted iron catalysts prepared using support materials with weak interaction towards iron

have displayed high activities and light olefins selectivities with a low methane production and an excellent mechanical and chemical stability *(23,25)*. However, still limited information is available about the effect of sodium, sulfur or a combination of both promoters on supported catalysts studied under the stringent reaction conditions used for the production of lower olefins from CO-rich synthesis gas. Most of the above mentioned promoter studies have been performed on precipitated or fused catalysts at temperatures lower than 300°C.

Here we discuss the effects of sodium and sulfur on iron catalysts supported on α- alumina *(23,26)* when the Fischer-Tropsch reaction is carried out at high temperatures (340 - 350°C). The catalysts have been prepared using an inert support to improve mechanical stability and to allow a better interaction between the promoters and the iron phase.

Experimental

Catalyst preparation and characterization

Preparation of an unpromoted supported catalyst. A supported catalyst with a nominal loading of 5 wt% Fe was prepared using the incipient wetness impregnation technique. Catalyst AFe was prepared with a solution of 1.726 g of ammonium iron citrate, $C_6H_8O_7.xFe^{3+}.yNH_3$ (Fluka, *purum* p.a. 14.5 - 16 wt% Fe (Appendix C, Table 1)), in 3.4 ml of demineralized water. For the preparation, 5 g of α-Al_2O_3 (10 m^2 g^{-1}; Pore volume 0.4 ml g^{-1}, AL4196E, BASF) were impregnated with the above mentioned solution until the support pores were filled. The impregnation steps were successively repeated until all the solution was incorporated to the support. After each impregnation step, the material was dried at 120°C under static air for 1 h. Finally, the catalyst precursors were dried overnight at 120°C under static air and calcined at 500°C (Heating ramp: 10 K min^{-1}) for 2 h under air flow.

Preparation of promoted supported catalysts. Catalysts AFe/Na and AFe/S were prepared with a solution of 1.726 g of ammonium iron citrate (Fluka) in 3.4 ml of demineralized water. The promoters were incorporated in the precursor solution adding 0.047 g of sodium citrate dihydrate, $HOC(COONa)(CH_2COONa)_2.2H_2O$ (Sigma-Aldrich, ACS reagent ≥ 99%) in the case of sodium promoted sample and 0.011 g of ferrous sulfate heptahydrate, $FeSO_4.7H_2O$ (Merck, for analysis) for the synthesis of sulfur promoted catalyst. It is important to note that sulfur has been added to the catalyst in the form of

a sulfate. It has been reported that the presence of sulfur as a sulfate or as a sulfide has a different effect on catalytic performance *(15)*.
AFe/S/Na and AFe/S/2Na were prepared using an aqueous solution of 1.726 g of ammonium iron citrate (J. T. Baker, 14.5-16 wt%, Na, S: ~750 mg/kg (Appendix C, Table 1)). For the preparation of sample AFe/S/2Na, 0.047 g of sodium citrate dihydrate (Sigma-Aldrich) was added to the precursor solution. The impregnation, drying and calcination steps were performed as described for the unpromoted supported catalysts.

Preparation of unsupported catalysts. A bulk unpromoted catalyst (BFe) was prepared by calcination of 2 g of FeO(OH) (Sigma-Aldrich, catalyst grade, 30-50 mesh) at 500°C (Heating ramp: 10 K min^{-1}) for 2 h under air flow. The bulk promoted catalyst (BFe/S/Na) was prepared by incipient wetness impregnation of 2 g of FeO(OH) with an aqueous solution of 0.243 g of sodium citrate dehydrate (Sigma-Aldrich) and 0.056 g of $FeSO_4.7H_2O$ (Merck) in 0.7 ml of demineralized water. After impregnation the catalyst precursor was dried at 120°C for 2 h under static air. The catalyst was finally calcined using the same procedure as described for the unpromoted bulk sample.

Fresh and spent catalysts characterization. Iron, sulfur and sodium contents were analyzed with ICP-OES (Inductively coupled plasma – optical emission spectroscopy) using a Spectro Ciros CCD spectrometer. The average iron oxide crystallite size for the unpromoted supported catalysts was determined by line broadening analysis of XRD (X-ray diffraction) patterns obtained with a Bruker AXS D8 ADVANCE diffractometer equipped with a $Co\kappa_{\alpha 1}$ source (λ = 0.1789 nm) using an angle range from 20° to 90° in 2θ.
Fresh and spent catalysts were analyzed with TEM (Transmission Electron Microscopy) to determine the size distribution of iron-containing particles. The images were obtained using a Philips Tecnai-20 FEG (200 kV) microscope equipped with an EDX and HAADF detector.
The extent of carbon deposition on the spent samples was determined with thermal gravimetric analysis (TGA) during carbon burn-off experiments performed in a Perkin Elmer Pyris 1 TGA under oxygen flow (10 ml min^{-1}). For these experiments, temperature was increased from 30°C to 600°C (Heating ramp: 5 K min^{-1}) and the sample remained under the final temperature for one hour. During the experiments a mass increase originated by re-oxidation was observed and was accounted for in the estimation of carbon lay-down.

Using a tapered element oscillating microbalance *(26,27)* (TEOM Series 1500 Pulse Mass Analyzer, Rupprecht & Patashnick Co., Inc.) carbon formation was measured under plug-flow conditions at 350°C, 20 bar and a H_2/CO = 1. Fresh catalysts after calcination, after reduction, and spent catalysts were analyzed with ^{57}Fe Mössbauer spectroscopy in transmission mode. Spectra were collected *in situ* at room temperature using a ^{27}Co (Rh) source. The calibration for the velocity was performed using an α-Fe foil. The measurement parameters were determined by fitting the spectra using subspectra with Lorentzian-shaped lines with the Mosswin 3.0i program.

Catalytic tests

Low pressure testing. The Fischer-Tropsch synthesis was performed at 1 bar and 350°C in a fixed bed reactor using 0.02 ± 0.005 g of catalyst (particle size 0.2 – 0.4 mm) and 0.2 g of SiC (0.2 mm) for bed dilution. The catalyst was reduced prior to reaction at 350°C with a mixture of H_2 and He (33% H_2 v/v, 60 ml min^{-1} total flow) for 2 h. After reduction, the feed flow was switched to a mixture of H_2 and CO (H_2/CO = 1 v/v, GHSV = 10500 h^{-1}). The reaction was carried out for 20 h. The CO conversion levels were lower than 1% to ensure differential operation thus limiting the extent of secondary reactions. Under these conditions the products remained in the gas phase and were analyzed with online gas chromatography (C_1 – C_{16}). CO_2 was not measured. Product selectivity was calculated as equivalent of carbon atoms in a product with respect to the total carbon atoms present in the hydrocarbons produced (%C). The activities and selectivities reported here were determined after 15 h of reaction.

Medium pressure testing. The Fischer-Tropsch reaction was carried out at 20 bar, 340°C and a H_2/CO ratio of 1 (v/v) in a high throughput testing unit fitted with fixed bed reactors and using a gas hourly space velocity of 3000 h^{-1}. 100 µl of catalyst (0.2 – 0.4 mm) were diluted with SiC (0.2 – 0.4 mm) to complete a volume of 200 µl. Prior to reaction the catalysts were reduced in a H_2/N_2 (90/10 volume basis) flow at 350°C for 2 h. Product selectivity was determined up to C_9 using online gas chromatography. The selectivity was calculated as equivalent carbon atoms in a product with respect to the total amount of carbon present in the hydrocarbon product (%C). Activities and selectivities were determined at CO conversion levels between 60 to 66%.

Results and discussion

The iron, sulfur and sodium loadings of the promoted and unpromoted catalysts are presented in Table 1. The first letter of the sample code corresponds to the type of catalyst: A was assigned to α-alumina supported samples and B to bulk (or unsupported) catalysts.

The Fe, S, and Na loadings determined with ICP were similar to the nominal loadings. For the S-promoted samples an S/Fe atomic ratio of 0.009 was expected while Na-promoted catalysts were prepared with a nominal composition of 0.22 Na/Fe (atomic ratio) with the exception of sample AFe/S/2Na for which a 0.45 Na/Fe ratio was intended.

Table 1. Composition of supported and bulk iron catalysts.

Sample	Iron precursor	Fe loading (wt%)[a]	Na loading (wt%)[a]	S loading (wt%)[b]
AFe	Ammonium Fe citrate	5.0	-	-
AFe/Na	Ammonium Fe citrate	4.9	0.22[b]	-
AFe/S	Ammonium Fe citrate	4.9	-	0.03
AFe/S/Na	Ammonium Fe citrate	5.0	0.19	0.03
AFe/S/2Na	Ammonium Fe citrate	5.0	0.39	0.03
BFe	FeO(OH)	71.8	-	-
BFe/S/Na	FeO(OH)	67.2	0.36	0.4[a]

[a] Measured with ICP

[b] Nominal loading

For the supported samples, the average Fe_2O_3 size calculated from the XRD line broadening using the Scherrer equation was approximately 15 nm. TEM analysis of the samples (Figure 1) showed that iron containing nanoparticles were well-distributed on the support material. The average Fe_2O_3 particle size of Na plus S promoted and unpromoted Fe/α-Al_2O_3 samples was 14 ± 5 nm and 15 ± 5 nm, respectively. BFe consisted of iron oxide crystallites with an average size of 16 ± 5 nm that had aggregated to larger clustered particles. BFe/S/Na showed similar morphology and average Fe_2O_3 particle size (15 ± 7 nm) although it contained a higher amount of small particles compared to the unpromoted sample.

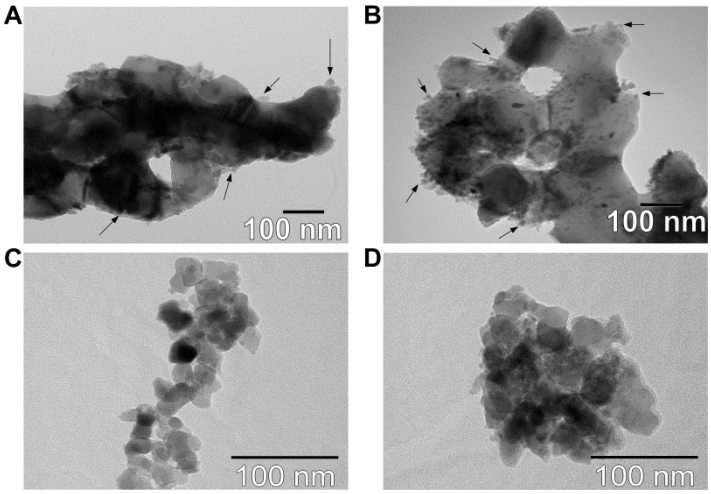

Figure 1. TEM images of fresh supported and bulk iron catalysts. The TEM analysis of fresh supported catalysts prepared by incipient wetness impregnation indicated similar average Fe_2O_3 particle sizes. (**A**) AFe; (**B**) AFe/S/Na; (**C**) BFe; (**D**) BFe/S/Na. The supported samples (5 wt% Fe) exhibited comparable average Fe_2O_3 crystallite sizes from XRD analysis. Fe_2O_3 particles are indicated by arrows.

Mössbauer spectroscopy analysis of the fresh catalysts (Appendix C, Table 2) provided information about the amount of small Fe_2O_3 nanoparticles present in the samples. Fe_2O_3 particles with a diameter smaller than 13.5 are superparamagnetic (SPM) *(28,29)*. The content of SPM Fe_2O_3 thus indicates the percentage of small iron oxide nanoparticles.

The results from Appendix B, Table 2 indicate that sample AFe showed a content of SPM Fe_2O_3 of 34%. The addition of sodium (sample AFe/Na) slightly increased the amount of SPM Fe_2O_3 from 34% to 40% whereas AFe/S displayed a lower content of SPM particles (21%). These results are in line with the observations of Bromfield *et al. (15)* for bulk S-promoted catalysts and Ribeiro *et al. (4)* for unsupported alkali-promoted samples. A/Fe/S/Na exhibited a low content of SPM Fe_2O_3 (17%) while the addition of extra sodium (Sample AFe/S/2Na) resulted in a large increase in the content of small Fe_2O_3 particles (54%).

In the case of bulk catalysts, BFe/S/Na showed a higher amount of small Fe_2O_3 particles (73%) compared with the unpromoted catalyst (15%). This result is in line with the observations from TEM analysis (Figure 1C and 1D).

The catalysts were also analyzed with Mössbauer spectroscopy after 2 h of reduction at 350°C under H_2/Ar flow to evaluate the influence of the

promoters on the extent of reduction. The unreduced samples contained only Fe^{3+} as shown in Appendix C, Table 2. The results of the analysis after reduction are summarized in Appendix C, Table 3. The supported samples promoted with Na, S, and Na/S showed a higher degree of reduction compared with the unpromoted catalyst. AFe/S was reduced to Fe^0 (66%) and Fe^{2+} (34%). The rest of the supported samples exhibited Fe^0 and Fe^{2+} along with unreduced Fe^{3+}. The addition of extra sodium to the Na/S promoted sample (AFe/S/2Na) resulted in a slightly higher content of Fe^{3+} similarly to the results observed by An *et al. (13)* for samples with a high sodium content. In the case of bulk catalysts, the Na/S promoted sample exhibited a lower concentration of Fe^0 compared with BFe. Both bulk catalysts showed a very high content of Fe^0 (> 70%) while most of the supported samples displayed lower concentrations of metallic iron (< 25%).

The catalysts were tested in the Fischer-Tropsch reaction at 350°C, 1 bar and a H_2/CO ratio of 1 (v/v) to determine the influence of sodium and/or sulfur on catalytic activity and product selectivity. The results of these low pressure measurements are summarized in Figure 2 and Table 2. The CO conversion levels were maintained below 1% to ensure differential operation in the reactor therefore limiting the extent of secondary reactions.

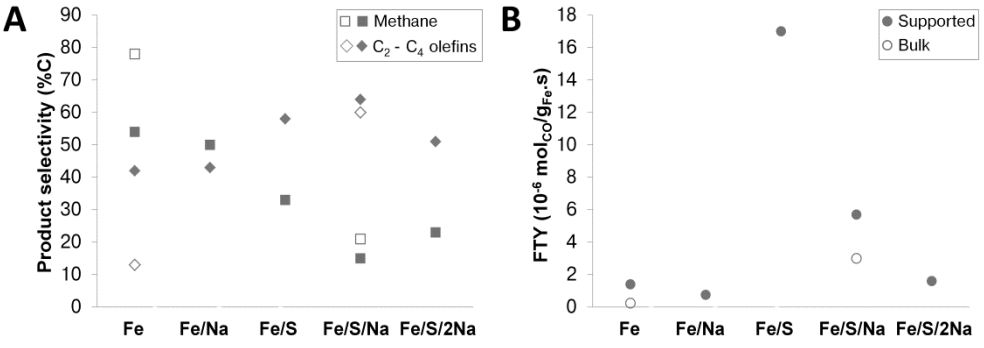

Figure 2. Catalytic performance of iron catalysts at 1 bar, 350°C and H_2/CO ratio of 1. Filled symbols correspond to supported catalysts, open symbols to bulk catalysts. (**A**) Methane (■,□) and C_2-C_4 olefins selectivity (◆,◇); (**B**) Iron time yield (●,○).

Sample AFe showed high C_2-C_4 olefins (~40 %C) and CH_4 (~55 %C) selectivities while promoted catalysts showed enhanced light olefins selectivity and lower methane production (Figure 2A). The addition of Na to the unpromoted sample led to a minor effect on product selectivity whereas

activity decreased by almost 50% (Figure 2B, sample AFe/Na). The negative effect of Na on activity was attributed to a higher extent of carbon deposition and will be discussed later.

Table 2. Catalytic activity and product selectivity of Fe catalysts under FTO conditions (1 bar, 350°C, H_2/CO = 1, TOS = 15 h).

Sample	FTY (10^{-5} $mol_{CO}/g_{Fe}.s$)	Product selectivity (%C)			
		CH_4	C_2-C_4 olefins	C_2-C_4 paraffins	C_{5+}
AFe	0.14	54	42	3	2
AFe/Na	0.08	50	43	4	3
AFe/S	1.70	33	58	3	5
AFe/S/Na	0.57	15	64	2	19
AFe/S/2Na	0.16	23	51	3	22
BFe	0.02	78	13	2	7
BFe/S/Na	0.30	21	60	3	16

On the contrary, the catalyst promoted with S showed a 12-fold increase in catalytic activity accompanied by a significant improvement on C_2-C_4 olefins selectivity while decreasing CH_4 production from 54 %C to 33 %C. Presumably, sulfur blocks the active sites for hydrogenation thus decreasing methane selectivity and increasing selectivity towards olefins. The C_{5+} selectivity was unaffected by the addition of sulfur which evidenced that the addition of this promoter did not increase the chain growth probability (α) (Appendix C, Figure 1). The high activity observed for the sulfur promoted sample might be explained by a decrease in the Fe - CO binding strength.Weaker CO binding strengths were observed for sulfur-containing cobalt catalysts during DRIFTS studies performed by Curtis *et al. (30)* which might be similar for iron catalysts. A decrease in binding strength between iron and carbon may result in an improvement of catalytic activity as shown by Cheng *et al. (31)* for a comparison between the CO hydrogenation activity of metallic iron and iron carbide. A schematic representation of the relationship between M-C bond strength and catalytic activity is shown in Appendix C, Figure 2.

The addition of Na plus S resulted in a major improvement of product selectivity for the supported catalysts, increasing the C_2-C_4 olefins content above 60 %C and decreasing CH_4 selectivity below 20 %C. A significant effect of Na and S on selectivity was also observed for bulk catalysts, as

lower olefins selectivity incremented from approximately 15 %C to 60 %C while methane production reduced from 80 %C to 20 %C. The Na plus S promoted samples showed a significant increase in chain growth probability from 0.30 to 0.50 for supported catalysts (Appendix C, Figure 1B) and from 0.30 to 0.40 for bulk materials (Appendix C, Figure 1A). From the Anderson-Schulz-Flory (ASF) plots it was observed that methane selectivity was below the predicted value for samples promoted with S and Na plus S, which we tentatively attributed to the possible blocking effect of S on hydrogenation sites. In contrast, extra addition of Na to AFe/S/Na resulted in lower C_2-C_4 selectivity and increased methane content.

The addition of Na and S not only improved product selectivity but it also enhanced catalytic activity (Figure 2B). Na and S promoted catalysts exhibited higher activities in comparison with unpromoted samples. Iron time yield was 4 and 12 times for higher for double promoted supported and bulk catalysts respectively.

Further addition of Na had a negative effect on product selectivity, as previously mentioned, but also on catalytic activity. AFe/S/2Na showed a lower iron time yield (1.6×10^{-6} mol_{CO} g_{Fe}^{-1} s^{-1}) in comparison with AFe/S/Na (5.7×10^{-6} mol_{CO} g_{Fe}^{-1} s^{-1}). These results indicated that an optimum amount of promoters might exist to obtain an adequate catalytic performance for the FTO reaction. This behavior was previously observed on studies performed for unsupported iron catalysts *(13,15)*.

The catalytic activity was plotted as a function of time on stream in Figure 3.

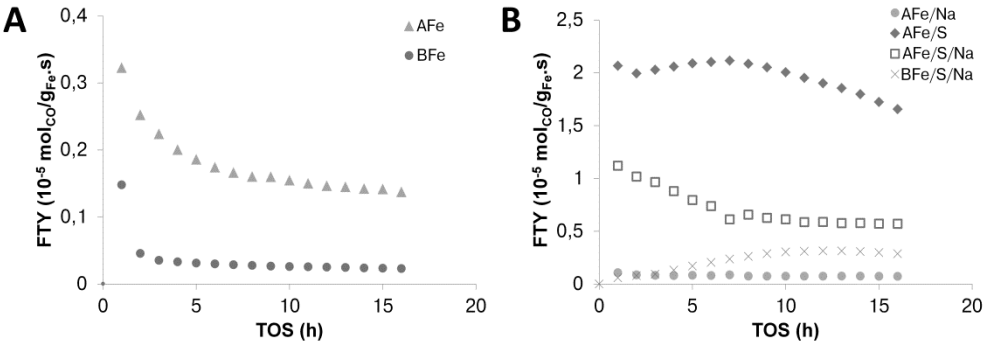

Figure 3. Catalytic activity as a function of time on stream. The reaction was performed at 1 bar, 350°C and a H_2/CO ratio of 1. (**A**) Unpromoted catalysts, (**B**) Promoted catalysts.

For all the samples, a decrease in activity was observed. Most probably deactivation was caused by coke lay-down. It is known that for this type of catalysts formation of carbon deposits is favored at high temperatures, low pressures and low H_2/CO ratios *(26)*.

At high reaction temperature it might be expected that sulfur associated to iron would be stripped from the catalysts, changing the catalytic performance of S-promoted catalysts as a function of time. However, plots of product selectivity as a function of time (Appendix C, Figure 3) showed that CH_4 and lower olefins selectivities remained relatively constant for the samples modified by addition of sulfur thus indicating that this promoter was not removed from the iron phase throughout the duration of the experiment.

The catalysts were also tested at 340°C and 20 bar to investigate their performance under industrially more relevant reaction conditions. The α-Al_2O_3 supported catalysts showed a stable catalytic activity for at least 20 h. The high stability of Na and S promoted catalyst during longer reaction times has been reported elsewhere *(23)*. Product selectivity of sulfur-promoted samples did not vary with time on stream suggesting that under the conditions tested sulfur remains in close contact with the iron phase. Activity and C_2-C_4 olefins selectivity as a function of time on stream are plotted in Appendix C, Figure 4 and the results of the catalytic tests are summarized in Table 3 and Figure 4.

Table 3. Catalytic performance of promoted and unpromoted supported and bulk Fe catalysts (20 bar, 340°C and H_2/CO = 1) [a]

Sample	FTY (10^{-5} molco/g_{Fe}.s)	Product selectivity (%C)				
		CH_4	C_2-C_4 olefins	C_2-C_4 paraffins	C_5+	Oxy.
AFe	6.7	27	35	24	14	0
AFe/Na	3.2	20	30	18	30	3
AFe/S	6.2	16	41	25	16	2
AFe/S/Na	12.3	19	51	19	11	1
AFe/S/2Na	2.5	27	38	12	3	19
BFe	0.5	32	40	9	15	4
BFe/S/Na	0.4	16	49	7	21	7

[a] Data reported at CO conversion between 60-66%; CO_2 :45 – 50% of CO converted.

AFe displayed a high activity for the FTO reaction but lower olefins selectivity was only 35 %C and methane selectivity was almost 30 %C (Table 3). Figure 5 displays the ASF plots for catalysts tested at 20 bar. AFe showed a product

selectivity which could be modeled with an α value of 0.63. The Na-promoted sample indeed showed lower CH_4 selectivity compared to the unpromoted sample as well as a higher selectivity towards longer hydrocarbons (30 %C to C_{5+}). The calculated α value for AFe/Na was 0.76 (Figure 5B). Research performed on alkali-promoted catalysts has shown that sodium, as well as potassium, increase chain growth probability *(10)*. Although the addition of Na reduced methane selectivity it did not increase the selectivity towards lower olefins and the catalytic activity decreased significantly.

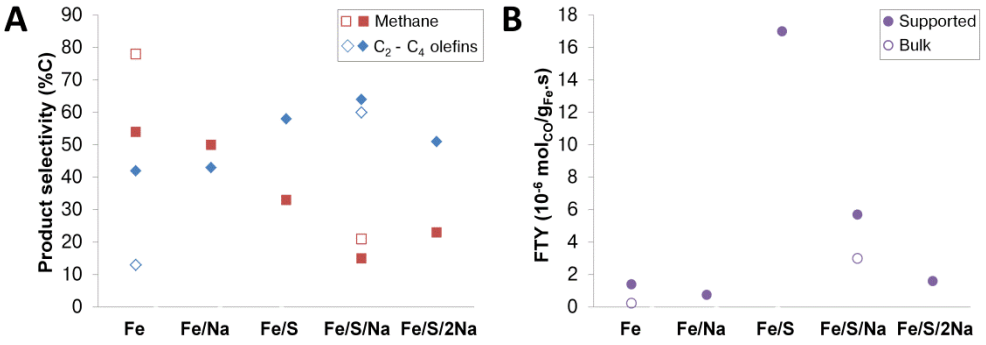

Figure 4. Catalytic performance of iron catalysts at 20 bar, 340°C and H_2/CO ratio of 1. Filled symbols correspond to supported catalysts, open symbols to bulk catalysts. (**A**) Methane (■,□) and C_2-C_4 olefins selectivity (◆,◇); (**B**) Iron time yield (●,○).

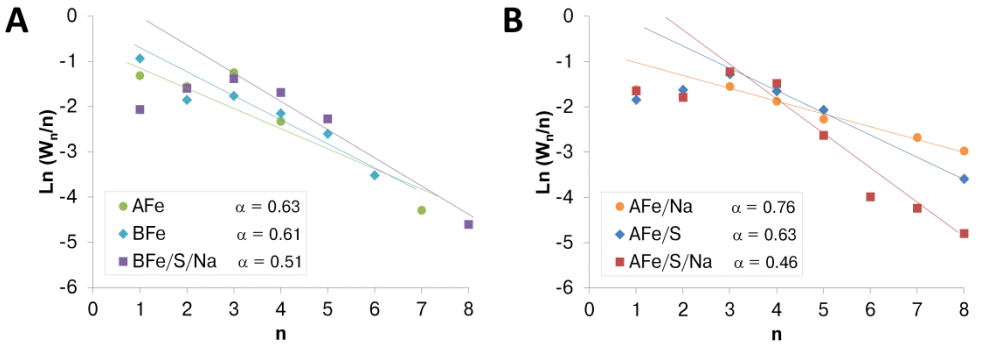

Figure 5. Anderson-Schulz-Flory plots. Iron based catalysts were tested in the Fischer-Tropsch reaction at 340°C, 20 bar and a H_2/CO = 1. Product selectivity was measured after 17 h time on stream.

The addition of S did not modify the chain growth probability (α = 0.63) compared to AFe but CH_4 selectivity was decreased from 27 %C to 16 %C.

Lower olefins selectivity was improved (41 %C) while catalytic activity was only slightly decreased (Figure 4). This result might indicate that sulfur selectively blocks sites that lead to chain termination via hydrogenation *(23)*. The combination of Na and S had a major impact on catalytic performance increasing activity approximately two times while increasing C_2-C_4 olefins selectivity above 50 %C. The calculated α for AFe/S/Na was 0.46. From the ASF model, a high C_2-C_4 selectivity is expected with such a low alpha value, but methane selectivity is predicted to be approximately 30 %C. Our results showed that for AFe/S and AFe/S/Na methane selectivity was far lower than the expected value from the ASF prediction (Fig. 5B). In the case of AFe/Na, methane selectivity was also below the modeled value but the largest deviations were observed on the samples promoted with sulfur.

The addition of extra Na to the Na/S-promoted sample exhibited high C_2-C_4 olefins (38 %C) and methane selectivity (27 %C) similar to the behavior observed for the unpromoted catalyst AFe. However, AFe/S/2Na showed a higher olefin to paraffin ratio and the highest oxygenates selectivity of all the catalysts tested (19 %C). Higher sodium content in catalyst AFe/S/2Na resulted in a catalytic activity almost 3 times lower than for AFe (Table 3).

Promoted and unpromoted bulk catalysts displayed an activity per gram of iron one order of magnitude lower than for supported samples. The product selectivity of the promoted bulk sample was largely improved by the addition of Na and S, increasing light olefins selectivity to about 50 %C in combination with a low methane production. Although highly selective bulk catalyst could be obtained, it is anticipated that these catalysts would show a high extent of carbon deposition. It has been demonstrated that bulk iron catalysts tested under stringent conditions (high temperature and low H_2/CO ratio) suffer from deactivation by coke lay-down and fragmentation due to the formation of carbon filaments *(23)*.

The spent samples after reaction at 340°C and 20 bar were analyzed with TEM to determine the level of sintering of iron containing particles and to assess the extent of formation of carbon deposits. TEM images of selected spent samples are shown in Figure 6.

Analysis of the TEM images of spent catalysts indicated that supported samples AFe and AFe/S/Na suffered from particle growth. The particle size distribution broadened as a result of an increase in the fraction of larger iron containing particles. Figures 6A and 6B show images of AFe (initial size: 15 $\pm$ 5 nm) and AFe/S/Na (initial size: 14 $\pm$ 5 nm) after reaction (Final size: AFe 16

± 10 nm; AFe/S/Na 16 ± 12 nm). In the case of bulk catalysts, most of the iron-containing particles were covered with a layer of carbon and even growth of carbon fibrils was observed (pointed by arrows in Fig. 6C and 6D). The unsupported Fe_2O_3 particles of sample BFe/S/Na showed more sintering as expected for a bulk catalyst with small Fe_2O_3 average particle size before reaction (15 ± 7 nm). The average particle size of the spent sample was 49 ± 35 nm. During reaction, some of the large iron-containing particles fragmented due to differences in Fe phase density and to the formation of carbon fibrils. The attrition of bulk catalysts at the micro and nanoscale under high temperatures and a CO-rich environment has been previously reported *(22,23)*.

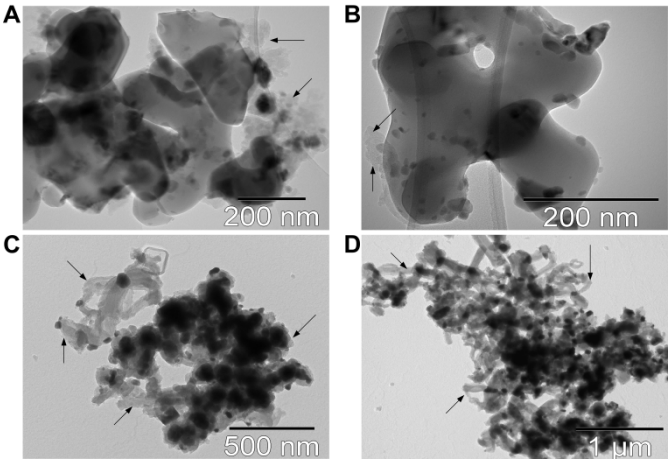

Figure 6. TEM images of spent catalyst. The catalyst were analyzed after reaction at 340°C and 20 bar (H_2/CO ratio = 1 v/v). Carbon deposits are indicated by arrows: (**A**) AFe, (**B**) AFe/S/Na, (**C**) BFe, (**D**) BFe/S/Na.

These results evidenced that high C_2-C_4 olefins selectivity and low methane production can be obtained by promoting unsupported catalysts with Na and S, however, bulk catalysts exhibited a low catalytic activity and very poor mechanical stability under the conditions tested.

Carbon burn-off experiments performed with thermogravimetric analysis (TGA) indicated that after 25 h of reaction, the unpromoted catalyst AFe exhibited a low amount of carbonaceous deposits (2 wt%) (Appendix C, Table 4). AFe/Na and AFe/S showed a higher extent of coke formation compared to the unpromoted sample. The addition of Na resulted in a 9 times increase in the amount of coke formed as it was expected for the higher C_{5+} selectivity observed during reaction (Table 3).

After 58 h of reaction, the Na and S promoted samples were analyzed to determine the extent of carbon deposition after longer reaction times. AFe/S/Na exhibited a carbon deposition level 8 times lower than for BFe/S/Na. Absence of stabilization by a support led to extensive aggregation of iron-containing particles; large particles are apparently more prone to formation of carbonaceous layers and/or carbon filaments.

Although the results of the TGA analysis performed on samples AFe/S/Na and AFe/S/2Na are not directly comparable as the samples were extracted of the reactor after different reaction times, it is clear that extra Na results in a higher amount of carbon deposition: AFe/S/Na showed only 3 wt% of carbon deposits after 55 h of reaction whereas AFe/S/2Na displayed an amount of coke 4 times higher after 25 h.

In situ carbon lay-down experiments were performed using the tapered element oscillating microbalance (TEOM) to obtain further information on the effect of promoters on carbon lay-down and to establish a fairer comparison between the samples. The advantage of using the TEOM for carbon lay-down measurements is that it provides information about carbon deposition under plug-flow conditions similarly to the reactors used during the catalytic tests *(26)*. The results of these experiments are shown in Figure 7.

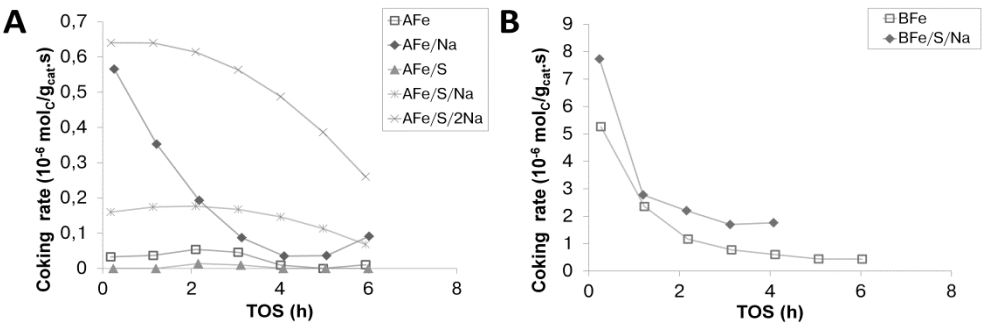

Figure 7. Carbon lay-down measurements of iron-based catalysts. The Fischer-Tropsch reaction was carried out at 350°C, 20 bar, H_2/CO = 1, GHSV = 180000 h^{-1}. (**A**) α-Al_2O_3 supported catalysts; (**B**) Bulk or unsupported catalysts.

The results of the TEOM experiments indicated that under low CO conversions (below 15%), AFe/S/2Na and AFe/Na had the highest initial coking rates among the supported samples (Figure 7 and Appendix C, Table 4). For these catalysts, the coking rates decreased rapidly with time. The samples AFe and

AFe/S showed a low amount of carbon deposits which is in line with the results observed with TGA for samples tested at 20 bar, 340°C and relatively high CO conversions (~60%). From these results it could be concluded that addition of sodium as a promoter increased the formation of coke.

AFe/S/Na showed a relatively low initial coking rate (1.6 x 10^{-7} mol_C g_{cat}^{-1} s^{-1}) in contrast to the results observed for sample BFe/S/Na which exhibited an initial carbon deposition rate almost 50 times higher. The significant differences in coking rates between these catalysts could be associated to the extreme sintering observed during reaction for unsupported catalysts (Fig. 3D). Large iron (carbide) particles are presumably more prone to carbon deposition as it has been observed for nickel catalysts *(32,33)*. Levels of carbon deposition of a supported Na and S-promoted catalyst can be decreased without affecting product selectivity by using synthesis gas with a higher H_2/CO ratio as has been shown by Koeken *et al*. *(26)*. This result indicates that success of the use of these catalysts is not only determined by an optimized catalyst but also by optimized process conditions (outside of the scope of this paper).

For the unsupported catalysts, BFe/S/Na displayed a higher coking rate than BFe (Figure 7B). Please note that for this reason, the experiment had to be stopped after 4 h of reaction to avoid breaking of the quartz element due to the expansion of the catalyst bed volume.

The catalysts were analyzed with *in situ* Mössbauer spectroscopy after reaction (1 bar) to determine if the addition of promoters had any impact in the levels of carbidization. The results of these experiments are summarized in Appendix C, Table 5. The promoted and supported samples showed higher carbide contents after reaction in comparison with AFe. High degrees of carbidization could be directly related to high catalytic activities. However, it is important to indicate that the catalytic activity might be greatly affected by the extent of carbon deposition especially during the measurements performed at 1 bar and low H_2/CO ratio. This reasoning might explain the lower activity observed for AFe/Na in comparison with AFe despite of its higher carbide content (Figure 2B). The sample with the double amount of sodium, AFe/S/2Na, showed a lower content of carbides after reaction compared with catalyst AFe/S/Na which is in agreement with the observations of An *et al. (13)* for samples with high sodium loadings.

Bulk catalysts displayed low activities when the experiments were carried out at 1 bar and 350°C although their extent of carbidization was extremely high

(95 - 100%). These results indicate that a high level carbide formation is not the only factor determining a high catalytic activity. The low activity observed for unsupported catalysts might be related to high levels of carbon deposition or to lower reactivity of larger carbide particles *(25)*.

Sodium and sulfur displayed distinct effects on the catalytic performance of supported iron catalysts. Sodium slightly decreased methane selectivity and favored chain growth probability probably caused by an increase of θ_C resulting from a stronger Fe - CO bond. However, a very high binding strength between iron and carbon might result in lower catalytic activity as depicted in the scheme in Appendix C, Figure 2 and as it was observed during the catalytic tests. On the other hand, sulfur had a major positive impact on product selectivity and catalytic activity presumably originated by the selective blockage of hydrogenation sites and the weakening of the Fe – CO bond. Although high C_2-C_4 olefins selectivity and activity as well as low methane production were achieved by promoting iron with low amounts of sulfur, the best catalytic performance was observed for the double promoted catalysts. This result points out to a synergistic effect between sodium and sulfur where the properties of each promoter are balanced by the presence of the other. Apparently, sodium assists to stabilize and anchor sulfur while sulfur enhances catalytic activity by weakening the iron-carbon bond at the surfaces of iron carbide nanoparticles. However, the location of the promoters on the active surface is still unknown and the nature of the interactions between sulfur, sodium and iron is not yet fully understood. The study of these interactions is part of ongoing research.

Conclusions

The effects of Na and S on Fe-based Fischer-Tropsch catalyst were studied. Sodium promotion of supported iron catalysts resulted in decreased methane selectivity and higher chain growth probability values when the catalysts were tested at 1 bar and 20 bar. However, the addition of sodium had a negative effect on catalytic activity possibly caused by an enhanced extent of carbon deposition as observed from TGA and TEOM experiments.

Modification of α-Al_2O_3 supported iron catalysts by addition of low loadings of sulfur had a positive impact on catalytic performance increasing lower olefins selectivity and catalytic activity while decreasing methane selectivity. The reduction of methane production was not associated to a shift of product selectivity to higher α values but probably it might be attributed to selective

blocking of hydrogenation sites by sulfur, which could at the same time explain the higher olefin selectivity.

The addition of low levels of sulfur and sodium to bulk iron catalysts greatly improved product selectivity for the FTO reaction, increasing the C_2-C_4 olefin selectivity and decreasing methane production. However, the high extent of coke lay-down observed under the selected reaction conditions (340°C, 20 bar and H_2/CO ratio of 1) caused fragmentation of the catalyst particles and carbon filament growth, evidencing the low mechanical stability of bulk promoted catalysts.

The combination of sodium plus sulfur as promoters for α-Al_2O_3 supported iron catalysts was effective to further increase lower olefins selectivity, decrease methane production while enhancing catalytic activity. The combined addition of these promoters increased carbon deposition slightly while the addition of higher amounts of sodium resulted in a decrease in catalytic activity possibly caused by the higher extent of carbon deposition.

The optimization of supported iron catalyst for the selective production of lower olefins from synthesis gas relies on many factors starting with the selection of a support material which confers mechanical stability while allowing an intimate contact between iron and the promoters. Additionally, the concentration of promoters has to be balanced carefully as low amounts of these elements have beneficial effects on catalytic performance while beyond the optimal level these might act as poisons.

Supplementary data

Product selectivity and catalytic activity as a function of time on stream, composition of the iron precursors, Anderson-Schulz-Flory plots, and *in situ* Mössbauer parameters are provided in Appendix C.

Acknowledgements

G. Bonte, Dr. A. Chojecki, Dr. A. C. J. Koeken, Dr. T. Davidian, and Dr. M. Ruitenbeek are thanked for the catalytic tests at 20 bar performed at Dow Benelux B.V. in Terneuzen. Dr. A. I. Dugulan is thanked for the Mössbauer spectroscopy measurements performed at the Fundamentals Aspects of Materials and Energy Group at the Technical University of Delft. Prof. Dr. Ir. E. J. M. Hensen (Technical University of Eindhoven) is thanked for his contribution in the discussion of the Mössbauer spectroscopy results. C. van

der Spek and J. D. Meeldijk are thanked for the TEM images. T. Zalm is thanked for ICP analysis.

References

1. A. P. Steynberg, M. E. Dry, Eds., *Fischer-Tropsch Technology (Series: Studies in surface science and catalysis No. 152)* (Elsevier, Amsterdam, 2004).
2. H. Arakawa, A. T. Bell, *Ind. Eng. Chem. Process. Des. Dev.* **22**, 97-103 (1983).
3. S. Li, S. Krishnamoorthy, A. Li, G. D. Meitzner, E. Iglesia, *J. Catal.* **206**, 202-217 (2002).
4. M. C. Ribeiro *et al.*, *J. Phys. Chem. C* **114**, 7895-7903 (2010).
5. X. An *et al.*, *Catal. Comm.* **8**, 1957-1962 (2007).
6. Y. Liu *et al.*, *J. Mol. Catal. A* **272**, 182-190 (2007).
7. B. Büssemeier, C. D. Frohning, G. Horn, W. Kluy, US Patent 4564642 (1986).
8. S. Li, A. Li, S. Krishnamoorthy, E. Iglesia, *Catal. Lett.* **77**, 197-205 (2001).
9. M. Sağlam, *Ind. Eng. Chem. Res.* **28**, 150-154 (1989).
10. M. E. Dry, G. J. Oosthuizen, *J. Catal.* **11**, 18-24 (1968).
11. J. Abbot, N. J. Clark, B. G. Baker, *Appl. Catal.* **26**, 141-153 (1986).
12. W. Ngantsoue-Hoc, Y. Zhang, R. J. O'Brien, M. Luo, B. H. Davis, *Appl. Catal. A* **236**, 77-89 (2002).
13. X. An *et al.*, *J. Mol. Catal. A* **263**, 266-272 (2007).
14. T. Riedel *et al.*, *Appl. Catal. A* **186**, 201-213 (1999).
15. T. C. Bromfield, N. J. Coville, *Appl. Catal. A* **186**, 297-307 (1999).
16. R. Crous, T. C. Bromfield, S. Booyens, European Patent Application No. EP2193841 (2010).
17. R. Crous, T. C. Bromfield, S. Booyens, US Patent 2012/0029096 A1 (2012).
18. B. Wu *et al.*, *Fuel* **83**, 205-212 (2004).
19. W. L. van Dijk, J. W. Niemantsverdriet, van der Kraan, A. M., van der Baan, H. S., *Appl. Catal.* **2**, 273-288 (1982).
20. T. C. Bromfield, N. J. Coville, *Appl. Surf. Sci.* **119**, 19-24 (1997).
21. B. Büssemeier, C. D. Frohning, B. Cornils, *Hydrocarb. Process.* **56**, 105-112 (1976).

22. D. S. Kalakkad, M. D. Shroff, S. D. Köhler, N. B. Jackson, A. K. Datye, *Appl. Catal. A* **133**, 335-350 (1995).
23. H. M. Torres Galvis *et al.*, *Science* **335**, 835-838 (2012).
24. H. J. Schulte, B. Graf, W. Xia, M. Muhler, *ChemCatChem* **4**, 350-355 (2012).
25. H. M. Torres Galvis *et al.*, *J. Am. Chem. Soc.* **134**, 16207-16215 (2012).
26. A. C. J. Koeken, H. M. Torres Galvis, T. Davidian, M. Ruitenbeek, K. P. de Jong, *Angew. Chem. Int. Ed.* **51**, 7190-7193 (2012).
27. D. Chen, E. Bjørgum, K. O. Christensen, R. Lødeng, A. Holmen, Eds., *In situ* catalyst characterization by the oscillating microbalance catalytic reactor (TEOM) *in Advances in catalysis*, Vol. 51, pp. 351-382 (Academic Press, Amsterdam, 2007).
28. T. Liu, L. Guo, Y. Tao, Y. B. Wang, W. D. Wang, *Nanostruct. Mater.* **11**, 487-492 (1999).
29. D. B. Bukur, M. Koranne, X. Lang, Rao, K. R. P. M., G. P. Huffman, *Appl. Catal. A* **126**, 85-113 (1995).
30. V. Curtis, C. P. Nicolaides, N. J. Coville, D. Hildebrandt, D. Glasser, *Catal. Today* **49**, 33-40 (1999).
31. J. Cheng *et al.*, *J. Phys. Chem.* **114**, 1085-1093 (2010).
32. D. Chen *et al.*, *J. Catal.* **229**, 82-96 (2005).
33. M. L. Toebes, J. H. Bitter, A. J. van Dillen, K. P. de Jong, *Catal. Today* **76**, 33-42 (2002).

Chapter 6

Effect of precursor on the catalytic performance of supported iron catalysts for the Fischer-Tropsch synthesis of lower olefins

Abstract

The Fischer-Tropsch-to-Olefins process (FTO) enables the direct synthesis of lower olefins from synthesis gas (CO + H_2) derived from alternative feedstocks such as natural gas, coal or biomass. A catalyst suitable for this process must comply with different requirements: high selectivity for C_2-C_4 olefins, low methane selectivity, high catalytic activity and excellent mechanical and chemical stability under demanding reaction conditions (high temperatures and low H_2/CO ratios). These features have been reported for a catalyst consisting of iron-containing nanoparticles promoted with sodium and sulfur dispersed on a weakly interactive support. In this study, Na plus S promoted alpha-alumina supported catalysts with loadings of 1 – 20 wt% Fe have been prepared using different iron precursor salts to investigate their effects on catalytic performance. The catalysts prepared from iron nitrate or ammonium iron citrate both consisted of iron nanoparticles of 15-20 nm and displayed high selectivity to lower olefins (> 50 %C) in combination with low methane selectivity (< 20 %C) when tested under industrially relevant conditions (340°C, 20 bar and H_2/CO = 1 v/v). The catalyst synthesized with ammonium iron citrate exhibited a higher catalytic activity and a much lower rate of carbon lay-down (factor 4 – 6) compared to the sample prepared with iron nitrate. Tentatively, the differences in catalytic performance are attributed to a more uniform distribution of the iron particles observed when ammonium iron citrate was used as precursor. These results suggest that the extent of aggregation of iron (carbide) nanoparticles affects their catalytic performance.

Adapted with permission from H. M. Torres Galvis, A. C. J. Koeken, J. H. Bitter, T. Davidian, M. Ruitenbeek, A. I. Dugulan, K. P. de Jong, *Effect of precursor on the catalytic performance of supported iron catalysts for the Fischer-Tropsch synthesis of lower olefins,* Catal. Today (2013), http://dx.doi.org/10.1016/j.cattod.2013.03.018.

Introduction

Lower olefins are used for the production of plastics, solvents, lubricants, pharmaceuticals, cosmetics and many other products. They are traditionally produced from oil refining processes, steam cracking of naphtha and by dehydrogenation of ethane and propane from natural gas. The need for alternative feedstocks and processes to produce these major building blocks from carbon sources other than oil has pushed research in this area during the last 40 years *(1,2)*.

An interesting alternative is to produce lower olefins from synthesis gas, a mixture of CO and H_2 derived from natural gas, coal or biomass. One of the processes that allow the conversion of synthesis gas into lower olefins without intermediate steps is the so called Fischer-Tropsch to Olefins (FTO) process *(3-5)*. Recently, selective, active and stable iron catalysts for this process have been reported *(6-9)*. These catalysts consist of iron-containing nanoparticles promoted with sodium and sulfur dispersed on a carrier material with low interaction towards iron. It has been shown that the nature of the support *(6)*, the size of iron carbide particles *(8)* and the amount and nature of promoters *(9)* play a crucial role in determining the performance for the selective production of lower olefins from synthesis gas.

Another aspect that may have a major impact on catalytic activity and product selectivity is the spatial distribution of the active carbide particles on the support material. Nanoparticle growth is one of the main deactivation pathways for many commercial catalysts *(10-17)*. This phenomenon has been studied extensively for processes involving the conversion of synthesis gas such as the production of methanol *(18-21)* and the Fischer-Tropsch synthesis of transportation fuels over cobalt catalysts *(22-24)*. Most recently our group has reported a tremendous impact of the distribution of copper nanoparticles on their stability for methanol synthesis *(18)*.

Strategies to mitigate active phase particle growth comprise alloying with a higher melting point metal to reduce their mobility *(25,26)*, increasing the metal-support interaction by using specific carriers *(27,28)* and the development of improved catalyst synthesis methods that allow a homogeneous distribution of the active particles on the support material *(18)*. The modification of the active phase by adding a metal with a higher melting point or the use of a carrier material with a stronger interaction with the active phase might have a negative impact on catalytic activity and product selectivity *(6)*. For this reason, modified catalyst preparation techniques that

maximize the inter-particle spacing without affecting its activity and selectivity are preferred. Improvements on the distribution of metal nanoparticles on a support have been reported using controlled thermal decomposition of metal nitrates *(18,29-31)*, confinement of metal nanoparticles *(32-34)*, and using chelated metal complexes as precursors during the impregnation of the support *(35,36)*.

The Fischer-Tropsch synthesis carried out in the presence of an iron catalyst has been mainly directed for the production of gasoline and light hydrocarbons. These catalysts are in general unsupported (bulk) materials and they have been investigated extensively. Limited studies have been performed on supported iron catalysts for the selective production of lower olefins from synthesis gas. The supported iron catalysts reported in literature were mainly prepared using high surface area carrier materials such as γ-Al_2O_3, SiO_2 or activated carbon. Generally, iron nitrate was the metal precursor of choice because of its high water solubility and low cost. The distribution of iron-containing nanoparticles on catalysts prepared using iron nitrate and high surface area supports may be quite uniform. Nevertheless, strong metal-support interactions hinder the formation of the active carbide phase thus resulting in a low catalytic activity *(6)*. The decrease in activity due to a strong interaction between the support and the iron-containing particles can be overcome by using an inert support *(6,7)*. The main disadvantage of using a carrier with low interaction toward the iron phase is that the metal (carbide) particles tend to aggregate during reaction resulting in deactivation by loss of active surface area. For this reason, it is necessary to use an iron precursor that will allow obtaining a homogeneous distribution of nanoparticles on the inert support. To this end, we have chosen to use chelated metal complexes.

In the present work we have prepared series (1 – 20 wt% Fe) of unpromoted α-alumina supported iron catalysts using two different iron precursors: an inorganic salt (iron nitrate) and a chelated metal complex (ammonium iron citrate). An additional series of sulfur and sodium promoted catalysts using both precursors were prepared for comparison. The catalysts have been tested for FTO to investigate the influence of the iron precursor on catalytic performance.

Experimental

Catalyst preparation

Preparation of unpromoted Fe/α-Al_2O_3 catalysts with iron nitrate. Five supported catalysts with different nominal iron loadings (1, 2, 5, 10 and 20 wt% Fe) were prepared using the incipient wetness impregnation technique. The series of catalysts XNFe, where X corresponds to the iron loading, were prepared using aqueous solutions of $Fe(NO_3)_3.9H_2O$ (Acros, ACS reagent ≥ 98%). The amounts of iron salt and demineralized water used to prepare the solutions are specified in Appendix D, Table 1. For the preparation, 5 g of α-Al_2O_3 (10 m^2 g^{-1}; Pore volume 0.4 ml g^{-1}, AL4196E, BASF) were impregnated with the iron nitrate solution until the support pores were filled. The impregnation steps were successively repeated until all the solution was incorporated to the support. After each impregnation step, the material was dried at 120°C under static air for 1 h. Finally, the catalyst precursors were dried overnight at 120°C under static air and calcined at 500°C (Heating ramp: 10°C min^{-1}) for 2 h under air flow.

Preparation of a promoted Fe/α-Al_2O_3 catalyst with iron nitrate. The catalyst 5NFeP, where P denotes promoted, was prepared using 1.9 g of $Fe(NO_3)_3.9H_2O$ which were dissolved in 1.5 ml of demineralized water (5 g of α-Al_2O_3 support). The promoters (S and Na) were incorporated in the precursor solution adding 0.042 g of sodium nitrate, $NaNO_3$ (Acros, ACS reagent ≥ 99%), and 0.005 g of ammonium sulfate $(NH_4)_2SO_4$ (Acros, for analysis ≥ 99.5%). The impregnation, drying and calcination steps were performed as described for the unpromoted supported catalysts.

Preparation of unpromoted Fe/α-Al_2O_3 catalysts with ammonium iron citrate. Five supported catalysts with different nominal iron loadings (1, 2, 5, 10 and 20 wt% Fe) were prepared using the incipient wetness impregnation technique. The series of catalysts XAFe, where X corresponds to the iron loading, were prepared using aqueous solutions of ammonium iron citrate, $C_6H_8O_7.xFe^{3+}.yNH_3$ (Fluka, *purum* p.a. 14.5 - 16 wt% Fe (Appendix D, Table 2)). The amounts of iron salt and demineralized water used to prepare the solutions are specified in Appendix D, Table 1. The impregnation, drying and calcination steps were performed as described for the unpromoted supported catalysts.

Preparation of promoted Fe/α-Al_2O_3 catalysts with ammonium iron citrate. Five supported catalysts with different nominal iron loadings (1, 2, 5, 10 and 20 wt% Fe) were prepared using the incipient wetness impregnation technique. The series of promoted catalysts XAFeP, where X corresponds to the iron loading and P denotes promoted, were prepared using aqueous solutions of ammonium iron citrate, $C_6H_8O_7.xFe^{3+}.yNH_3$, which contained the sodium and sulfur promoters (J. T. Baker, 14.5 - 16 wt%, Na, S: ~750 mg/kg (Appendix D, Table 2)). The impregnation, drying and calcination steps were performed as described for the unpromoted supported catalysts.

Catalyst characterization

Iron, sulfur and sodium contents were analyzed with ICP-OES (Inductively coupled plasma – optical emission spectroscopy) using a Spectro Ciros CCD spectrometer. The average iron oxide crystallite size was determined by line broadening analysis of XRD (X-ray diffraction) patterns obtained with a Bruker AXS D8 ADVANCE diffractometer equipped with a $Co_{K\alpha 1}$ source (λ = 0.1789 nm) using an angle range from 20° to 90° in 2θ.

Fresh and spent catalysts were analyzed with TEM (Transmission Electron Microscopy) to determine the size and spatial distribution of iron-containing particles. The images were obtained using a Philips Tecnai-20 FEG (200 kV) microscope equipped with EDX and HAADF detectors.

Carbon present on spent catalyst samples was determined with thermal gravimetric analysis (TGA) carbon burn-off performed in a Perkin Elmer Pyris 1 TGA under oxygen flow (10 ml min^{-1}). For these experiments, temperature was increased from 30°C to 600°C (Heating ramp: 5°C min^{-1}) and the sample remained under the final temperature for one hour.

Using a tapered element oscillating microbalance *(37,38)* (TEOM Series 1500 Pulse Mass Analyzer, Rupprecht & Patashnick Co., Inc.) carbon formation was measured under plug-flow conditions at 350°C, 20 bar and H_2/CO = 1 v/v. Fresh catalysts after calcination, after reduction, and spent catalysts were analyzed with ^{57}Fe Mössbauer spectroscopy in transmission mode. Spectra were collected *in situ* at room temperature using a ^{27}Co (Rh) source. The calibration for the velocity was performed using an α-Fe foil. The measurement parameters were determined by fitting the spectra using subspectra with Lorentzian-shaped lines with the Mosswin 3.0i program.

Catalytic tests

Low pressure testing. The Fischer-Tropsch synthesis was performed at 1 bar and 350°C in a fixed-bed reactor using 0.02 ± 0.005 g of catalyst (particle size 0.2 – 0.4 mm) and 0.2 g of SiC (0.2 mm) for bed dilution. The catalysts were reduced prior to reaction at 350°C with a mixture of H_2 and He (33% H_2 v/v, 60 ml min^{-1} total flow) for 2 h. After reduction, the feed flow was switched to a mixture of H_2 and CO (H_2/CO = 1 v/v, GHSV = 10500 h^{-1}). The reaction was carried out for 20 h. The CO conversion levels were lower than 1% to ensure differential operation thus limiting the extent of secondary reactions. Under these conditions the products remained in the gas phase and were analyzed with online gas chromatography (C_1 – C_{16}). CO_2 was not measured. The product selectivity was calculated on a carbon atom basis: (moles of product Y) x (carbon atoms in product Y)/(total carbon atoms in hydrocarbons produced). The activities and selectivities reported here were determined after 15 h of reaction.

Medium pressure testing. The Fischer-Tropsch reaction was carried out at 20 bar, 340°C and a H_2/CO ratio of 1 (v/v) in a high throughput testing unit fitted with fixed-bed reactors and using a gas hourly space velocity of 3000 h^{-1}. 100 μl of catalyst (0.2 - 0.4 mm) were diluted with SiC (0.2 - 0.4 mm) to complete a volume of 200 μl. Prior to reaction the catalysts were reduced in a H_2/N_2 (90/10 volume basis) flow at 350°C for 2 h. Product selectivity was determined up to C_9 using online gas chromatography. Product selectivity was calculated on a carbon atom basis excluding CO_2: (moles of product Y) x (carbon atoms in product Y)/(total carbon atoms in hydrocarbons produced).

Results and discussion

The samples with 5 wt% iron loading were analyzed with ICP-Optical emission spectroscopy to determine the composition of the calcined catalysts. The results of this analysis are summarized in Appendix D, Table 3. The promoted catalysts 5NFeP and 5AFeP showed similar sulfur and sodium contents (~ 0.2 wt% Na and 0.03 wt% S).

The XRD analysis of 5 wt% Fe and 10 wt% Fe catalysts demonstrated that samples prepared with different iron precursors and with the same iron loading had similar diffraction patterns. The analysis of the patterns indicated that the iron phase present in the calcined catalysts was Fe_2O_3 and that comparable average iron oxide crystallite sizes were obtained regardless the iron precursor

used (Appendix D, Figure 1). The average Fe_2O_3 crystallite size determined from XRD was ~ 17 nm and ~ 21 nm for the samples with 5 wt% Fe and 10 wt% Fe, respectively.

Although the average crystallite size of Fe_2O_3 was the same for the samples prepared with the nitrate and AIC precursors with the same iron loading, TEM analysis revealed that the spatial distribution of iron-containing particles on the alumina support was strongly dependent on the precursor used. Figures 1A and 1C show TEM micrographs of two calcined Fe/α-Al_2O_3 catalysts with a nominal iron loading of 5 wt%.

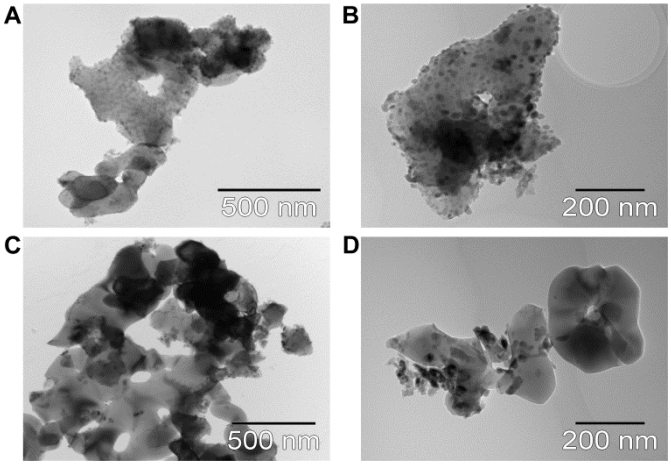

Figure 1. TEM images of supported iron catalysts. The TEM analysis of supported catalysts prepared by incipient wetness impregnation with different iron precursors indicated similar average Fe_2O_3 particle sizes. Calcined catalysts: (**A**) 5AFeP, (**C**) 5NFe; After reduction: (**B**) 5AFeP; (**D**) 5NFe.

Catalyst 5AFeP (Figure 1A) exhibited a quite uniform distribution of Fe_2O_3 particles on α-Al_2O_3. In the case of catalyst 5NFe (Figure 1C) it was observed that many areas of the alumina support were not covered with iron oxide (empty areas) while some other parts of the carrier material presented high local loadings of Fe_2O_3 particles with a high extent of aggregation (cluster formation). The differences between the two samples were even clearer after they were subjected to a reduction treatment under H_2 at 350°C for 2 h (Figures 1B and 1D).

The number-average sizes of iron-containing particles in unpromoted or promoted samples were comparable, despite of the precursor used, and only

limited sintering was observed after reduction (Table 1). The particle size distributions for these samples are included in the Appendix D (Figure 2, calcined catalysts; Figure 3, reduced catalysts). The differences observed in the distribution of Fe_2O_3 particles on the support when using nitrate or AIC precursors is ascribed to the nature of these iron salts. Upon drying, iron nitrate redistributes and crystallizes on the surface of the support. On the contrary, AIC forms a gel-like phase that interacts with the support leading to a highly dispersed compound with poor crystallization and uniform distribution. It is known that the viscosity of aqueous solutions of AIC increases during drying limiting the redistribution of the impregnation solution *(36)*.

Table 1. Average particle sizes obtained by TEM of iron-containing particles of supported catalysts.

Sample	Particle size (nm)	
	Fresh	After reduction[a]
5AFe	15 ± 5	-
5AFeP	14 ± 5	15 ± 5
5NFe	15 ± 7	17 ± 7

[a] Reduction at 1 bar, 350°C and H_2/Ar = 0.5 v/v for 2 h.

Differences in the size distribution of iron oxide particles were observed for different iron loadings as it was evidenced by Mössbauer spectroscopy. The results of the analysis indicated that calcined catalysts with lower iron loadings had higher contents of small or superparamagnetic iron oxide particles (particles with sizes smaller than 13 nm *(39-41)* as it is shown in Appendix D, Figure 4. The differences in size distribution of Fe_2O_3 particles were ultimately reflected in dissimilar levels of reduction and carbidization (reaction at 1 bar, 350°C, H_2/CO = 1, TOS = 20 h) (Appendix D, Figure 5). The content of Fe^{3+} after reduction showed a decreasing trend with increasing iron loading whereas the carbidization levels increased with iron content. The unpromoted and promoted catalysts with an iron loading of 5 wt% Fe prepared with both precursors showed a total carbidic content between 70 and 90% (Appendix, Table 4).

The series AFe, NFe and AFeP were tested in the Fischer-Tropsch reaction at 1 bar, 350°C and H_2/CO = 1 to study the influence of iron loading on selectivity and activity. The results of the catalytic tests at low pressure are presented in Table 2 and Figure 2.

Table 2. Catalytic activity and product selectivity under FTO conditions (1 bar, 350°C, H_2/CO = 1, TOS = 15 h) of Fe catalysts

	FTY (10^{-6} molCO/g_{Fe}.s)	Product selectivity (%C)			
		CH_4	C_2-C_4 olefins	C_2-C_4 paraffins	C_{5+}
1AFe	2.80	27	66	1	6
2AFe	1.90	29	63	2	6
5AFe[a]	1.40	54	42	3	2
10AFe	0.70	52	41	1	6
20AFe	0.40	51	43	2	4
1NFe	2.70	27	59	1	13
2NFe	2.20	40	53	1	6
5NFe	0.95	75	23	1	1
10NFe	0.80	68	27	1	4
20NFe	0.70	57	33	2	8
1AFeP	7.60	25	61	1	13
2AFeP	6.30	21	61	1	17
5AFeP[a]	5.70	15	64	2	19
10AFeP	1.10	27	54	1	18
20AFeP	1.90	42	42	2	14
5NFeP	4.18	15	60	2	23

[a] Data from Ref. *(9)*.

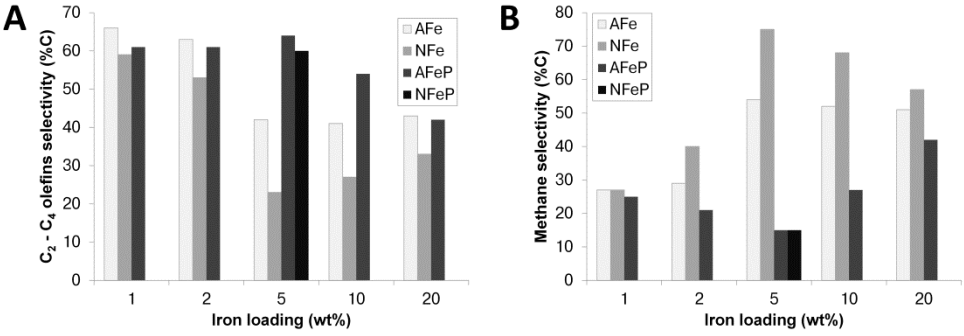

Figure 2. Product selectivity of iron catalysts at 1 bar, 350°C and H_2/CO ratio of 1 (TOS = 15 h). (**A**) C_2-C_4 olefins; (**B**) Methane selectivity.

Figure 2 shows that the lower olefins and methane selectivities of catalysts with an iron loading of 1 wt% Fe were similar irrespective of the nature presence or absence of promoters or the iron precursor. The differences in selectivity between the catalysts series were significant at intermediate iron

loadings (5 – 10 wt% Fe). The unpromoted samples prepared with AIC exhibited higher C_2-C_4 olefins selectivity and lower methane selectivities in comparison with the samples prepared with iron nitrate.

Although the average iron particle size did not increase extensively during reduction for the catalyst prepared with iron nitrate (Table 1), it was observed that the particles that were close to each other, as a consequence of poor precursor distribution, tended to aggregate further increasing the amount of large particles (> 15 nm) as shown in Appendix D, Figure 3B. Presumably, iron-containing particles sintered even further under reaction conditions bringing about larger differences in average particle size and dissimilarities in product selectivity.

The promoted catalysts with 5 wt% Fe prepared with AIC showed the highest C_2-C_4 olefins selectivity (64 %C for 5AFeP) in combination with a low methane production (15 %C for 5AFeP). It is known that the addition of sodium and sulfur, in low concentrations, to supported iron catalysts improves olefin selectivity while limiting methane formation *(8,9)*. All the catalysts tested at 1 bar and 350°C showed a chain growth probability (α) lower than 0.6. The Anderson-Schulz-Flory (ASF) plots of the product distribution for the different samples are included in Appendix D, Figure 6.

The selectivities of the catalysts with the highest iron loading tended to converge (Figure 2) irrespective of the precursor or the presence of promoters. α-Alumina is a support with a very low surface area (~10 m^2 g^{-1}) which inhibits to obtain a uniform distribution of iron particles and also to achieve narrow particle size distributions. When high iron loadings are used, the available area to distribute a large amount of particles is too small and a high extent of aggregation of the particles was inevitable regardless of the iron precursor used.

The iron-weight based catalytic activity showed a decreasing trend with increasing iron loading for the three series of catalysts (Table 2). The iron time yield (FTY) of unpromoted samples was lower in comparison with the promoted series AFeP, with the exception of catalyst 10AFeP (Figure 3A). In Figure 3B, FTY is plotted as a function of time on stream for different catalysts with an iron loading of 5 wt%. Catalyst 5AFeP showed a very high initial activity which decreased rapidly and stabilized after 10 h of reaction. After 15 h of reaction, FTY of the promoted catalyst prepared with AIC was 4 and 6 times higher than for the unpromoted catalysts prepared with AIC and iron nitrate respectively.

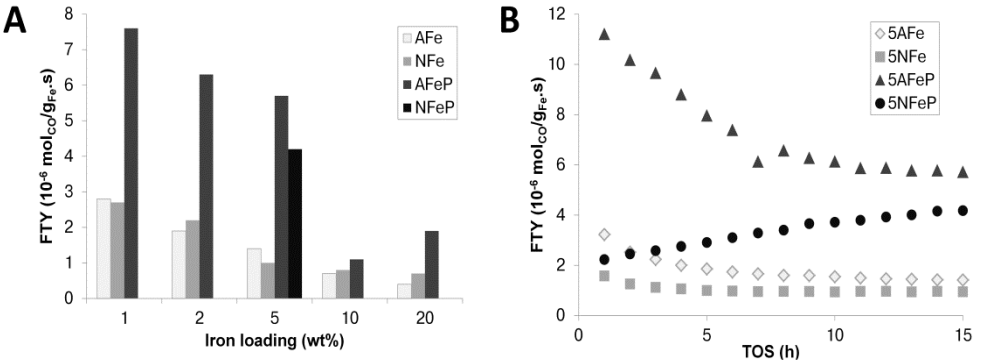

Figure 3. Catalytic activity of iron catalysts at 1 bar, 350°C and H_2/CO ratio of 1. The reaction was performed at 1 bar, 350°C and a H_2/CO ratio of 1. (**A**) Iron time yield as a function of iron loading (TOS = 15 h), (**B**) Iron time yield as a function of time on stream for 5 wt% Fe catalysts.

Iron time yield showed a similar decreasing trend when increasing iron loading for catalysts prepared using carbon nanofibers (CNF) as support material (1 – 20 wt% Fe) and AIC as iron precursor *(8)*. The promoted CNF supported catalysts showed an increasing trend in C_2-C_4 olefins selectivity and a decrease in methane production with an increase in iron loading when tested at 350°C, 1 bar and H_2/CO = 1 v/v for 15 h whereas the promoted α-Al_2O_3 supported catalysts, prepared with AIC, showed opposite trends. In the case of CNF supported catalysts, iron loading is directly related to particle size, thus higher iron contents result in larger iron-containing particles (~2 nm at 1 wt% Fe and ~9 nm at 20 wt% Fe). The iron nanoparticles supported on CNF have narrow size distributions and they are homogeneously distributed on the support *(8)*. In contrast, the particles dispersed on α-Al_2O_3 have very broad size distributions and they are more aggregated as a consequence of the low surface area (10 m^2 g^{-1} in comparison to 150 m^2 g^{-1} for CNF). The increase of iron loading cannot be directly associated with the average particle size (15 to 21 nm for loadings between 1 and 20 wt% Fe) for α-Al_2O_3 supported catalysts but it is related to particle size distribution and their spatial distribution on the support as observed from TEM analysis. The extent of aggregation of iron nanoparticles increases with iron loading and the unpromoted catalysts tend to exhibit a behavior typical from bulk or unsupported catalysts such as lower activity, higher methane production and fragmentation of large iron (carbide) particles *(6,9,42)*.

The catalysts with an iron loading of 5 wt% were tested in the Fischer-Tropsch reaction at 20 bar, 340°C and H_2/CO of 1 to investigate the influence of the iron precursor on catalytic performance under more industrially relevant conditions. The results of the catalytic tests at medium pressure are presented in Table 3 and Figure 4.

Table 3. Catalytic performance of promoted and unpromoted 5 wt% Fe catalysts (20 bar, 340°C and H_2/CO = 1, TOS = 25 h) [a]

Sample	FTY (10^{-5} $mol_{CO}/g_{Fe}.s$)	CO conversion (%)	Product selectivity (%C)				
			CH_4	C_2-C_4 olefins	C_2-C_4 paraffins	C_{5+}	Oxy.
5AFe	6.7	58	27	35	24	14	0
5AFeP	8.2	69	19	51	19	11	1
5NFeP	3.1	49	9	54	0	35	3

[a] CO_2 :45 – 50% of CO converted.

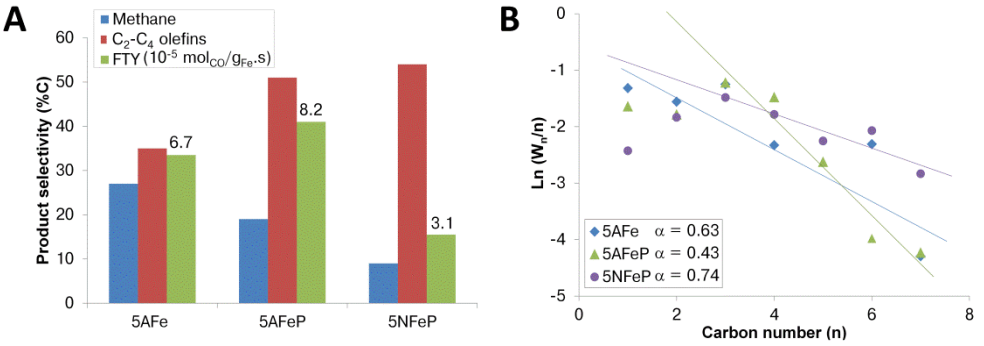

Figure 4. Catalytic performance of iron catalysts at 20 bar, 340°C and H_2/CO ratio of 1, TOS = 25 h. (**A**) Methane and C_2-C_4 olefins selectivity and iron time yield; (**B**) Anderson-Schulz-Flory plots of the product distribution.

The unpromoted catalyst 5AFe exhibited a high activity after 25 h of reaction at 340°C, 20 bar and H_2/CO = 1 v/v. The lower olefins and methane selectivities for this catalyst were moderate (35 %C and 27 %C, respectively). This sample showed a product distribution that followed the ASF model (Figure 4B) with α = 0.63 (calculated including C_1).

Catalyst 5AFeP displayed the highest catalytic activity of the three samples tested, accompanied with a high C_2-C_4 olefins selectivity (51 %C) and low methane production (19 %C). This catalyst showed a low chain growth probability (α = 0.43, excluding C_1 and C_2) and methane selectivity was

below the ASF prediction caused by the addition of the Na and S promoters (Figure 4B). Interestingly, a better selectivity for the FTO reaction was observed for the catalyst prepared with iron nitrate (54 %C C_2-C_4 olefins; 9 %C CH_4). Sample 5NFeP displayed a C_{5+} selectivity three times higher than the one observed for 5AFeP. The increased selectivity to longer hydrocarbon chains was reflected in a higher α (0.74, excluding C_1 and C_2, in comparison to 0.43 for 5AFeP) and a very large deviation of methane selectivity from the ASF model was also observed. However, 5NFeP exhibited a catalytic activity that was almost three times lower than the promoted catalyst prepared with AIC.

The differences observed in the catalytic activity of promoted samples prepared with AIC or iron nitrate might be attributed to dissimilarities in the distribution of the iron-containing particles on the support. Under the stringent reaction conditions that were applied during the catalytic tests some particle growth was expected was expected disregarding the precursor that has been used for the preparation of the samples.

TEM images of the spent catalysts are shown in Figure 5. After 25 h of reaction, 5AFe exhibited limited sintering as indicated in Table 4. The promoted samples were tested for longer times on stream and both of them displayed broader size distributions. The histograms corresponding to the iron (carbide) particle size distribution of samples 5AFeP and 5NFe are presented in Appendix D, Figure 7.

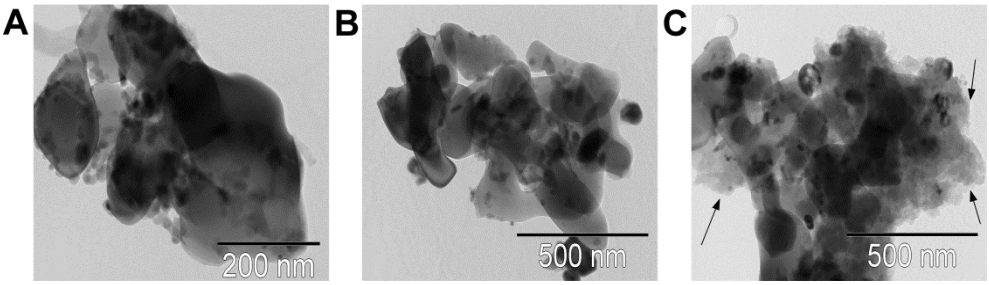

Figure 5. TEM images of spent catalyst. The catalyst were analyzed after reaction at 340°C and 20 bar (H_2/CO ratio = 1). (**A**) 5AFe (TOS = 25 h), (**B**) 5AFeP (TOS = 55 h), (**C**) 5NFeP (TOS = 58 h). The carbon deposits are indicated with arrows.

Figure 5B shows that the spent 5AFeP catalysts contained larger iron (carbide) particles as well as smaller particles well-distributed on the α-Al_2O_3 surface. In the case of 5NFeP (Figure 5C) different features could be identified: the

catalyst was covered with large amounts of amorphous carbon with small iron (carbide) particles embedded in it and large iron (carbide) particles (> 50 nm) which seemed to have fragmented. A magnified image of these "broken" particles has been included in Appendix D, Figure 8. As a result of fragmentation, it is difficult to estimate the real level of sintering of the sample prepared with iron nitrate. The small particles originated from the fragmentation of larger iron (carbide) particles decreased the average particle size of the spent 5NFeP catalyst making it comparable to the results observed for sample 5AFeP (Table 4).

Table 4. Average iron (carbide) particle size of spent catalysts tested at 20 bar, 340°C, H_2/CO = 1, GHSV = 3000 h^{-1}.

Sample	Average size before reaction (nm)	Average size after reaction (nm)	TOS (h)
5AFe	15 ± 5	15 ± 8	25
5AFeP	14 ± 5	18 ± 14	55
5NFeP	15 ± 7	18 ± 14	58

The higher levels of carbon deposition that were apparent from the TEM micrographs were confirmed by carbon burn-off experiments (TGA) and *in situ* carbon lay-down measurements performed with the TEOM (Table 5 and Figure 6). The spent promoted sample prepared with iron nitrate exhibited a coke formation level six times higher than the amount of coke determined for spent 5AFeP as determined from TGA (Table 5). The initial coking rate of sample 5NFeP was four times higher than for 5AFeP during the *in situ* measurements performed with a TEOM at 350°C, 20 bar and a H_2/CO = 1 v/v. After 6 h of reaction the coking rate of catalyst 5NFeP decreased to approximately 70% of its initial value, however, the amount of coke formed per gram of catalysts was almost five times higher than for the promoted sample prepared with the AIC precursor (Figure 6).

From these results it is shown that very selective catalysts for the FTO process (high C_2-C_4 olefins selectivity and low methane production) can be synthesized using different iron precursors in combination with Na and S as promoters. However, it is crucial to obtain a uniform distribution of the iron (carbide) particles on the support, maximizing inter-particle distances to restrict the extent of aggregation of the active particles and thereby to limit the

deposition of carbon. Further study is proposed to investigate the aggregation of the particles at different times on stream and/or under milder reaction conditions, for instance, at low pressures, where limited particle growth is expected, or at higher H_2/CO ratios to decrease the coking rates *(38)*.

Table 5. Carbon lay-down measurements. Carbon burn-off experiments performed with TGA on samples tested at 20 bar, 340°C, H_2/CO = 1, GHSV = 3000 h^{-1}. *In situ* carbon lay-down measurements carried out on the TEOM at 20 bar, 350°C, H_2/CO = 1, GHSV = 180000 h^{-1}.

Sample	TGA		Initial coking rate (10^{-6} molc/g_{cat}.s)
	Carbon deposition (wt%)	TOS (h)	TEOM
5AFe	2	25	0.03
5AFeP	3	55	0.16
5NFeP	19	58	0.68

[a] After 1 hour

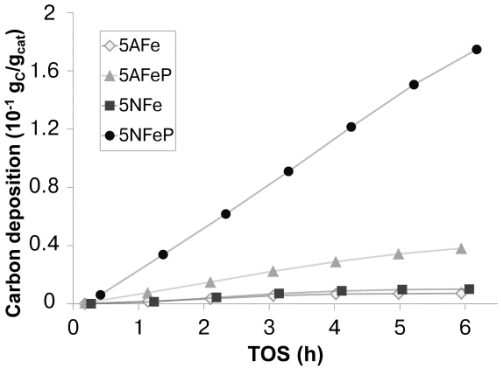

Figure 6. Carbon lay-down measurements of iron-based catalysts. The Fischer-Tropsch reaction was carried out at 350°C, 20 bar, H_2/CO = 1, GHSV = 180000 h^{-1}.

Conclusions

The influence of the iron precursor at loadings of 1 – 20 wt% Fe on the catalytic performance of Fe-based FTO catalysts was studied. The catalysts prepared with ammonium iron citrate exhibited a more uniform distribution of iron (oxide) particles on α-Al_2O_3 compared with the samples prepared with iron nitrate based on analysis with TEM of the calcined and the reduced catalysts (before catalysis). The unpromoted and promoted samples with 5 wt% Fe showed similar average iron (oxide) crystallite sizes regardless the nature of the precursor.

Similar product selectivities with both precursors were observed for unpromoted and promoted samples with an iron loading of 1 wt% when the catalysts were tested in the Fischer-Tropsch reaction at low pressure (1 bar, 350 °C). With an iron loading of 5 or 10 wt% Fe the unpromoted catalysts prepared with AIC showed higher C_2-C_4 olefins selectivity and lower methane production in comparison with the samples prepared with iron nitrate. These differences in product selectivity were tentatively attributed to the dissimilar extent of aggregation of iron-containing particles observed for the different precursors at intermediate loadings.

Catalysts with a high extent of aggregation of iron nanoparticles behaved similarly to unsupported or bulk catalysts exhibiting lower catalytic activities and high methane selectivity *(6,9)*. Iron-containing particles that were highly aggregated in the calcined catalysts during reaction formed larger crystals that fragmented due to carbon deposition and density differences which have been typically observed for unsupported (bulk) catalysts.

The Na plus S promoted catalysts prepared with different iron precursors exhibited high selectivity to light olefins (> 50 %C) and methane levels below the selectivity expected from the Anderson-Schulz-Flory model (< 20 %C) when tested in the Fischer-Tropsch reaction at medium pressure (20 bar, 350 °C). Although the promoted catalyst (5 wt% Fe) prepared with iron nitrate exhibited a remarkable selectivity for the FTO process (54 %C lower olefins, 9 %C methane), it also displayed a high selectivity towards longer-chain hydrocarbons (35 %C), low activity and extensive formation of coke deposits.

The promoted catalyst prepared with ammonium iron citrate (AIC) displayed high light olefins selectivity (~ 50 %C), low methane formation (~ 20 %C), high catalytic activity and low levels of carbon lay-down despite of some growth of the iron (carbide) particles.

The spatial distribution of Na plus S-promoted iron nanoparticles on a weakly interactive support is suggested to have a large impact not only on product selectivity and catalytic activity but also on the extent of formation of carbon deposits which directly affects the chemical and mechanical stability of Fe-based systems.

Supplementary data

Results of XRD analysis, particle size distributions, composition of the iron precursor solutions and of Na plus S-promoted catalysts, Anderson-Schulz-Flory plots, and *in situ* Mössbauer parameters are provided in Appendix D.

Acknowledgements

G. Bonte, Dr. A. Chojecki, Dr. A. C. J. Koeken, Dr. T. Davidian, and Dr. M. Ruitenbeek are thanked for the catalytic tests at 20 bar performed at Dow Benelux B.V. in Terneuzen. Dr. A. I. Dugulan is thanked for the Mössbauer spectroscopy measurements performed at the Fundamentals Aspects of Materials and Energy Group at the Technical University of Delft. Prof. Dr. Ir. E. J. M. Hensen (Technical University of Eindhoven) is thanked for his contribution in the discussion of the Mössbauer spectroscopy results. C. van der Spek and J. D. Meeldijk are thanked for the TEM images. T. Zalm is thanked for ICP analysis.

References

1. C. Wang, L. Xu, Q. Wang, *J. Nat. Gas Chem.* **12**, 10-16 (2003).
2. M. Janardanarao, *Ind. Eng. Chem. Res.* **29**, 1735-1753 (1990).
3. E. Schwab, A. Weck, J. Steiner, K. Bay, *Oil Gas Eur. Mag.* **1**, 44-47 (2010).
4. B. Sun, K. Xu, L. Nguyen, M. Qiao, F. Tao, *ChemCatChem* **4**, 1498 (2012).
5. E. de Smit, B. M. Weckhuysen, *Chem. Soc. Rev.* **37**, 2758 (2008).
6. H. M. Torres Galvis *et al.*, *Science* **335**, 835-838 (2012).
7. H. J. Schulte, B. Graf, W. Xia, M. Muhler, *ChemCatChem* **4**, 350-355 (2012).
8. H. M. Torres Galvis *et al.*, *J. Am. Chem. Soc.* **134**, 16207-16215 (2012).
9. H. M. Torres Galvis *et al.*, *J. Catal.* **303**, 22-30 (2013).
10. C. H. Bartholomew, *Appl. Catal. A* **212**, 17 (2001).
11. D. L. Trimm, *Appl. Catal. A* **212**, 153 (2001).
12. Y. Nagai *et al.*, *Catal. Today* **175**, 133-140 (2011).
13. B. Lindström, L. J. Pettersson, *Catal. Lett.* **74**, 27-30 (2001).
14. R. J. Liu *et al.*, *Appl. Catal. A* **282**, 111-121 (2005).
15. K. O. Christensen, D. Chen, R. Lødeng, A. Holmen, *Appl. Catal. A* **314**, 9-22 (2006).
16. A. K. Datye, Q. Xu, K. C. Kharas, J. M. McCarty, *Catal. Today* **111**, 59 (2006).
17. G. Jacobs *et al.*, *Appl. Catal. A* **233**, 215 (2002).
18. G. Prieto, J. Zečević, H. Friedrich, K. P. de Jong, P. E. de Jongh, *Nature Mater.* **12**, 34-39 (2013).
19. W. J. Shen, A. Kobayashi, Y. Ichihashi, Y. Matsumura, M. Haruta, *Catal. Lett.* **73**, 161-165 (2001).
20. J. T. Sun, I. S. Metcalfe, M. Sahibzada, *Ind. Eng. Chem. Res.* **38**, 3868-3872 (1999).
21. M. Kurtz, H. Wilmer, T. Genger, O. Hinrichsen, M. Muhler, *Catal. Lett.* **86**, 77-80 (2003).
22. A. M. Saib *et al.*, *Catal. Today* **154**, 271-282 (2010).

23. G. L. Bezemer, T. J. Remans, A. P. van Bavel, A. I. Dugulan, *J. Am. Chem. Soc.* **132**, 8540-8541 (2010).
24. Ø. Borg *et al.*, *J. Catal.* **259**, 161-164 (2008).
25. M. V. Twigg, M. S. Spencer, *Top. Catal.* **22**, 191 (2003).
26. C. S. Chen, W. H. Cheng, S. S. Lin, *Appl. Catal. A* **257**, 97 (2004).
27. M. Montes, J. B. Soupart, M. de Saedeleer, B. K. Hodnett, B. Delmon, *J. Chem. Soc. , Faraday Trans. 1* **80**, 3209 (1984).
28. R. Riva, H. Miessner, R. Vitali, G. del Piero, *Appl. Catal. A* **196**, 111 (2000).
29. J. R. A. Sietsma *et al.*, *Angew. Chem. Int. Ed.* **46**, 4547-4549 (2007).
30. P. Munnik *et al.*, *J. Phys. Chem. C* **115**, 14698-14706 (2010).
31. M. Wolters, P. Munnik, J. H. Bitter, P. E. de Jongh, K. P. de Jong, *J. Phys. Chem. C* **115**, 3332 (2011).
32. R. Dehghan-Niri *et al.*, *Catal. Sci. Technol. ,* **DOI: 10.1039/c2cy20325a** .
33. P. M. Arnal, M. Comotti, F. Schüth, *Angew. Chem.* **118**, 8404 (2006).
34. T. M. Eggenhuisen, J. P. den Breejen, D. Verdoes, P. E. de Jongh, K. P. de Jong, *J. Am. Chem. Soc.* **132**, 18318-18325 (2010).
35. J. Y. Carriat, M. Che, M. Kermarec, M. Verdaguer, A. Michalowicz, *J. Am. Chem. Soc.* **120**, 2059 (1998).
36. A. J. van Dillen, Terörde, Robert J. A. M., D. J. Lensveld, J. W. Geus, K. P. de Jong, *J. Catal.* **216**, 257-264 (2003).
37. D. Chen, E. Bjørgum, K. O. Christensen, R. Lødeng, A. Holmen, Eds., *In situ* catalyst characterization by the oscillating microbalance catalytic reactor (TEOM) *in Advances in catalysis*, Vol. 51, pp. 351-382 (Academic Press, Amsterdam, 2007).
38. A. C. J. Koeken, H. M. Torres Galvis, T. Davidian, M. Ruitenbeek, K. P. de Jong, *Angew. Chem. Int. Ed.* **51**, 7190-7193 (2012).
39. Z. Liu, C. Sun, G. Wang, Q. Wang, G. Cai, *Fuel Process. Technol.* **62**, 161-172 (2000).
40. T. Liu, L. Guo, Y. Tao, Y. B. Wang, W. D. Wang, *Nanostruct. Mater.* **11**, 487-492 (1999).
41. D. B. Bukur, M. Koranne, X. Lang, Rao, K. R. P. M., G. P. Huffman, *Appl. Catal. A* **126**, 85-113 (1995).
42. D. S. Kalakkad, M. D. Shroff, S. D. Köhler, N. B. Jackson, A. K. Datye, *Appl. Catal. A* **133**, 335-350 (1995).

Chapter 7a

Summary, concluding remarks and perspectives

Lower olefins (ethylene, propylene and butylenes) are important commodity chemicals used for the manufacture of, amongst others, plastics, solvents and lubricants to cosmetics and drugs. C_2 to C_4 olefins are conventionally produced by steam cracking of naphtha. In view of economic, strategic, and environmental reasons there is a growing necessity to produce these key chemical building blocks from non-oil derived sources.

Many processes have been devised to obtain lower olefins from synthesis gas, a mixture of CO and H_2 that can be obtained from different carbon-containing feedstocks. Methanol-to-olefins (MTO) and Dimethyl ether-to-olefins (DMTO) are syngas-based processes that involve the synthesis of an intermediate. A direct route for the conversion of syngas into lower olefins is the so-called Fischer-Tropsch-to olefins (FTO) process.

Promoted iron catalysts are the choice for FTO as they show low methane selectivity at the high reaction temperatures necessary to drive product distribution to shorter hydrocarbon chains and exhibit high olefin selectivity.

The use of iron-based catalysts is advantageous for the conversion of CO-rich syngas such as the gas obtained from gasification of coal or biomass. The use of Fe-based catalysts eliminates the need of an upstream water gas shift process to adjust the H_2/CO ratio. Iron is more resistant to poisoning by contaminants present in coal or biomass-based syngas in comparison to catalysts used for the conversion of syngas into methanol or DME.

Iron-based catalysts are highly complex in view of the chemical and physical changes they undergo during activation and reaction. Iron oxide, usually present in the fresh catalysts as hematite (α-Fe_2O_3), can be transformed into multiple phases including other Fe oxides, iron carbides and metallic iron. There are at least five iron oxides and six iron carbides that have been reported to be present during the Fischer-Tropsch reaction or in fresh or pretreated catalysts.

To achieve active and selective catalysts for the FTO reaction it is necessary to add small amounts of other elements to modify the properties of iron (carbide). In general, promoters are added to reduce methane selectivity and to increase the selectivity towards C_2-C_4 olefins. The complexity of promoted bulk iron catalysts is not only related to the different iron phases present in the working catalysts but also to the presence of modifying elements and their intricate interactions with the active phase.

As mentioned before, iron catalysts experience physical changes during reaction. Large iron oxide crystals transform into iron carbide when they are

put in contact with syngas. Internal forces originated by density differences of the iron phases and by nucleation of carbon filaments result in fragmentation of iron-containing particles. This might lead to problems during operation such as fouling of separation equipment or plugging of the catalyst bed. The stability of iron-based catalysts can be improved by dispersing iron nanoparticles on a support or carrier material.

The complexity of iron catalysts increases further when introducing a support material as a result of the interactions between the active phase and the carrier. Additionally, structure sensitivity starts to play a role when iron (carbide) particle size is decreased from micrometers to the nanometer range and the spatial distribution of the particles on the support might influence catalytic properties. Other factors that determine the performance of FTO catalysts are reaction conditions and pretreatment processes.

The present work is mainly focused on the study of the properties of iron-based catalysts that have an influence on activity, selectivity and stability during the conversion of synthesis gas into lower olefins.

Chapter 2 provides a literature review of syngas-based processes that have been proposed for the production of C_2-C_4 olefins and describes in detail the different catalysts for the Fischer-Tropsch synthesis of light olefins based on scientific publications and patents. It is shown that promoted and supported iron-based catalysts are promising for the FTO process as they can exhibit high stability and activity, high C_2-C_4 olefins selectivity and low methane production.

The influence of the nature of the support on the catalytic properties of Fe-based systems is discussed in **Chapter 3**. Na and S-promoted and supported catalysts were prepared by impregnation of ammonium iron citrate on conventional high surface area carriers and on supports with weak interactions toward iron. Three bulk catalysts, unpromoted Fe_2O_3, Fe-Ti-Zn-K and Fe-Cu-K-SiO_2 were prepared and tested for comparison. At 1 bar, Fe/CNF and Fe/α-Al_2O_3 catalysts displayed the highest C_2-C_4 olefins selectivity and the lowest methane production. These catalysts were five to ten times more active than the catalysts prepared with γ-Al_2O_3 or SiO_2 as carrier. A similar behavior was observed when the catalysts were tested under industrially relevant conditions (20 bar). Mössbauer spectroscopy of spent catalysts after reaction at 1 bar revealed that the formation of the carbide phase was inhibited in Fe/SiO_2 and Fe/γ-Al_2O_3 due to strong interactions between iron and support thus explaining their lower activity. After reaction at 20 bar, Fe/CNF and Fe/α-Al_2O_3 (10 wt%

Fe) displayed limited sintering and low levels of carbon deposition (< 10 wt%) whereas Fe-Cu-K-SiO_2 showed extensive coke formation (~ 40 wt%) and low stability reflected in particle fragmentation.

Chapter 4 deals with the study of iron (carbide) particle size effects on activity of selectivity. Na and S-promoted and unpromoted catalysts were prepared by impregnation of ammonium citrate on carbon nanofibers. The size of iron-containing particles was varied by changing iron loading. Additional unpromoted samples were prepared by a colloidal route. The initial surface-specific activity of both promoted and unpromoted catalysts increased with decreasing particle size when the samples were tested at 1 and 20 bar. The particle size effect observed for iron catalysts at high temperature contrasted with results reported for Co, Ru and Fe catalysts tested at low temperatures. It was proposed that the high activity exhibited by smaller iron carbide particles is related to enhanced methane formation on their corners and edges. The influence of iron particle size on selectivity was marginal for unpromoted catalysts whereas methane production increased and C_2-C_4 olefins selectivity decreased with decreasing particle size for Na plus S-promoted catalysts. These results point out that the smallest promoted iron carbide particles were the most active but the least selective.

The influence of Na and S promoters on catalytic performance was investigated in **Chapter 5** using Fe/α-Al_2O_3 catalysts prepared by impregnation of ammonium iron citrate. The addition of Na increased the chain growth probability and decreased methane production while decreasing catalytic activity possibly originated by enhanced carbon lay-down. The modification of Fe catalysts with low amounts of sulfur resulted in higher activity and C_2-C_4 olefins selectivity and lower methane production without affecting chain growth probability. It was put forward that sulfur selectively blocked the hydrogenation sites leading to enhanced olefin selectivity and low methane formation. High C_2-C_4 olefins selectivity and low methane selectivity was also observed for Na and S-promoted bulk catalysts. However, these catalysts exhibited extensive carbon lay-down and low stability reflected in the fragmentation of catalyst particles.

Chapter 6 covered the effect of iron precursor on activity, selectivity and stability. The study was performed using iron nitrate or ammonium iron citrate as precursors for the preparation of Na plus S-promoted and unpromoted Fe/α-Al_2O_3 catalysts. TEM analysis of the samples revealed that a more uniform distribution of iron-containing particles was achieved when using ammonium

iron citrate as precursor. The Na plus S-promoted catalysts (5 wt% Fe) showed high C_2-C_4 olefins selectivity and low methane formation regardless of the iron precursor used. However, the catalysts prepared with iron nitrate displayed a lower activity and extensive carbon deposition. Calcined catalysts that showed a high extent of aggregation of iron particles displayed low activities and high methane selectivities during reaction. Iron nanoparticles that were highly aggregated sintered under reaction conditions and subsequently fragmented as it has been reported for unsupported catalysts.

The Fischer-Tropsch reaction on iron-based catalysts has been studied for almost a century. However, the reaction mechanism has not been completely elucidated yet and there is still debate on the assignment of the actual active site(s). It is expected that further development of characterization techniques, especially *operando* and *in situ* analysis of working catalysts under industrially relevant conditions, will provide insights on the reaction and the effects of the catalyst properties on activity, selectivity and stability. A better understanding of the particle size effects, the active phase-support interactions and the influence of promoters and precursors on catalytic performance will contribute to the development and optimization of Fe-based catalysts for the production of lower olefins from synthesis gas.

Industrial development of supported Fe catalysts for the FTO process might be achieved by using supports with moderate-to-low interactions towards iron that permit the formation of the active carbide phase but that simultaneously provide sufficient mechanical anchoring for iron nanoparticles to avoid particle growth. It is recommended to explore new synthesis methods to maximize interparticle spacing and to achieve narrower particle size distributions and more homogeneous distribution of iron nanoparticles on the support.

Suggestion for academic research include the investigation of the iron particle size effects on carbon lay-down during reaction using the TEOM (Tapered Element Oscillating Microbalance) and the effects on surface coverage and residence times on reaction intermediates using SSITKA (Steady-State Isotopic Transient Kinetic Analysis). The use of in situ Mössbauer spectroscopy analysis might provide additional information on metal-support interactions at reaction conditions relevant for industrial application. Advances in *in situ* microscopy techniques would be a powerful tool in the future to study the aggregation and fragmentation of iron-containing particles during reaction conditions.

Chapter 7b

Nederlandse samenvatting

Lagere olefines, zoals etheen, propeen en buteen, zijn belangrijke chemicaliën voor een breed scala aan producten zoals plastics, oplosmiddelen, smeermiddelen, cosmetica en medicijnen. De C_2 tot C_4 olefines worden traditioneel gemaakt door het stoomkraken van nafta, maar vanwege economische, strategische en milieutechnische redenen is er een groeiende vraag om deze chemicaliën via een andere route te produceren zodat er geen olie voor nodig is. Er zijn veel processen bekend waarbij lagere olefines gemaakt worden uit synthesegas (syngas), een gas dat bestaat uit CO en H_2 en wat verkregen kan worden door koolstofhoudende materialen te vergassen. De zogenaamde Methanol-naar-Olefines (MTO) en Dimethylether-naar-Olefines (DMTO) processen zijn beide gebaseerd op syngas waarbij eerst een tussenproduct wordt gemaakt namelijk methanol of dimethylether. Een directe route voor de conversie van syngas naar lagere olefines is het proces dat we Fischer-Tropsch-naar-Olefines (FTO) noemen.
Voor FTO zijn gepromoteerde ijzerkatalysatoren veelal de beste keuze, omdat ze bij de hoge temperaturen die nodig zijn om de koolstofketens kort te houden en een hoog olefine gehalte te verkrijgen, toch een relatief lage selectiviteit naar methaan hebben. Daarbij is het gebruik van ijzer-gebaseerde katalysatoren voordelig als syngas gebruikt wordt dat relatief veel CO bevat, zoals dat verkregen uit biomassa of steenkool. Dit komt doordat ijzer zelf actief is in de water-gas-shift-reactie, waardoor verdere behandeling om de H_2/CO verhouding te veranderen niet nodig is. IJzer is ook beter bestand tegen vervuiling die aanwezig is in syngas gemaakt uit biomassa of steenkool, vergeleken met de katalysatoren die gebruikt worden om syngas om te zetten naar methanol of dimethylether.
IJzer-gebaseerde katalysatoren zijn erg complex met betrekking tot de fysische en chemische veranderingen die ze tijdens activatie en reactie ondergaan. Zo kan ijzeroxide, dat meestal in de katalysator aanwezig is als hematiet (α-Fe_2O_3), omgezet worden in verscheidene fases zoals andere ijzeroxides, ijzercarbides en metallisch ijzer. Ten minste vijf ijzeroxides en zes ijzercarbides zijn gerapporteerd in ijzerkatalysatoren direct na synthese, na de voorbehandeling of tijdens de Fischer-Tropschreactie.
Om een hoge activiteit en selectiviteit te verkrijgen in de FTO reactie is het nodig om kleine hoeveelheden van andere elementen toe te voegen om zo de eigenschappen van het ijzer te veranderen. Zo worden promotoren gebruikt om de selectiviteit naar methaan te reduceren terwijl die naar C2 tot C4 olefines verhoogd wordt. Gepromoteerde ongedragen ijzerkatalysatoren zijn dan ook

niet alleen complex vanwege de vele verschillende ijzerfases, maar ook vanwege de aanwezigheid van deze additionele elementen en hun interacties met de katalytisch actieve plaatsen.

Zoals genoemd ondergaat ijzer veel veranderingen tijdens de reactie. Zo transformeren grote ijzerkristallen naar ijzercarbide als ze in contact komen met synthesegas. Vanwege grote interne krachten die ontstaan door verschillen in dichtheid tussen de verscheidene ijzerfases en door nucleatie van koolstoffilamenten kunnen de ijzerdeeltjes fragmenteren. Dit kan voor vervuiling zorgen in de scheidingsapparaten of voor verstoppingen van het katalysatorbed. De stabiliteit van ijzer-gebaseerde katalysatoren kan verbeterd worden door kleine ijzerdeeltjes te dispergeren op een dragermateriaal.

Het introduceren van een dragermateriaal compliceert het geheel echter nog verder, vanwege interacties tussen het dragermateriaal en de actieve fase. Ook gaat structuurgevoeligheid een rol spelen wanneer de grootte van ijzer(carbide)deeltjes wordt verkleind van micrometers naar nanometers en kan de distributie van de deeltjes op het dragermateriaal invloed hebben op de katalytische eigenschappen. Andere factoren die invloed hebben op de FTO-reactie zijn de reactiecondities en de voorbehandeling.

Het huidige werk richt zich voornamelijk op de eigenschappen van ijzerkatalysatoren die invloed hebben op de activiteit, selectiviteit en stabiliteit tijdens de omzetting van synthesegas naar lagere olefines.

Hoofdstuk 2 geeft een overzicht van de literatuur over processen die gebaseerd zijn op het omzetten van synthese gas naar C_2-C_4 olefines en beschrijft de verschillende katalysatoren die gebruikt worden voor de Fischer-Tropsch-reactie van lagere olefines gebaseerd op wetenschappelijke artikelen en patenten in detail. Hieruit blijkt dat gepromoteerde ijzer-gebaseerde katalysatoren op een dragermateriaal veelbelovend zijn voor het FTO proces omdat ze een hoge activiteit en stabiliteit tonen terwijl de selectiviteit naar C_2-C_4 olefines hoog is en die naar methaan laag.

De invloed van het dragermateriaal op de katalytische eigenschappen van ijzer-gebaseerde katalysatoren wordt besproken in **Hoofdstuk 3**. Gedragen en met natrium en zwavel gepromoteerde katalysatoren werden bereid door middel van een impregnatie met ammoniumijzercitraat op conventionele dragers met een hoog interne oppervlakte en op materialen die weinig interactie tonen met ijzer. Drie katalysatoren, zonder dragen, te weten Fe_2O_3, Fe-Ti-Zn-K en Fe-Cu-K-SiO_2 werden ook bereid en getest ter vergelijking. Bij 1 bar toonde Fe/koolstofnanovezels (CNF) en Fe/α-Al_2O_3 katalysatoren de hoogste

selectiviteit naar C_2-C_4 olefines en de laagste methaanproductie. Deze katalysatoren waren ook vijf tot tien keer actiever dan de katalysatoren bereid met γ-Al_2O_3 of SiO_2 als dragermateriaal. Een vergelijkbaar gedrag werd geobserveerd wanneer de katalysatoren getest werden onder industrieel relevante condities (20 bar). Mössbauer spectra van de katalysatoren na reactie bij 1 bar toonde dat de formatie van de carbide fase werd tegen gehouden in de Fe/SiO_2 en Fe/γ -Al_2O_3 katalysatoren door de sterke interactie tussen het ijzer en het dragermateriaal, wat de lage activiteit van deze katalysatoren verklaarde. Na reactie bij 20 bar vertoonde Fe/CNF en Fe/α-Al_2O_3 (10 wt% Fe) gelimiteerde samenklontering van de ijzerdeeltjes en een relatief lage hoeveelheid van koolstofdepositie (< 10 wt%), terwijl Fe-Cu-K-SiO_2 veel meer koolstof formatie (~40 wt%) vertoonde samen met een lage mechanische stabiliteit vanwege fragmentatie van de katalysatordeeltjes.

Hoofdstuk 4 betreft een studie van het effect van de grootte van ijzer(carbide)deeltjes op de activiteit en selectiviteit. Na- en S-gepromoteerde en ongepromoteerde katalysatoren werden bereid door middel van impregnatie van ammoniumijzercitraat op koolstofnanovezels. De grootte van de ijzerhoudende deeltjes werd gevarieerd door de belading van ijzer te veranderen. Extra ongepromoteerde katalysatoren werden gesynthetiseerd via een colloïdale route. De initiële oppervlaktespecifieke activiteit van zowel gepromoteerde als ongepromoteerde katalysatoren ging omhoog als de deeltjesgrootte kleiner werd wanneer katalysatoren getest werden bij 1 en 20 bar. Dit effect van deeltjesgrootte voor ijzer bij hoge temperaturen staat in contrast met resultaten die gerapporteerd zijn voor Co-, Ru- en Fe-katalysatoren getest bij lagere temperaturen. De hypothese is dat de hoge activiteit gemeten bij kleinere deeltjes te maken heeft met een versnelde vorming van methaan op de hoeken en randen van deze deeltjes. De invloed van deeltjesgrootte op de selectiviteit was marginaal voor ongepromoteerde katalysatoren terwijl de methaanproductie was verhoogd en de selectiviteit naar C2-C4 olefines verminderde naarmate de deeltjes kleiner werden voor de Na- en S-gepromoteerde katalysatoren. Hieruit was te concluderen dat de kleinste gepromoteerde ijzercarbide deeltjes de hoogste activiteit toonden, samengaand met de laagste selectiviteit.

De invloed van Na- en S-promotoren op de katalytische prestatie werd onderzocht in **Hoofdstuk 5** met Fe/α-Al_2O_3-katalysatoren bereid door middel van impregnatie van ammoniumijzercitraat. De additie van Na verhoogde de kans op groei van langere koolstofketens en verminderde de methaanproductie

alsmede de katalytische activiteit, mogelijk door een verhoogde koolstofdepositie. Modificatie van ijzerkatalysatoren met kleine hoeveelheden zwavel resulteerde in een hogere activiteit en C_2-C_4 olefines selectiviteit en een lagere selectiviteit naar methaan, terwijl de lengte van de koolstofketens gelijk bleef. Dit werd verklaard doordat zwavel selectief de actieve sites blokkeert waar hydrogenatie plaats vindt, wat leidt tot een hogere olefine-selectiviteit en minder methaanproductie. De hoge C_2-C_4 selectiviteit en lage methaanproductie werd ook waargenomen voor Na- en S-gepromoteerde ongedragen katalysatoren. Deze katalysatoren kampten echter met een erg hoge koolstofdepositie en lage stabiliteit door fragmentatie van de katalysatordeeltjes.

Hoofdstuk 6 betreft het effect van de ijzerprecursor op de activiteit, selectiviteit en stabiliteit. Deze studie werd uitgevoerd door ijzernitraat en ammoniumijzercitraat te vergelijken als precursor voor de bereiding van Na- en S-gepromoteerde en ongepromoteerde Fe/α-Al_2O_3 katalysatoren. TEM analyse van de katalysatoren toonde dat ammoniumijzercitraat resulteerde in een meer uniforme distributie van de ijzerhoudende deeltjes. De Na- en S-gepromoteerde katalysatoren (5 wt% Fe) toonde een hoge selectiviteit naar C_2-C_4 olefines en lage methaanproductie ongeacht welke ijzerprecursor werd gebruikt. De katalysatoren bereid met ijzernitraat hadden echter een lagere activiteit en was er meer koolstofdepositie. Gecalcineerde katalysatoren waarbij de deeltjes sterk geaggregeerd waren, toonden een lage activiteit en hoge methaan selectiviteit tijdens de reactie. IJzerdeeltjes die erg geaggregeerd waren, sinterden ook tijdens de reactie en konden vervolgens fragmenteren zoals eerder gezien voor ongedragen katalysatoren.

De Fischer-Tropschreactie met katalysatoren gebaseerd op ijzer wordt al bijna 100 jaar bestudeerd. Toch is het reactiemechanisme nog niet volledig bekend en wordt er nog steeds gediscussieerd over wat de actieve plaatsen precies zijn. Verwacht wordt dat verdere ontwikkeling van karakterisatietechnieken, met name *operando* en *in situ* analyse van katalysatoren tijdens reactie onder industrieel relevante condities meer informatie kan bieden over de reactie en de invloed van de katalysatoreigenschappen op de activiteit, selectiviteit en stabiliteit. Een beter begrip op het effect van de deeltjesgrootte, de interactie tussen de actieve fase en het dragermateriaal en de invloed van promotoren en precursors op de katalytische prestaties is van groot belang voor het ontwerp en de optimalisatie van ijzerkatalysatoren voor de productie van lagere olefines uit synthesegas.

Industriële ontwikkeling van gedragen Fe katalysatoren voor het FTO proces zou bereikt kunnen worden door dragermaterialen te gebruiken die een lage tot gemiddelde interactie met ijzer tonen, zodat de formatie van de actieve carbide fase mogelijk is terwijl er wel voldoende mechanische verankering is voor de ijzernanodeeltjes om verdere groei van deeltjes te voorkomen. Het wordt aanbevolen nieuwe synthesemethodes te onderzoeken waarmee een maximale afstand tussen de individuele nanodeeltjes te verkrijgen is, en waarbij een nauwe deeltjesgrootte distributie te verkrijgen is voor een goed gedispergeerde en homogene katalysator.
Suggesties voor academisch onderzoek zijn het onderzoeken van het effect van deeltjesgrootte op de koolstofafzetting tijdens reactie met een TEOM (Tapered Element Oscillating Microbalance) en het effect op de oppervlaktebedekkingsgraad en residentietijden van reactieintermediëren door middel van SSITKA (Steady-State Isotopic Transient Kinetic Analysis). Het gebruik van *in situ* Mössbauer spectroscopische analyse kan extra informatie bieden over de interactie tussen de actieve fase en het dragermateriaal onder relevante reactiecondities. Verdere ontwikkelingen in *in situ* microscopische technieken zouden erg waardevol kunnen zijn om de aggregatie en fragmentatie van ijzerhoudende deeltjes tijdens reactiecondities te bestuderen.

Appendices

Appendix A

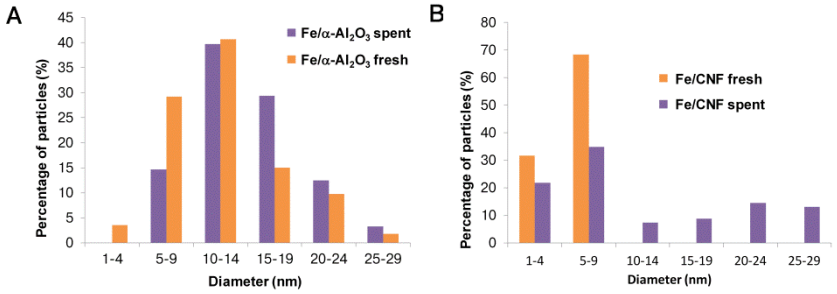

Figure 1. Particle size distribution of iron nanoparticles. (**A**) 12 wt% Fe/α-Al2O3, (**B**) Fe/CNF. Fresh catalysts: dark-colored bars. The spent catalysts (light-colored bars) were analyzed after reaction at 340°C, 20 bar and H2/CO ratio of 1 (TOS = 64 h).

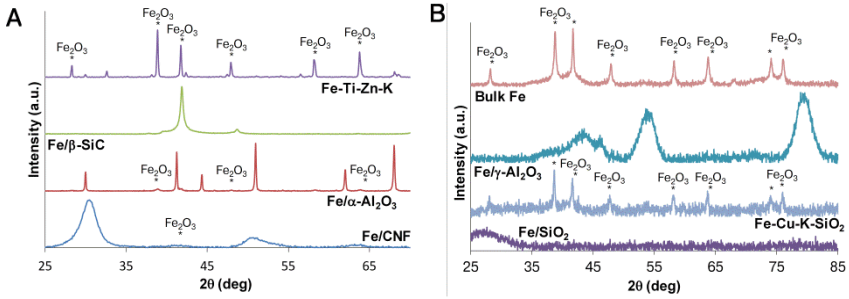

Figure 2. X-ray diffraction of supported and bulk Fe catalysts. Diffraction lines related to iron were not observed in catalysts supported on β-SiC (**A**), γ-Al2O3 and SiO2 (**B**).

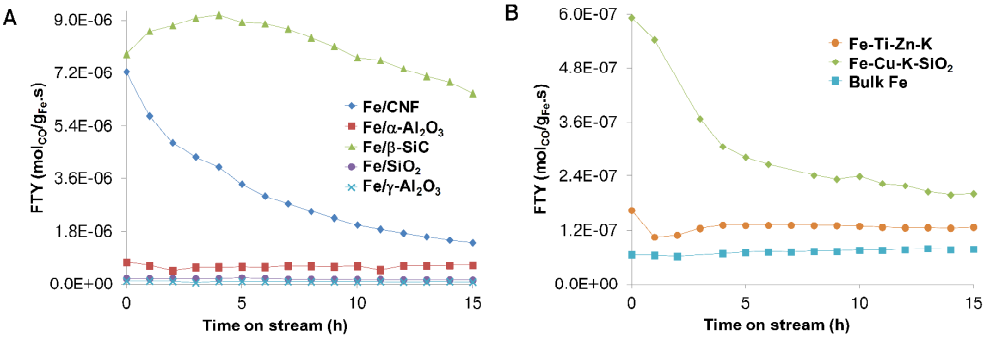

Figure 3. Catalytic activity as a function of time of iron catalysts for the Fischer-Tropsch to Olefins process at 1 bar. Catalytic activity was measured at T = 350°C, P = 1 bar, H2/CO ratio of 1, and low CO conversion levels (0.5-1%). (**A**), Iron time yield for supported Fe catalysts. (**B**), Iron time yield as a function of time on stream (TOS) for Fe bulk catalysts.

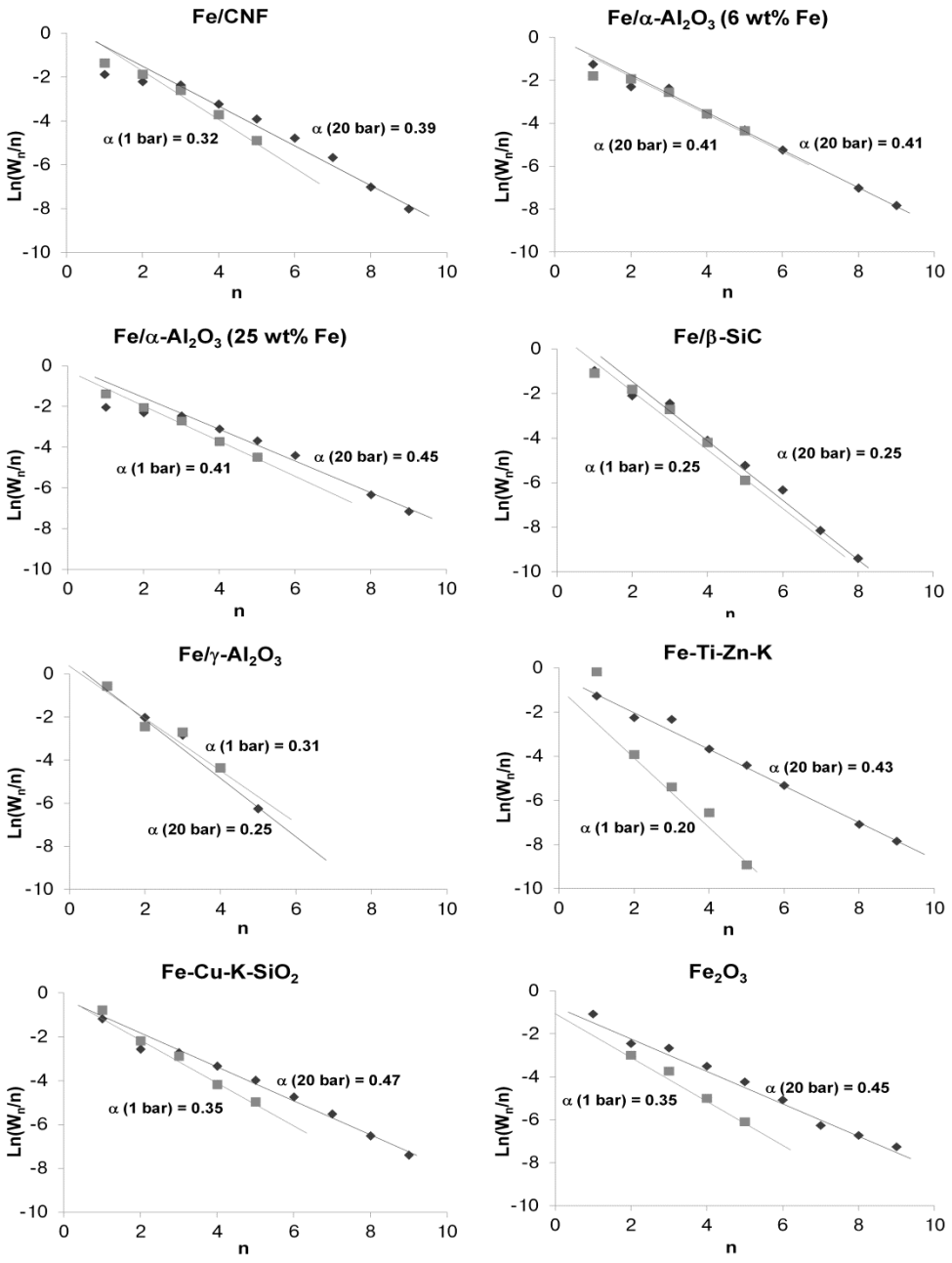

Figure 4. Anderson-Schulz-Flory plots. (■) Product distribution at 350°C, 1 bar and H_2/CO ratio of 1 (TOS = 15 h). (◆) Product distribution at 340°C, 20 bar and H_2/CO ratio of 1 (TOS = 64 h). W_n is the weight fraction of a product with n number of carbon atoms; α is the chain growth probability and $1-\alpha$ is the probability of chain termination.

Table 1. Catalytic results from the literature on supported iron catalysts tested under high temperature conditions.

Catalyst	Fe (wt%)	P (bar)	T (°C)	H_2/CO	CO conv. (%)	FTY ($mol_{CO\ to\ HC}/g_{Fe}.s$)	Selectivity (%C)		
							CH_4	C_2-C_4 olefins	C_{5+}
Fe/Al_2O_3 *(1)*	20	15	280	1	22	N. A.	26	9	35
Fe-Pr/HT γ-Al_2O_3 *(2)*	2	8	280	0.5	5.4*	$1.95x10^{-5}$	5	51	42
Fe-Pr/HT γ-Al_2O_3 ** (TOS = 64 h)	2	20	350	1	18	$4.3x10^{-5}$	42	23	8
Fe/AC *(3)*	4	10	275	1	2.24*	$1.7x10^{-5}$‡	35	38†¶	9
Fe/AC *(4)*	4.4	1	350	1	2.3	$1.6x10^{-4}$‡ $4.6x10^{-5}$§	18	60†#	5
Fe/CNT *(5)*	10.8	20	275	2	86	N. A.	9	13	70
Fe-Mn/C *(6)*	1.53	1	309	3	1.3*	N. A.	38	39	0
Fe-Ru-K/CNT *(7)*	9.8	8	275	2	25	$1.0x10^{-4}$	15	N. A.	46
Fe-K/C spheres *(8)*	8.9	8	275	2	N.A.	$1.8x10^{-5}$	3	4	92

* CO converted to hydrocarbons; † Selectivity towards C_2 and C_3 olefins; ‡ Initial activity; § Iron time yield after 20 h; N.A. = data not available.

**This sample was prepared in our laboratory according to the procedure described by Baker *et al.(2)* and tested for comparison under our reaction conditions.

Please note that the activated carbon supported systems deactivated rapidly: ¶ the activity of this catalyst decreased 50% from its initial value after 17 h (H_2/CO ratio of 3) and # for this catalyst, activity decreased 71% after 20 h.

References

1. J. Barrault, C. Forquy, J. C. Menezo, R. Maurel, *React. Kinet. Catal. Lett.* **15**, 153-158 (1980).
2. B. G. Baker, N. J. Clark, H. Macarthur, E. Summerville, WO8400702 (1984).
3. J. M. Martín-Martínez, M. A. Vannice, *Ind. Eng. Chem. Res.* **30**, 2275 (1991).
4. A. P. B. Sommen, F. Stoop, K. van der Wiele, *Appl. Catal.* **14**, 277-288 (1985).
5. R. M. Malek Abbaslou, A. Tavasoli, A. K. Dalai, *Appl. Catal. A* **355**, 33-41 (2009).
6. J. Venter, M. Kaminsky, G. L. Geoffroy, M. A. Vannice, *J. Catal.* **105**, 155-162 (1987).
7. M. C. Bahome *et al.*, *Appl. Catal. A* **328**, 243-251 (2007).
8. H. Xiong, M. Moyo, M. A. M. Motchelaho, L. L. Jewell, N. J. Coville, *Appl. Catal. A* **388**, 168-178 (2010).

Table 2. Iron loading and average Fe_2O_3 crystallite size of fresh Fe catalysts.

Sample	Fe_2O_3 crystallite size* (nm)	Fe loading† (wt%)
Fe/CNF	7	12
Fe/α-Al_2O_3	21	13
Fe/β-SiC	N.A.	8
Fe/SiO_2	N. A.	13
Fe/γ-Al_2O_3	N. A.	13
Fe-Ti-Zn-K	50	72
Fe-Cu-K-SiO_2	40	32
Bulk Fe	30	63

N. A.: Not applicable

* Determined by X-ray diffraction (XRD).

† Determined by X-ray fluorescence (XRF).

Table 3. Elemental analysis of the fresh catalysts determined with XRF (X-Ray Fluorescence).

Sample	Na (wt%)	Al (wt%)	Si (wt%)	Ca (wt%)	Sx (wt%)	Mn (wt%)	K (wt%)	Cr (wt%)
Fe/α-Al_2O_3 (12 wt%)	0.594	43.19	0.14	0.022	0.132	0.049	-	0.025
Fe/β-SiC	0.245	0.091	41.42	0.028	0.045	0.036	-	0.015
Fe/SiO_2	0.473	0.060	37.79	-	0.052	0.057	-	0.023
Fe/γ-Al_2O_3	0.496	42.28	0.137	-	0.062	0.057	-	0.020
Fe-Cu-K-SiO_2	-	0.090	19.5	-	-	-	8.05	-
Bulk Fe	-	0.036	0.238	0.017	-	-	-	-

Mössbauer Spectroscopy

The Mössbauer spectral contributions consisting of quadrupole-split center lines are assigned to high-spin Fe^{3+} in an octahedral environment and, most likely, correspond to superparamagnetic Fe_2O_3 in the fresh samples. In magnetic nanocrystals with dimensions lower than 13.5 nm *(1,2)* the thermal energy is high enough to induce the random fluctuation of the magnetic moments, cancelling out the magnetic ordering. At low temperatures or in larger particles, the coupling forces prevail over the thermal energy, causing the magnetic moments of neighboring atoms to align and the Mössbauer spectra becomes magnetically split (hyperfine sextuplets are observed).

References

1. Liu, T., Guo, L., Tao, Y., Wang, Y. B. & Wang, W. D. *Nanostruct. Mater.* **11**, 487-492 (1999).
2. Bukur, D. B., Koranne, M., Lang, X., Rao, K. R. P. M. & Huffman, G. P. *Appl. Catal. A* **126**, 85-113 (1995).

Table 4. Mössbauer parameters of fresh Fe catalysts. Experimental uncertainties: Isomer shift: IS ± 0.01 $mm.s^{-1}$; Quadrupole splitting: QS ± 0.01 $mm.s^{-1}$; Line width: Γ ± 0.01 $mm.s^{-1}$; Hyperfine field: ± 0.1 T; Spectral contribution: ±3%.

Sample	IS ($mm.s^{-1}$)	QS ($mm.s^{-1}$)	Γ ($mm.s^{-1}$)	Hyperfine field (T)	Phase	Spectral Contribution (%)
Fe/CNF	0.36	0.81	0.58	-	α-Fe_2O_3 (SPM)	100
Fe/α-Al_2O_3	0.34	0.81	0.83	-	α-Fe_2O_3 (SPM)	24
	0.38	-0.21	0.46	50.8	α-Fe_2O_3	76
Fe/β-SiC	0.33	0.80	0.57	-	α-Fe_2O_3 (SPM)	82
	0.39	-0.14	1.32	47.0*	α-Fe_2O_3	18
Fe/SiO_2	0.34	0.90	0.51	-	α-Fe_2O_3 (SPM)	97
	0.39	-0.20	0.51	51.7	α-Fe_2O_3	3
Fe/γ-Al_2O_3	0.31	0.97	0.57	-	α-Fe_2O_3 (SPM)	100
Fe-Ti-Zn-K	0.39	0.56	0.45	-	α-Fe_2O_3 (SPM)	9
	0.38	-0.21	0.50	50.2	α-Fe_2O_3	91
Fe-Cu-K-SiO_2	0.33	0.73	0.49	-	α-Fe_2O_3 (SPM)	87
	0.40	-0.21	0.47	51.8	α-Fe_2O_3	13
Bulk Fe	0.33	0.72	0.51	-	α-Fe_2O_3 (SPM)	67
	0.39	-0.23	0.48	51.6	α-Fe_2O_3	33

* Mean magnetic hyperfine field.

Table 5. Mössbauer parameters of spent Fe catalysts after 15 h of reaction at T = 350°C, P = 1 bar and H_2/CO ratio of 1. Experimental uncertainties: Isomer shift: IS ± 0.01 $mm.s^{-1}$; Quadrupole splitting: QS ± 0.01 $mm.s^{-1}$; Line width: Γ ± 0.01 $mm.s^{-1}$; Hyperfine field: ± 0.1 T; Spectral contribution: ±3%.

Sample	IS ($mm.s^{-1}$)	QS ($mm.s^{-1}$)	Γ ($mm.s^{-1}$)	Hyperfine field (T)	Phase	Spectral Contribution (%)
Fe/CNF	0.21	-	0.71	16.4	χ-Fe_5C_2 (I)	6
	0.28	-	0.71	20.3	χ -Fe_5C_2 (II)	6
	0.23	-	0.71	10.1	χ -Fe_5C_2 (III)	3
	0.31	0.74	0.71	-	Fe^{3+}	85
Fe/α-Al_2O_3	0.20	-	0.38	18.0	χ-Fe_5C_2 (I)	31
	0.26	-	0.35	21.4	χ -Fe_5C_2 (II)	28
	0.22	-	0.45	10.7	χ -Fe_5C_2 (III)	20
	0.32	0.98	0.70	-	Fe^{3+}	21
Fe/β-SiC	0.37	0.96	0.78	-	Fe^{3+}	66
	0.19	-	0.44	18.5	χ-Fe_5C_2 (I)	14
	0.25	-	0.44	21.9	χ -Fe_5C_2 (II)	13
	0.29	-	0.41	10.9	χ -Fe_5C_2 (III)	7
Fe/SiO_2	0.34	1.04	0.63	-	Fe^{3+}	100
Fe/γ-Al_2O_3	0.35	0.98	0.73	-	Fe^{3+}	90
	0.85	2.38	0.70	-	Fe^{2+}	10
Fe-Ti-Zn-K	0.23	-	0.77	18.1	χ-Fe_5C_2 (I)	18
	0.28	-	0.72	21.7	χ -Fe_5C_2 (II)	17
	0.24	-	0.41	11.5	χ -Fe_5C_2 (III)	7
	0.44	0.50	0.55	-	Fe^{3+}	8
	0.70	2.00	0.53	-	Fe^{2+}	5
	0.30	-	0.58	46.9*	Fe_3O_4 (I)	12
	0.68	-	0.54	44.1*	Fe_3O_4 (II)	8
	0.57	-	2.01	36.6*	Fe_3O_4 (II)†	25

* Mean magnetic hyperfine field; † Smear sextet.

Table 6. Catalytic performance at 20 bar. Catalytic tests performed at 340°C and H_2/CO ratio of 1; results after 64 h on stream.

Sample	Total CO conversion (%)	CO_2 (% of CO converted)	Chain growth probability α
Fe/CNF	88	42	0.39
Fe/α-Al_2O_3 (6 wt% Fe)	77	46	0.41
Fe/α-Al_2O_3 (12 wt% Fe)	81	41	0.39
Fe/α-Al_2O_3 (25 wt% Fe)	80	40	0.45
Fe/β-SiC	77	42	0.25
Fe/γ-Al_2O_3	10	20	0.25
Fe-Ti-Zn-K	79	41	0.43
Fe-Cu-K-SiO_2	79	37	0.47
Bulk Fe	97	34	0.45

$$CO + 2H_2 \rightleftarrows (-CH_2-) + H_2O \quad \mathbf{A}$$

$$CO + H_2O \rightleftarrows CO_2 + H_2 \quad \mathbf{B}$$

$$2CO + H_2 \rightleftarrows (-CH_2-) + CO_2 \quad \mathbf{C}$$

Equation 1. Reaction equations. (**A**), General Fischer-Tropsch reaction. (**B**), Water gas shift (WGS) reaction. (**C**), Overall Fischer-Tropsch reaction valid on catalysts with WGS activity such as iron.

Appendix B

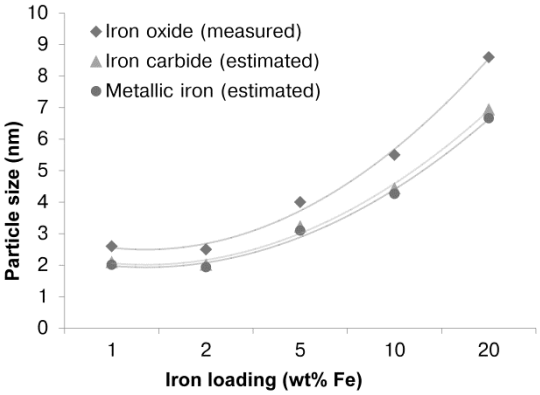

Figure 1. Iron oxide and carbide particle sizes as a function of iron loading. The average Fe_2O_3 particle size determined from TEM analysis increases with the increase of iron loading for samples prepared by impregnation.

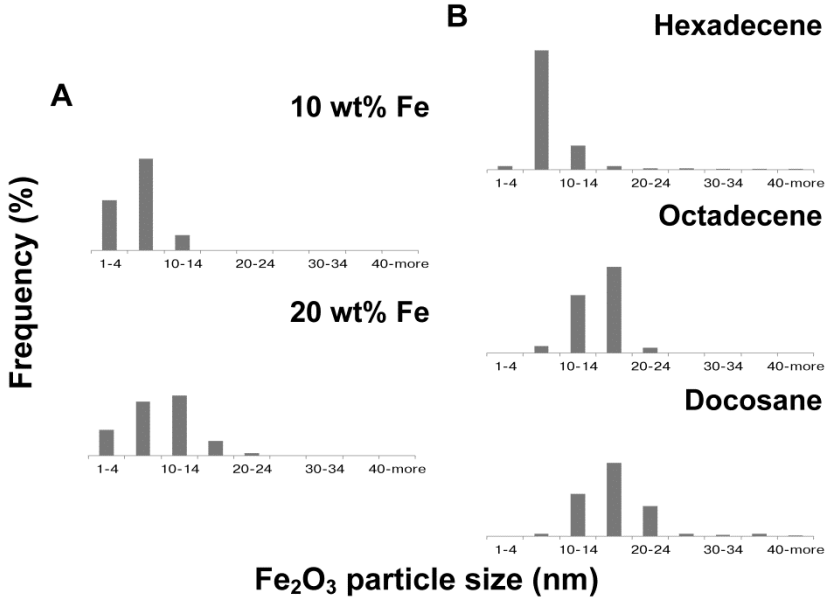

Figure 2. Particle size distribution of iron oxide. TEM analysis was used to determine the size distribution of Fe_2O_3 particles supported on CNF. (**A**) Samples prepared by incipient wetness impregnation; (**B**) Samples prepared with colloidal synthesis using different solvents; Top: Hexadecene, Middle: Octadecene; Bottom: Docosane.

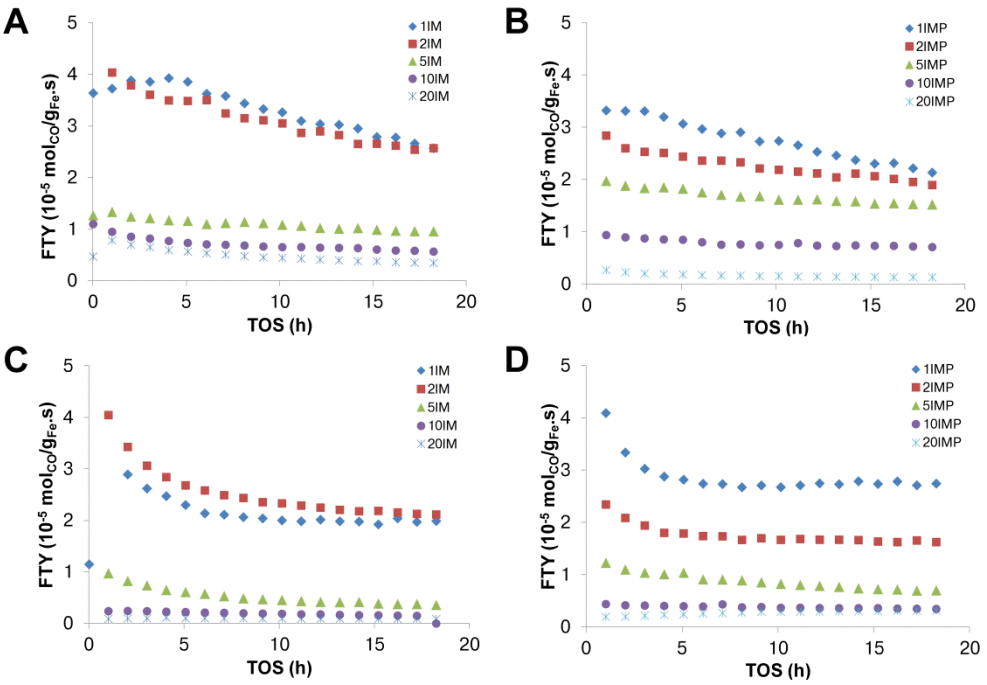

Figure 3. Iron time yield (FTY) as a function of time on stream. The activity of Fe/CNF catalysts decreased with an increase in iron carbide particle size. Results at 250°C: (**A**) unpromoted; (**B**) promoted. Results at 350°C: (**C**) unpromoted; (**D**) promoted. The reaction was performed at 1 bar and H_2/CO = 1 v/v.

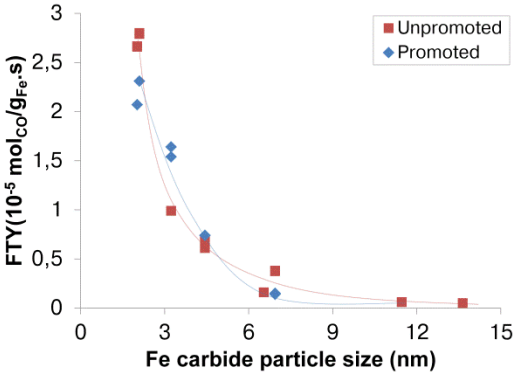

Figure 4. Iron time yield (FTY) as a function of particle size (TOS = 15 h). The activity of Fe/CNF catalysts (unpromoted (■); promoted (◆)) decreased with an increase in iron particle size. The reaction was performed at 250°C, 1 bar and H_2/CO = 1 v/v.

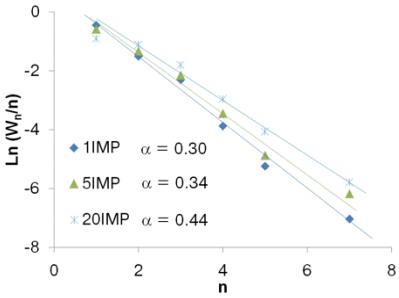

Figure 5. Anderson-Schulz-Flory (ASF) plots for promoted Fe/CNF catalysts. The reaction was performed at 350°C, 1 bar and a H_2/CO ratio of 1 (v/v). The results reported here were measured after 15 h of reaction. W_n is the weight fraction of a product with n number of carbon atoms; α is the chain growth probability.

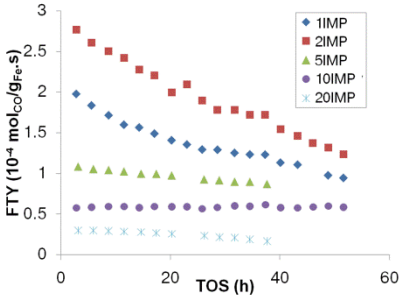

Figure 6. Iron time yield as a function of time on stream for promoted catalysts. The reaction was carried out at 340°C, 20 bar and a H_2/CO ratio of 1 (v/v).

Table 1. Average iron carbide particle sizes of selected spent catalysts determined by TEM analysis

Sample	Fe carbide size (nm)	
	1 bar, 350°C, TOS = 20 h	20 bar, 340°C, TOS = 40 h
1IMP	2.2 ± 0.8	3.1 ± 1.7
2IMP	3.1 ± 3.0	N.M.
5IMP	3.4 ± 1.5	11.1 ± 6.4
10IMP	5.1 ± 2.4	N.M.
20IMP	8.9 ± 4.0	13.5 ± 9.5

N.M.: Not measured

Table 2. Catalytic activity of promoted supported iron catalysts under FTO conditions (20 bar, 340°C, and H_2/CO = 1) and composition of iron phases after reaction (1 bar, 350°C, H_2/CO = 1, TOS = 20h)

Sample	Fe carbide size (nm)[a]	FTY (10^{-5} $mol_{CO}/g_{Fe}.s$)[b]	TOFx10 (s^{-1})[b]	Iron phase composition[c]		
				Carbides	Fe^{2+} [d]	Fe^{3+} [e]
Fe/CNF	~4	1.54	0.13	33	28	39
Fe/AC	< 4	0.33	0.03	29	55	16
Fe/γ-Al_2O_3	< 4	0.16	0.01	0	88	12

Note: The catalysts were prepared by incipient wetness impregnation of ammonium iron citrate. Nominal Fe loading: 10 wt%.

[a] Estimated sizes; [b] Determined at TOS = 35 h; [c] Results of *in situ* Mössbauer spectroscopy measurements; [d] Possible oxidic species; [e] Possible superparamagnetic carbides.

Table 3. *In situ* Mössbauer parameters of promoted supported iron catalysts under FTO conditions (1 bar, 350°C and H_2/CO = 1). Time on stream = 15 h. Experimental uncertainties: Isomer shift: IS ± 0.01 $mm.s^{-1}$; Quadrupole splitting: QS ± 0.01 $mm.s^{-1}$; Line width: Γ ± 0.01 $mm.s^{-1}$; Hyperfine field: ± 0.1 T; Spectral contribution: ±3%.

Sample	IS ($mm.s^{-1}$)	QS ($mm.s^{-1}$)	Hyperfine field (T)	Γ ($mm.s^{-1}$)	Phase	Spectral contribution (%)
2IM	0.20	0.48	-	0.70	Fe_xC (SPM)	48
	1.09	0.54	-	1.01	Fe^{2+}	44
	0.43	0.71	-	0.30	Fe^{3+}	8
10IM	1.06	0.18	-	0.81	Fe^{2+}	51
	0.20	0.38	-	0.71	Fe_xC (SPM)	32
	0.21	-	17.8	0.51	χ-Fe_5C_2 (I)	8
	0.22	-	10.7	0.37	χ-Fe_5C_2 (III)	5
	0.23	-	20.7	0.37	χ-Fe_5C_2 (II)	4
2IMP	0.20	0.57	-	0.81	Fe_xC (SPM)	43
	0.39	0.82	-	0.61	Fe^{3+}	38
	0.90	1.09	-	1.02	Fe^{2+}	8
	0.21	-	16.4	0.43	χ-Fe_5C_2 (I)	5
	0.23	-	20.2	0.36	χ-Fe_5C_2 (II)	3
	0.22	-	9.2	0.40	χ-Fe_5C_2 (III)	3
10IMP	1.05	0.35	-	0.66	Fe^{2+}	42
	0.19	0.39	-	0.62	Fe_xC (SPM)	31
	0.21	-	17.3	0.52	χ-Fe_5C_2 (I)	10
	0.23	-	10.4	0.54	χ-Fe_5C_2 (III)	9
	0.25	-	21.2	0.49	χ-Fe_5C_2 (II)	8

Note: Fe^{2+} and Fe^{3+} are possible oxidic species.

Table 4. Comparison of initial and steady state apparent TOF

Sample	Initial Fe carbide size (nm)	Initial apparent TOF x 10 (s^{-1}) TOS = 1 h	Fe carbide size after 40 h (nm)	Steady state apparent TOF x 10 (s^{-1}) TOS = 40 h
1IMP	2.1	1.1	3.1 ± 1.7	0.8
5IMP	3.2	0.9	11.1 ± 6.4	2.6
20IMP	6.9	0.6	13.5 ± 9.5	0.6

Table 5. *In situ* Mössbauer parameters of promoted supported iron catalysts after reduction in H_2 for 2 h (1 bar, 350°C). Experimental uncertainties: Isomer shift: IS ± 0.01 $mm.s^{-1}$; Quadrupole splitting: QS ± 0.01 $mm.s^{-1}$; Line width: Γ ± 0.01 $mm.s^{-1}$; Hyperfine field: ± 0.1 T; Spectral contribution: ± 3%.

Sample	IS ($mm.s^{-1}$)	QS ($mm.s^{-1}$)	Hyperfine field (T)	Γ ($mm.s^{-1}$)	Phase	Spectral contribution (%)
2IM	0.93	1.22	-	0.94	Fe^{2+}	51
	0.39	0.74	-	0.62	Fe^{3+}	49
10IM	1.06	-	-	0.89	Fe^{2+}	84
	0.31	0.22	-	0.33	Fe^{3+}	10
	0.01	-	-	0.37	Fe^{0}	6
2IMP	0.39	0.77	-	0.70	Fe^{3+}	72
	0.90	1.40	-	0.85	Fe^{2+}	28
10IMP	1.07	0.36	-	0.75	Fe^{2+}	77
	0.32	0.26	-	0.40	Fe^{3+}	16
	0.01	-	-	0.44	Fe^{0}	7

Note: Fe^{2+} and Fe^{3+} are possible oxidic species.

Appendix C

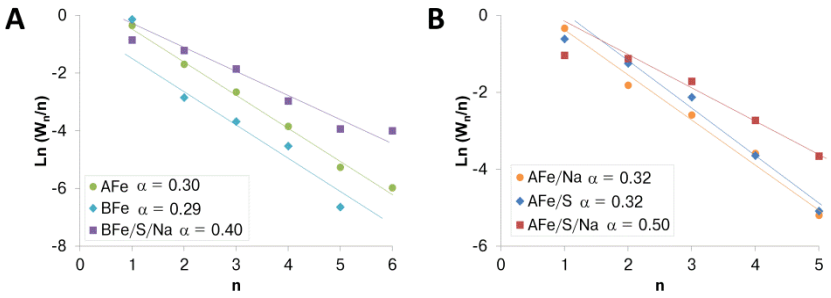

Figure 1. Anderson-Schulz-Flory plots. The catalysts were tested in the Fischer-Tropsch reaction at 350°C, 1 bar and a H_2/CO = 1. (**A**) Unpromoted and bulk promoted, (**B**) Supported promoted.

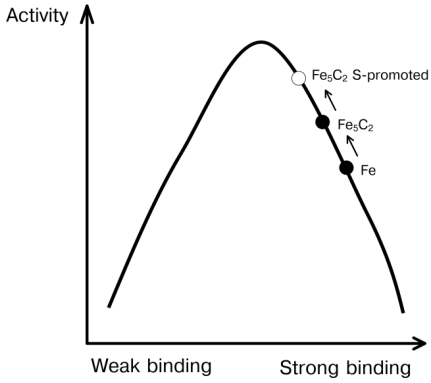

Figure 2. Volcano plot of CO hydrogenation activity versus binding strength of Fe-C. Adapted from Cheng *et al.(Ref. 31, Chapter 5)*.

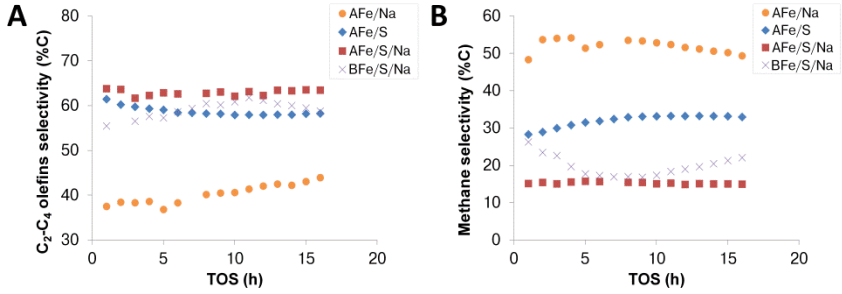

Figure 3. Product selectivity as a function of time on stream. The reaction was performed at 1 bar, 350°C and a H_2/CO ratio of 1. (**A**) Lower olefins, (**B**) Methane.

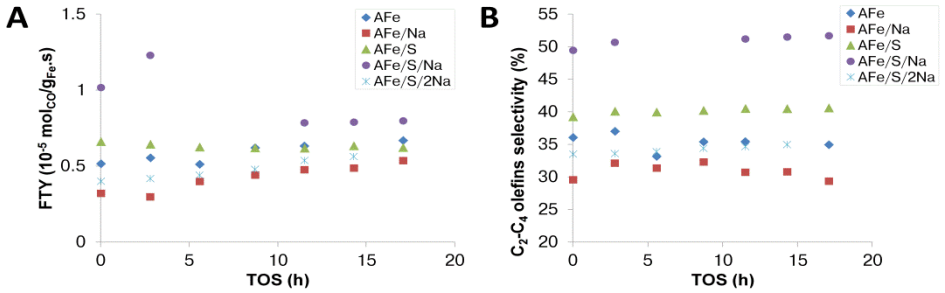

Figure 4. Catalytic activity as a function of time on stream for Fe/α-Al_2O_3 catalysts (5 wt% Fe). The reaction was performed at 20 bar, 340°C and a H_2/CO ratio of 1.

Table 1. Catalytic results from the literature on iron catalysts for the selective production of lower olefins from synthesis gas.

Catalyst	Fe (wt%)	P (bar)	T (°C)	H_2/CO	CO conv. (%)	FTY ($mol_{CO\ to\ HC}/g_{Fe}.s$)	Selectivity (%C)		
							CH_4	C_2-C_4 olefins	C_{5+}
Fe-Ti-Zn-K *(1)*	72	10	340	1	87*	N.A.	10	75	15
Fe-Ti-Zn-K¶ (TOS = 64 h)	72	20	340	1	79	$4.9x10^{-4}$	24	28	10
Fe-Pr/HT γ-Al_2O_3 *(2)*	2	8	280	0.5	5.4**	$1.95x10^{-5}$	5	51	42
Fe-Pr/HT γ-Al_2O_3¶ (TOS = 64 h)	2	20	350	1	18	$4.3x10^{-5}$	42	23	8
Fe/AC *(3)*	4.4	1	350	1	2.3	$1.6x10^{-4}$‡ $4.6x10^{-5}$§	18	60†	5
Fe-K-Mn/Silicalite-2 *(4)*	9.5	20	347	2	90.4	N.A.	22	70	8
Fe/N-CNT *(5)*	36	25	340	1	50	$3.9x10^{-4}$	8	92#	-
Fe-Na-S *(6)*	-	20	330	4	41*	N.A.	9	39	34

* Syngas conversion; ** CO converted to hydrocarbons; † Selectivity towards C_2 and C_3 olefins; ‡ Initial activity; § Iron time yield after 20 h; # olefin selectivity in the fraction C_2-C_6; HT = Heat-treated; N.A. = data not available.

¶ These samples were prepared in our laboratory according to the procedures described by Büssemeier *et al. (1)* and Baker *et al. (2)*, respectively, and tested for comparison under our reaction conditions.

References

1. B. Büssemeier, C. D. Frohning, G. Horn, W. Kluy, US Patent No. 4564642 (1986).
2. B. G. Baker, N. J. Clark, H. Macarthur, E. Summerville, International Patent Application No. WO8400702 (1984).
3. A. P. B. Sommen, F. Stoop, K. van der Wiele, *Appl. Catal.* **14**, 277-288 (1985).

4. L. Xu, Q. Wang, Y. Xu, J. Huang, *Catal. Lett.* **31**, 253-266 (1995).
5. H.J. Schulte, B. Graf, W. Xia, M. Muhler, *ChemCatChem* **4**, 350-355 (2012).
6. R. Crous, T. C. Bromfield, S. Booyens, US Patent No. 2012/0029096 A1 (2012).

Table 2. Compositions of the iron precursors determined by ICP

Sample	Ca (mg/kg)	Na (mg/kg)	K (mg/kg)	S (mg/kg)	Fe (wt%)
AIC J. T. Baker	115	753	56	759	13
AIC Fluka	128	256	46	27	14

Table 3. Mössbauer parameters of fresh iron catalysts. Experimental uncertainties: Isomer shift: IS ± 0.01 $mm.s^{-1}$; Quadrupole splitting: QS ± 0.01 $mm.s^{-1}$; Line width: Γ ± 0.01 $mm.s^{-1}$; Hyperfine field: ± 0.1 T; Spectral contribution: ±3%.

Sample	IS ($mm.s^{-1}$)	QS ($mm.s^{-1}$)	Hyperfine field (T)	Γ ($mm.s^{-1}$)	Phase	Spectral contribution (%)
AFe	0.37 0.33	-0.20 0.81	49.3 -	0.47 0.74	α-Fe_2O_3 α-Fe_2O_3 (SPM)	66 34
AFe/Na	0.37 0.33	-0.20 0.79	49.3[a] -	0.26 0.63	α-Fe_2O_3 α-Fe_2O_3 (SPM)	60 40
AFe/S	0.37 0.34	-0.20 0.81	49.6[a] -	0.24 0.59	α-Fe_2O_3 α-Fe_2O_3 (SPM)	79 21
AFe/S/Na	0.37 0.32	-0.20 0.84	49.6 -	0.41 0.66	α-Fe_2O_3 α-Fe_2O_3 (SPM)	83 17
AFe/S/2Na	0.33 0.37	0.79 -0.21	- 49.2[a]	0.59 0.23	α-Fe_2O_3 (SPM) α-Fe_2O_3	54 46
BFe	0.37 0.33	-0.20 0.79	49.2[a] -	0.25 0.78	α-Fe_2O_3 α-Fe_2O_3 (SPM)	85 15
BFe/S/Na	0.37 0.33	-0.21 0.69	49.3[a] -	0.26 0.64	α-Fe_2O_3 (SPM) α-Fe_2O_3	73 27

[a] Mean hyperfine field

Table 4. Mössbauer parameters of reduced iron catalysts. Reduction performed at 350°C and 1 bar under H_2/Ar flow for 2 h. Experimental uncertainties: Isomer shift: IS ± 0.01 mm.s^{-1}; Quadrupole splitting: QS ± 0.01 mm.s^{-1}; Line width: Γ ± 0.01 mm.s^{-1}; Hyperfine field: ± 0.1 T; Spectral contribution: ±3%.

Sample	IS (mm.s^{-1})	QS (mm.s^{-1})	Hyperfine field (T)	Γ (mm.s^{-1})	Phase	Spectral contribution (%)
AFe	1.08	0.50	-	0.63	Fe^{2+}	39
	0.33	0.68	-	0.89	Fe^{3+}	20
	0.00	-	34.4	0.37	Fe^{0}	13
	0.21	-	21.5	0.84	Fe^{3+}	10
	0.67	-	45.1	1.46	Fe_3O_4(II)	8
	0.04	-	-	0.77	Fe^{0} (SPM)	6
	0.24	-	48.6	1.46	Fe_3O_4(I)	4
AFe/Na	1.06	0.58	-	0.49	Fe^{2+}	70
	0.39	0.16	-	0.39	Fe^{3+}	11
	0.06	-	-	0.51	Fe^{0} (SPM)	11
	0.01	-	33.0	0.22	Fe^{0}	8
AFe/S	0.01	-	33.0	0.27	Fe^{0}	51
	0.98	0.46	-	0.86	Fe^{2+}	34
	0.06	-	-	0.85	Fe^{0} (SPM)	15
AFe/S/Na	1.07	0.53	-	0.52	Fe^{2+}	56
	0.00	-	34.3	0.33	Fe^{0}	18
	0.05	-	-	0.70	Fe^{0} (SPM)	8
	0.65	-	46.8	0.53	Fe_3O_4(II)	8
	0.37	-	-	0.61	Fe^{3+}	7
	0.34	-	49.9	0.31	Fe_3O_4(I)	3
AFe/S/2Na	1.06	0.63	-	0.49	Fe^{2+}	63
	0.01	-	33.0	0.23	Fe^{0}	16
	0.36	0.20	-	0.39	Fe^{3+}	12
	0.04	-	-	0.47	Fe^{0} (SPM)	9
BFe	0.01	-	33.0	0.30	Fe^{0}	79
	0.33	-	-	0.89	Fe^{3+}	13
	1.20	0.59	-	0.53	Fe^{2+}	8
BFe/S/Na	0.01	-	33.0	0.33	Fe^{0}	70
	0.33	-	-	0.85	Fe^{3+}	7
	1.08	0.64	-	0.53	Fe^{2+}	23

Table 5. Carbon lay-down measurements. Carbon burn-off experiments performed with TGA on samples tested at 20 bar, 340°C, H_2/CO = 1, GHSV = 3000 h^{-1}. *In situ* carbon lay-down measurements carried out on the TEOM at 20 bar, 350°C, H_2/CO = 1, GHSV = 180000 h^{-1}.

Sample	TGA		Initial coking rate (10^{-6} molc/g_{cat}.s) TEOM
	Carbon deposition (wt%)	TOS (h)	
AFe	2	25	0.03
AFe/Na	18	24	0.57
AFe/S	7	25	Below detection limit
AFe/S/Na	3	55	0.16
AFe/S/2Na	12	25	0.64
BFe/S/Na	24	58	7.73

Table 6. *In situ* Mössbauer parameters of promoted supported iron catalysts under FTO conditions (1 bar, 350°C and H_2/CO = 1). Time on stream = 20 h. Experimental uncertainties: Isomer shift: IS ± 0.01 $mm.s^{-1}$; Quadrupole splitting: QS ± 0.01 $mm.s^{-1}$; Line width: Γ ± 0.01 $mm.s^{-1}$; Hyperfine field: ± 0.1 T; Spectral contribution: ±3%.

Sample	IS ($mm.s^{-1}$)	QS ($mm.s^{-1}$)	Hyperfine field (T)	Γ ($mm.s^{-1}$)	Phase	Spectral contribution (%)
AFe	0.27	-	21.9	0.54	χ-Fe_5C_2 (II)	33
	0.20	-	18.9	0.51	χ-Fe_5C_2 (I)	27
	0.29	0.94	-	0.72	Fe^{3+}	21
	0.20	-	11.5	0.38	χ-Fe_5C_2 (III)	12
	1.13	0.88	-	0.66	Fe^{2+}	7
AFe/Na	0.18	-	18.2	0.48	χ-Fe_5C_2 (I)	30
	0.26	-	21.2	0.43	χ-Fe_5C_2 (II)	28
	1.02	0.48	-	0.68	Fe^{2+}	19
	0.19	0.48	-	0.68	Fe^{3+} (SPM Fe_xC)	12
	0.21	-	11.3	0.34	χ-Fe_5C_2 (III)	11
AFe/S	0.27	0.62	-	0.86	Fe^{3+} (SPM Fe_xC)	26
	0.20	-	18.3	0.39	χ-Fe_5C_2 (I)	25
	0.26	-	21.7	0.32	χ-Fe_5C_2 (II)	19
	1.05	0.28	-	0.81	Fe^{2+}	18
	0.23	-	11.1	0.39	χ-Fe_5C_2 (III)	12
AFe/S/Na	0.23	-	18.7	0.46	χ-Fe_5C_2 (I)	28
	0.28	-	22.5	0.45	χ-Fe_5C_2 (II)	28
	0.15	-	10.4	0.50	χ-Fe_5C_2 (III)	19
	1.07	0.51	-	0.58	Fe^{2+}	14
	0.19	0.73	-	0.68	Fe^{3+} (SPM Fe_xC)	11

Table 6 (continuation)

Sample	IS ($mm.s^{-1}$)	QS ($mm.s^{-1}$)	Hyperfine field (T)	Γ ($mm.s^{-1}$)	Phase	Spectral contribution (%)
AFe/S/2Na	0.19	-	18.1	0.48	χ-Fe_5C_2 (I)	27
	0.26	-	21.5	0.43	χ-Fe_5C_2 (II)	26
	1.04	0.47	-	0.68	Fe^{2+}	21
	0.24	0.39	-	0.68	Fe^{3+} (SPM Fe_xC)	14
	0.24	-	11.0	0.34	χ-Fe_5C_2 (III)	12
BFe	0.19	-	18.4	0.45	χ-Fe_5C_2 (I)	41
	0.27	-	21.5	0.37	χ-Fe_5C_2 (II)	35
	0.21	-	11.3	0.35	χ-Fe_5C_2 (III)	19
	0.29	0.34	-	0.66	Fe^{3+}	5
BFe/S/Na	0.18	-	18.4	0.47	χ-Fe_5C_2 (I)	42
	0.26	-	21.4	0.41	χ-Fe_5C_2 (II)	36
	0.22	-	11.1	0.47	χ-Fe_5C_2 (III)	22

Appendix D

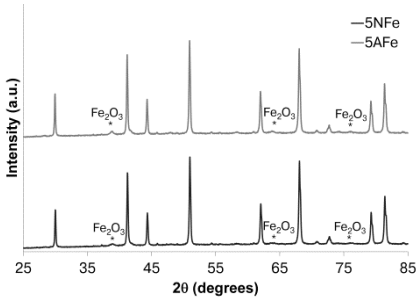

Figure 1. Diffraction patterns of fresh catalysts. Similar patterns were obtained for catalysts prepared with different iron precursors: iron nitrate (5NFe) and ammonium iron citrate (5AFe).

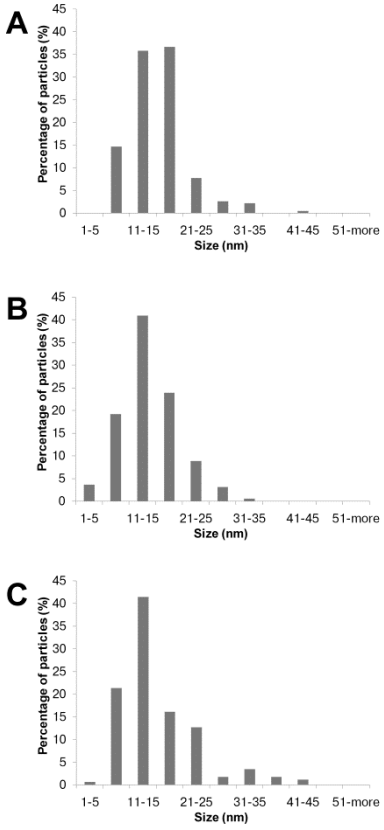

Figure 2. Particle size distribution of calcined catalysts. (**A**) 5AFe, (**B**) 5AFeP, (**C**) 5NFe.

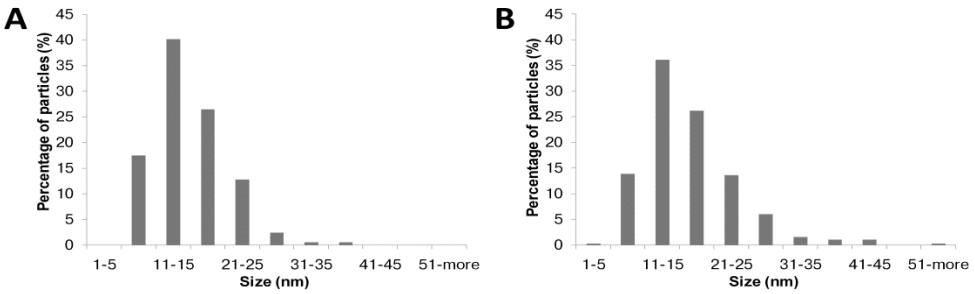

Figure 3. Particle size distribution of reduced catalysts. Reduction was carried out at 350°C, 1 bar and a H_2/Ar = 0.5 v/v. (**A**) 5AFeP, (**B**) 5NFe.

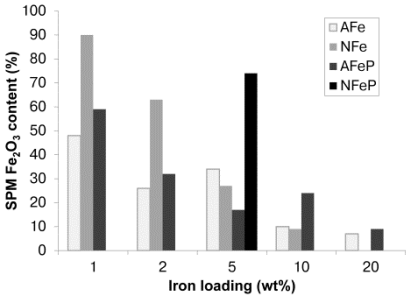

Figure 4. Content of SPM Fe_2O_3 in calcined catalysts as a function of iron loading determined by Mössbauer spectroscopy. The catalysts with lower iron loadings contained higher amounts of small Fe_2O_3 particles.

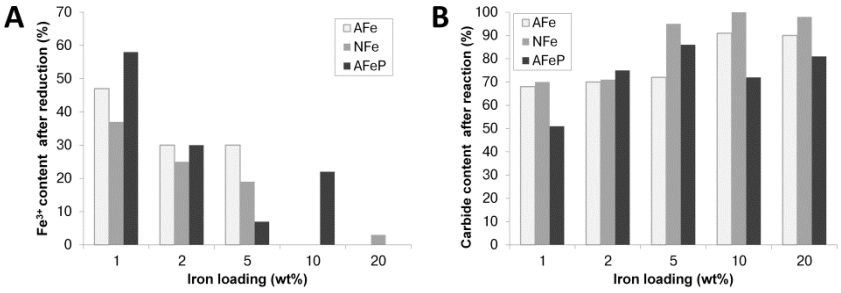

Figure 5. Fe^{3+} and carbidic content as a function of iron loading determined by *in situ* Mössbauer spectroscopy. (**A**) Reduced catalysts, (**B**) spent catalysts. The catalysts were reduced under H_2 at 1 bar and 350°C for 2 h. The spent catalysts were analyzed to determine the carbide content after reaction at 1 bar, 350°C, H_2/CO = 1 and TOS = 20 h.

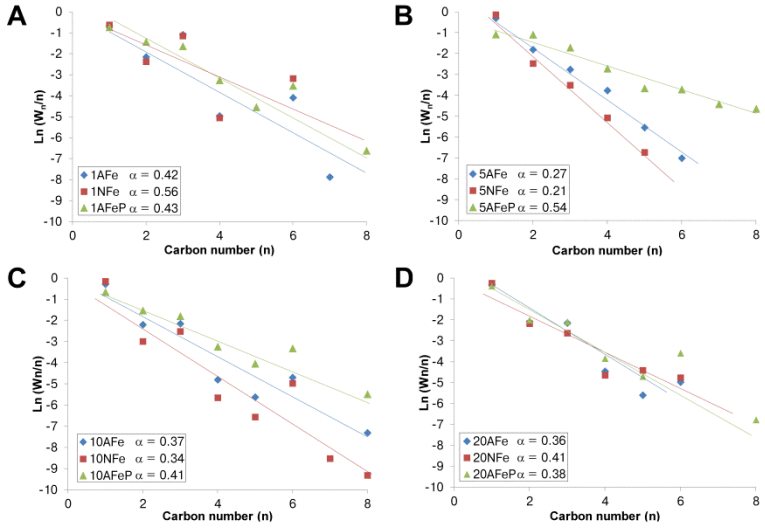

Figure 6. Anderson-Schulz-Flory plots. The catalysts were tested at 350°C, 1 bar and a H_2/CO = 1. (**A**) 1 wt% Fe, (**B**) 5 wt% Fe, (**C**) 10 wt% Fe, (**D**) 20 wt% Fe.

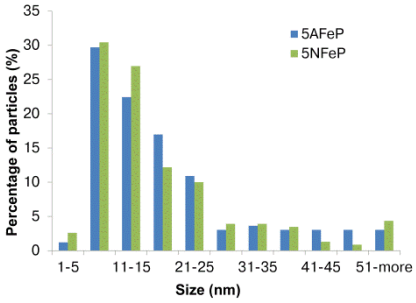

Figure 7. Particle size distribution of spent promoted catalysts. The catalysts had been used at 340°C, 20 bar and a H_2/CO = 1. Time on stream: 5AFeP = 55 h; 5NFeP = 58 h.

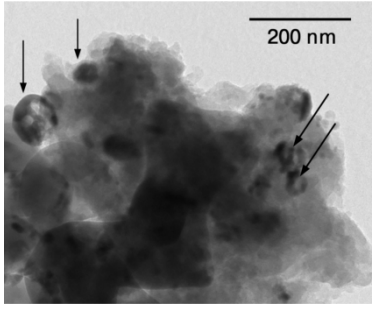

Figure 8. Magnification of fragmented iron (carbide) particles indicated by arrows (Sample 5NFeP, Figure 5C)

Table 1. Composition of iron precursor solutions (for 2 g of α-Al_2O_3 support)

Sample	Iron precursor	Mass iron salt (g)	Volume demineralized H_2O (ml)
1NFe	Iron nitrate	0.146	0.6
2NFe	Iron nitrate	0.295	0.4
5NFe	Iron nitrate	0.761	0.4
10NFe	Iron nitrate	1.607	0.8
20NFe	Iron nitrate	3.617	1.8
1AFe	Ammonium iron citrate	0.132	0.5
2AFe	Ammonium iron citrate	0.268	0.6
5AFe	Ammonium iron citrate	0.690	1.3
10AFe	Ammonium iron citrate	1.457	2.7
20AFe	Ammonium iron citrate	3.279	6.9

Note: The same amounts of ammonium iron citrate and demineralized water were used for the preparation of promoted catalysts series XAFeP.

Table 2. Compositions of the ammonium iron citrate determined by ICP

Sample	Ca (mg/kg)	Na (mg/kg)	K (mg/kg)	S (mg/kg)	Fe (wt%)
AIC J. T. Baker	115	753	56	759	13
AIC Fluka	128	256	46	27	14

Table 3. Composition of unpromoted and S and Na promoted iron catalysts.

Sample	Iron precursor	Fe loading (wt%)[a]	Na loading (wt%)	S loading (wt%)[a]
5AFe	Ammonium Fe citrate	5.0	-	-
5NFe	Iron nitrate	4.8	-	-
5AFeP	Ammonium Fe citrate	5.0	0.19[a]	0.03
5NFeP	Iron nitrate	5.0	0.22[b]	0.03

[a] Measured with ICP

[b] Nominal loading

Table 4. *In situ* Mössbauer parameters of promoted supported iron catalysts (5 wt% Fe) under FTO conditions (1 bar, 350°C and H_2/CO = 1). Time on stream = 20 h. Experimental uncertainties: Isomer shift: IS ± 0.01 $mm.s^{-1}$; Quadrupole splitting: QS ± 0.01 $mm.s^{-1}$; Line width: Γ ± 0.01 $mm.s^{-1}$; Hyperfine field: ± 0.1 T; Spectral contribution: ±3%.

Sample	IS ($mm.s^{-1}$)	QS ($mm.s^{-1}$)	Hyperfine field (T)	Γ ($mm.s^{-1}$)	Phase	Spectral contribution (%)
5AFe	0.27	-	21.9	0.54	χ-Fe_5C_2 (II)	33
	0.20	-	18.9	0.51	χ-Fe_5C_2 (I)	27
	0.29	0.94	-	0.72	Fe^{3+}	21
	0.20	-	11.5	0.38	χ-Fe_5C_2 (III)	12
	1.13	0.88	-	0.66	Fe^{2+}	7
5AFeP	0.23	-	18.7	0.46	χ-Fe_5C_2 (I)	28
	0.28	-	22.5	0.45	χ-Fe_5C_2 (II)	28
	0.15	-	10.4	0.50	χ-Fe_5C_2 (III)	19
	1.07	0.51	-	0.58	Fe^{2+}	14
	0.19	0.73	-	0.68	Fe^{3+} (SPM Fe_xC)	11
5NFe	0.19	-	18.4	0.45	χ-Fe_5C_2 (I)	35
	0.26	-	21.2	0.40	χ-Fe_5C_2 (II)	32
	0.19	-	11.4	0.34	χ-Fe_5C_2 (III)	15
	0.24	0.78	-	0.83	Fe^{3+} (SPM Fe_xC)	13
	1.10	0.99	-	0.54	Fe^{2+}	5
5NFeP	0.19	-	18.0	0.41	χ-Fe_5C_2 (I)	27
	0.27	-	21.5	0.40	χ-Fe_5C_2 (II)	27
	0.27	0.43	-	0.94	Fe^{3+} (SPM Fe_xC)	19
	0.21	-	10.9	0.44	χ-Fe_5C_2 (III)	14
	1.07	0.42	-	0.70	Fe^{2+}	13

Note: After reaction the spent catalysts showed the presence of iron carbides (χ-Fe_5C_2, SPM Fe_xC) and iron in oxidic form (Fe^{2+}, Fe^{3+}).

List of publications and presentations

Publications

H. M. Torres Galvis and K. P. de Jong, **Catalysts for production of lower olefins from synthesis gas: A review.**
ACS Catal. (2013), http://dx.doi.org/10.1021/cs4003436

H. M. Torres Galvis, A. C. J. Koeken, J. H. Bitter, T. Davidian, M. Ruitenbeek, A. Iulian Dugulan and K. P. de Jong, **Effect of precursor on the catalytic performance of supported iron catalysts for the Fischer-Tropsch synthesis of lower olefins.**
Catal. Today (2013), http://dx.doi.org/10.1016/j.cattod.2013.03.018

H. M. Torres Galvis, A. C. J. Koeken, J. H. Bitter, T. Davidian, M. Ruitenbeek, A. Iulian Dugulan and K. P. de Jong, **Effects of sodium and sulfur on catalytic performance of supported iron catalysts for the Fischer-Tropsch synthesis of lower olefins.**
J. Catal. **303** (2013) 22-30.

H. M. Torres Galvis, J. H. Bitter, T. Davidian, M. Ruitenbeek, A. Iulian Dugulan and K. P. de Jong, **Iron Particle Size Effects for Direct Production of Lower Olefins from Synthesis Gas**.
J. Am. Chem. Soc. **134** (2012) 16207-16215.

A. C. J. Koeken, H. M. Torres Galvis, T. Davidian, M. Ruitenbeek and K. P. de Jong, **Suppression of Carbon Deposition in the Iron-Catalyzed Production of Lower Olefins from Synthesis Gas**.
Angew. Chem. Int. Ed. **51** (2012) 7190-7193.

H. M. Torres Galvis, J. H. Bitter, C. B. Khare, M. Ruitenbeek, A. Iulian Dugulan and K. P. de Jong, **Supported Iron Nanoparticles as Catalysts for Sustainable Production of Lower Olefins**.
Science **335** (2012) 835-838. Featured in *ChemCatChem* **4** (2012) 751-752.

B. Luigjes, S. M. C. Woudenberg, R. de Groot, J. D. Meeldijk, H. M. Torres Galvis, K. P. de Jong, A. P. Philipse and B. H. Erné, **Diverging Geometric and Magnetic Size Distributions of Iron Oxide Nanocrystals.**
J. Phys. Chem. C **115** (2011) 14598-14605.

Production of lower olefins from synthesis gas,
H. M. Torres Galvis, J. H. Bitter and K. P. de Jong. Patent applications EP 2 314 557 A1 and WO 2011/049456 A1 (2011).

Oral presentations

H. M. Torres Galvis, A. C. J. Koeken, M. Ruitenbeek, A.I. Dugulan, J. H. Bitter and K. P. de Jong, *Stable, Selective and active iron catalysts for the production of lower olefins from synthesis gas,* 23rd North American Catalysis Society Meeting 2013, Louisville, Kentucky, USA, June 2013.

H. M. Torres Galvis, A. I. Dugulan, J. H. Bitter and K. P. de Jong, *Na plus S promoted Fe catalysts for the selective production of lower olefins from synthesis gas,* 15th International Congress on Catalysis 2012, München, Germany, July 2012.

H. M. Torres Galvis, A. I. Dugulan, J. H. Bitter and K. P. de Jong, *Na plus S promoted Fe catalysts for the selective production of lower olefins from synthesis gas,* SynFuel 2012, München, Germany, June 2012 (Keynote lecture).

H. M. Torres Galvis, A. I. Dugulan, J. H. Bitter and K. P. de Jong, *Supported iron-based catalysts for the Fischer-Tropsch synthesis of lower olefins,* 2012 American Institute of Chemical Engineers Spring Meeting, Houston, Texas, USA, April 2012.

H. M. Torres Galvis, A. I. Dugulan, J. H. Bitter and K. P. de Jong, *Supported iron-based catalysts for the Fischer-Tropsch synthesis of lower olefins,* 13th Netherlands' Catalysis and Chemistry Conference, Noordwijkerhout, The Netherlands , March 2012.

H. M. Torres Galvis, J. H. Bitter and K. P. de Jong, *Supported iron-based catalysts for the Fischer-Tropsch synthesis of lower olefins,* TransACTS symposium, Lunteren, The Netherlands, January 2012 (Plenary lecture).

H. M. Torres Galvis, J. H. Bitter and K. P. de Jong, *Stable iron catalysts for the selective production of lower olefins from synthesis gas*, Europacat X, Glasgow, Scotland, August-September 2011.

H. M. Torres Galvis, A. C. J. Koeken, J. H. Bitter and K. P. de Jong, *Supported iron-based catalysts for the Fischer-Tropsch synthesis of lower*

olefins, 2011 American Institute of Chemical Engineers Spring Meeting, Chicago, Illinois, USA, March 2011.

H. M. Torres Galvis, A. I. Dugulan, J. H. Bitter and K. P. de Jong, *Iron-based catalysts for the Fischer-Tropsch synthesis of lower olefins studied by Mössbauer spectroscopy*, 12th Netherlands' Catalysis and Chemistry Conference, Noordwijkerhout, The Netherlands, February-March 2011.

H. M. Torres Galvis, J. H. Bitter and K. P. de Jong, *Supported Iron-based catalysts for the Fischer-Tropsch synthesis of lower olefins*, 11th Netherlands Catalysis and Chemistry Conference, Noordwijkerhout, The Netherlands, March 2010.

Poster presentations

H. M. Torres Galvis, A. C. J. Koeken, M. Ruitenbeek, A. I. Dugulan, J. H. Bitter and K. P. de Jong, *Stable, selective and active iron catalysts for the production of lower olefins from synthesis gas*, 10th Novel Gas Conversion Symposium, Doha, Qatar, March 2013.

H. M. Torres Galvis, , J. H. Bitter and K. P. de Jong, *Novel iron catalysts for the selective production of lower olefins from synthesis gas*, 22nd North American Catalysis Society Meeting, Detroit, Michigan, USA, June 2011.

H. M. Torres Galvis, J. H. Bitter and K. P. de Jong, *Highly dispersed iron on carbon nanofibers for the Fischer-Tropsch synthesis of lower olefins*, 9th Novel Gas Conversion Symposium, Lyon, France, May-June 2010.

Acknowledgements

When it comes to thank people for all their support and help it is difficult to fit the words in just a couple of pages, especially after meeting so many wonderful people through all these years.

I would like to start thanking my supervisors Krijn de Jong and Harry Bitter. Harry, I am very glad I had the chance to work with you. You helped me very much when I started in the group and you were always available for me when I needed advice. We are missing your jokes and good humor in the group. I wish you great success in your new position in Wageningen.

Krijn, I appreciate dearly everything I have learned under your tuition, not only the scientific and technical knowledge but also other professional and personal skills from which I am sure I will profit in the future. You are a great example as a scientist, a manager and a family man. I would like to thank you for giving me the opportunity of being part of the Inorganic Chemistry and Catalysis group. I still remember when I applied for the Ph.D. position I mentioned that I would be honored to work with you and your staff. Indeed, I am honored to work in a group with professors who are top in their respective fields and with many young talented researchers. I feel very proud of this.

All of the high quality research done in the group is possible not only by a deep understanding of science but also by having solid technical support. For this reason I would like to give special thanks to Ad Mens, Ad van der Eerden, Fouad, Marjan, Vincent, Rien, Monique and Dymph. I appreciate very much your willingness to help, your patience and your diligence. I also would like to acknowledge the great work of Cor and Hans while analyzing and imaging my samples with TEM.

During my project I had the opportunity of collaborating with people outside the group who contributed greatly to its success. First, I would like to express my gratitude for the input and hard work of Matthijs Ruitenbeek and his team at Dow Benelux in Terneuzen. Matthijs, I am very grateful to you for all the fruitful discussions, the time you took to schedule and supervise the experiments that we performed at Dow and your immense contribution to our papers. It has been a pleasure to work with you and your people. Many thanks to Thomas, Chaitya, Adam and Ard for their help and their involvement in the project and to the technical staff from Dow that took care of the experimental part.

I am also very thankful to Iulian Dugulan from TU Delft for his contribution with the analysis of my samples with Mössbauer spectroscopy. Iulian, your participation in this project has been crucial.
I would like to acknowledge the ACTS-ASPECT program not only for their financial support but also for giving me the opportunity to meet and discuss with our industrial partners and to learn from their experience. Many thanks to all the Industrial Contact Group members for their input and suggestions: Leon van de Oetelaar from Albemarle, Peter Berben from BASF, Marcel Janssen from Exxon Mobil, Michiel Verhaak from Shell, and Mike Watson and Leon van de Water from Johnson Matthey. I would like to thank as well Robert Terörde (BASF) for the nice discussions during the ASPECT meetings.
My time in the group has been wonderful; I have fulfilled many scientific and professional achievements and at the same time, I have enjoyed a very friendly and warm working atmosphere. I have to thank Johan and Emiel for helping me when I just arrived to the group with learning how to use the setup, how to prepare the catalysts and how to do the FT magic.
Ard, thank you very much for your help. I appreciate very much your contribution to my work and all the times that we fought the green monster in the DA room ☺. Thanks for solving my questions and for all the nice discussions.
Many thanks to Peter Munnik for translating my summary (in view of my still incipient Dutch level). Volgende keer ga ik proberen om in het Nederlands te schrijven!.
I want to give recognition to the work of my students Daan, Daniel, Anna and Huub. Also, I would like to thank Ana Raquel and Sophia for their contribution.
Since I have been around for such a long time, I have managed to switch offices three times (!!). It has been a good chance to share my space with many great colleagues and friends: Adri, Inge, Rene, Upakul, Peter Munnik, Jinbao, Peter Hausoul, Bart, Ilona, Davide, Mustafa, Inés G. and Inés L. Thanks to all for making the working space a great place to be.
Sometimes in life there are dark moments when one can feel a bit hopeless. I am glad that during those times I had the help of so many friends that lend me a hand when I needed it most. Many, many, many thanks to Adri, Inge, Davide, María, Oscar, Karin, Liz, Juan, Nicole and Ana Raquel. I will never forget what you have done for me. Infinite thanks to Diana (mi alma

compañera), Gilito and Casitas for being there for me no matter time difference and distance between us.
Now I would like to mention special thanks to the moving crew: Javi, Sandra, Gonzalo, Fernando, Joe, Rob, Dilek, Jinbao, Inés G., Oscar, Karin, Peter N. and Wenhao. Thanks guys for helping us moving our things to our new little mansion, for painting walls and installing lamps in less than a day… We wouldn't have been able to make it without your help.
It has been a fantastic journey, full of enjoyable moments in conferences and also in social events: Thanks to Carlo, Jovana, Tamara, Zoran, Luis, Eduardo, Qingyun, Siswati, Nadia, Agnieska, Ignacio, Philipp, Sankara, Elena, Clare, Sonia, and many others for the these wonderful times.
There is a special place in my heart for two amazing friends: Upakul Deka and Peter Ngene. Guys, you have been more than friends to me. You're family. Peter, thank you very much for all your support, for taking care of me, for helping me so many times and praying for me and my family like a real brother. I miss our long talks and I am very grateful for your friendship. I hope God fills your life (and of course, Oge, Armstrong and little Deborah) with many more blessings.
Deka…no words…only laughs. We've had so many nice moments and I will cherish them forever. Thanks for taking care of me: watching out what I ate while we were in München, tying my shoelaces when I couldn't reach my feet, playing bodyguard while David was away, and just for making me laugh so much. I hope we keep on sharing happy times like those.
I would like to thank my supervisors during my Master studies in TU Eindhoven, Patrick Wenmakers and John van der Schaaf, for taking me closer to the catalysis world and for teaching me so many things that have been very useful during my PhD.
My last few paragraphs are dedicated to my family and the people that have supported me all along, believing in me and helping me to realize my dreams.
Sra. Ofelia Castro: muchas gracias por el apoyo y todas las cosas que aprendí durante mi tiempo en Plastinova. Agradezco mucho su generosidad y su comprensión.
Signor Valente: Jamás olvidare todo lo que ha hecho por mí. Si no fuera por su gran generosidad nunca hubiera podido alcanzar este sueño. Le agradezco mucho por toda su ayuda y espero que algún día pueda retribuirle aunque sea un poco. Muchas gracias a usted, a la Signora Lucia y a Barbara por hacerme sentir parte de la familia cada vez que estuve en Segrate. Grazie di tutto cuore.

También quiero dar gracias especiales a mis suegros, María Teresa y Darío. Les agradezco mucho por su cariño, su generosidad y por apoyarnos cuando lo hemos necesitado.
Nada de esto hubiera sido posible sin el apoyo y el amor de mis padres. Pap y madrecilla pilla: les agradezco mucho por todo lo que me han dado. No tengo palabras para expresar cuanto los amo y cuanto aprecio su esfuerzo. Soy una mejor persona gracias a ustedes, a su buen ejemplo y su dedicación. Espero que estén tan orgullosos de mí como yo lo estoy de ustedes. Gracias por creer en mí y por sus enseñanzas que son más valiosas que el oro y las riquezas materiales. Espero que algún día mis hijos lleguen a apreciarme tanto como yo los amo y los extraño.
Last but not least… to my little family: Cami, Mariana y David. My little princesses: I am so lucky to have you by my side. Sometimes, when things make no sense, I just have to look at you, with your beautiful big eyes and amazing smiles, to find the light. Thanks for behaving so well when mom had to work at home.
Esposito: thanks for taking care of the girls and our house when I had to work late or during the weekends. Without your help all of this would have been even tougher. I hope we can celebrate soon that there are two new doctors in the family. Un besote.

Curriculum Vitae

Hirsa M. Torres Galvis was born on the 5th of May 1979 in Bogotá, Colombia. She completed secondary school education in 1995 from Colegio San José in Bogotá, Colombia. In 1996 she was admitted into Universidad Nacional de Colombia in Bogotá and she received a bachelor degree (BSc) in Chemical Engineering in 2003 with a major in polymers. From 2003 to 2005 she worked as production manager at Plastinova S.A., a synthetic rubber compounding company, in Bogotá, Colombia. In March 2005, she started a Master of Science degree program in process engineering at the Technical University of Eindhoven. Her thesis project: "Development of a platinum on Hairy Foam catalyst" was carried out at the Chemical Reactor Engineering group (SCR) under the supervision of Prof. Dr. Ir. J. C. Schouten, Dr. Ir. J. van der Schaaf, Dr. Ir. B. F. M. Kuster and Dr. Ir. P. W. A. M. Wenmakers. After obtaining her Master of Science (MSc.) degree in 2007, she started her PhD studies at the Inorganic Chemistry and Catalysis group under the supervision of Prof. Dr. Ir. K. P. de Jong and Prof. Dr. J. H. Bitter. Her research was funded by the ACTS-ASPECT program of The Netherlands Organization for Scientific Research (NWO). The results obtained during this period are described in this thesis and were presented at different international conferences.